MINISTRY OF EDUCATION
TECHNICAL UNIVERSITY
OF CLUJ-NAPOCA, ROMANIA
FACULTY OF ELECTRICAL ENGINEERING

PhD THESIS

Permanent Magnet Synchronous Machine for Electric Vehicles Propulsion

PhD Student:
Eng. Cristina-Adina MOLDOVAN (căs. BILAȚIU)

PhD Supervisor:
Prof. Claudia Steluța MARȚIȘ

Examination committee:
Chair: Assoc. Prof. **Mircea Ruba**, PhD – Technical University of Cluj-Napoca, Romania;
PhD Supervisor: Prof. **Claudia Steluța Marțiș**, PhD – Technical University of Cluj-Napoca, Romania;

Members:
Prof. **Nicolae Muntean**, PhD – Politehnica University Timisoara, Romania;

Assoc. Prof. **Ciprian Șorandaru**, PhD – Politehnica University Timisoara, Romania;

Prof. **Loránd Szabó**, PhD – Technical University of Cluj-Napoca, Romania.

– Cluj-Napoca –
2023

str. Memorandumului nr. 28, 400114 Cluj-Napoca, România
tel. +40-264-401200, fax +40-264-592055, secretariat tel. +40-264-202209, fax +40-264-202280
www.utcluj.ro

ACKNOWLEDGMENTS

First and foremost I am deeply grateful to my scientific advisor prof. Claudia Steluța MARȚIȘ for her continuous support shown me over the years, for giving me confidence and motivation, for her patience and immense knowledge. Her guidance and constant encouragement helped me to discover my abilities and to look confident towards my career.

I want to thank my colleagues in the department for all the help and support offered during these years, all the constructive discussions and time spent together.

I would like to thank my beloved husband Andrei, my marvellous parents Anca and Marcel, and my family as a whole for all the sacrifices they have done for me, for their continuous support and for their unconditional love. Without them, I would not have been able to achieve my goals.

Last, but not the least, I thank my friends for supporting me every time, for creating unforgettable moments and experiences.

THANK YOU!

TABLE OF CONTENTS

ABBREVIATIONS

PMSM	Permanent Magnet Synchronous Machine
IPMSM	Interior Permanent Magnet Synchronous Machine
PM	Permanent Magnet
EV	Electric Vehicle
ICE	Internal Combustion Engine
FEA	Finite Element Analysis
FEM	Finite Element Method
DC	Direct Current
AC	Alternative Current
RMS	Root mean square
DTC	Direct Torque Control
FOC	Field Oriented Control
MTPA	Maximum Torque per Ampere
HiL	Hardware in the Loop

1. Introduction

1.1 Motivation and objectives

In recent years, electric vehicles have become more and more popular. Air pollution, global warming, the threatening shortage in terms of natural resources, and also the increased market demand in this direction, have led to the increasingly accelerated development of this sector.

In such a continuously changing world, engineers in the field and designers must always find the best solution to meet the market's requirements, while continuously supporting progress and innovation.

The development of an electrical machine is a complex task, considering that this involves expertise in a variety of domains, including electromagnetics, computer science, mathematical modelling and numerical methods, optimization, mechanics, thermodynamics, acoustics, etc. In addition, the selection of the right electrical machine type, for a given application, is challenging too considering that the advantages of each type of machine must be maximized according to the requirements. Even so, the development of new electrical machines that meet the requirements of the market is impetuously necessary, the contribution of each specialist being a real breath of fresh air in an industry that is taking up more and more land.

Looking back, from the beginning of the expansion of this market until now, it can be seen an exponential increase in the number of electric vehicles sold in the world. If this statistic is reported to Europe, the trend is also an increasing one. According to the International Energy Agency (IEA), in 2022, 1.6 million of electrical vehicles were sold in Europe, compared to 2012 when 18000 sales were recorded. In this regard, Fig. 1.1 highlights a graph of the electrical vehicles sold in Europe between 2012 and 2022.

It can be noticed that the expansion of the market is as obvious as possible, the production of new electrical vehicles being in a continuous and accelerated development.

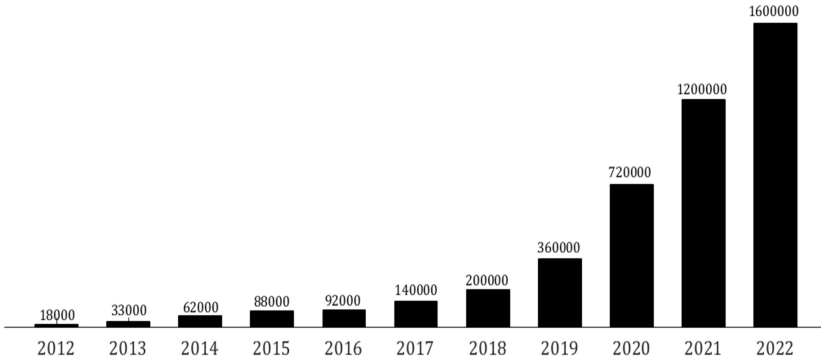

Fig.1. 1 Electrical vehicles sold in Europe between 2012 and 2022 (based on IEA data)

The main objective of this doctoral thesis is to design, analyse and validate an Interior Permanent Magnet Synchronous Machine for the propulsion of an electric vehicle developed to work as a mobile charging station. The research and development work was performed in the frame of a national funded research project entitled "Smart conductive charging station, fixed and mobile, for electric propulsion transportation - SMiLE-EV (PCCDI 36/2018).

The author designed the electrical machine by taking into account the requirements and limitations given by the application, and also taking into account the phenomena that occur when the machine is operating and their impact on the performances of the entire drive system. The validation of the designed model was carried out by laboratory testing within the Department of Electrical Machines and Drives of the Technical University of Cluj-Napoca.

"We keep moving forward, opening new doors, and doing new things, because we're curious and curiosity keeps leading us down new paths."

Walt Disney

1.2 Thesis organization

This thesis comprises six chapters that are briefly presented below.

In the **second chapter**, the main characteristics of PMSMs, such as their particularities, the advantages and disadvantages compared to other electrical machines available on the market, or their applicability in the industry, are highlighted. Next, a brief classification of PMSMs based on different criteria is provided. Among the considered criteria, there are: the air-gap flux orientation, the positioning of the permanent magnets on the rotor, etc.

At the end of this chapter, the constructive elements of PMSMs, along with certain constructive variants of IPMSMs that already exist on the market, as well as the operating principle are addressed.

The **third chapter** is, for the most part, dedicated to the theoretical background necessary for the implementation of design, analysis and optimization processes of an electrical machine. In this regard, the algorithm for generating the machine specifications based on the requirements, as well as the algorithm for the pre-sizing of an IPMSM, are detailed. The pre-sizing stage aims to determine the main geometrical characteristics of the machine. Also, in the design process, particularities, such as the influence of the number slots-poles combination, the influence of the winding configuration on the machine's performances, but also the characteristics of the materials used in the construction of the machine's elements, are taken into account.

Next, the implementation algorithm of performing an electromagnetic analysis using specialized calculation software packages (in this case, JMAG Designer) is highlighted, as well as the main characteristics of the thermal and mechanical analyses, but also the optimization process of an electrical machine particularities.

In addition, the dynamic model of the machine, based on the mathematical model, is presented, as well as some online and offline techniques for parameter estimation and calculation.

At the end of the chapter, the impact of the saturation and cross-saturation phenomena on the machine's parameters is addressed, together with the four levels of complexity used in the development of electrical machines models, based on the aforementioned phenomena.

Chapter four deals with the actual design and analysis of the machine that made the subject of this thesis, based on the theoretical background presented in the previous chapter.

Therefore, starting from the main geometrical characteristics and requirements, the specifications of the electrical machine are generated. Afterward, it goes to the preliminary design stage, in which the chosen type of machine and its particularities, the materials used in the construction of its main elements, the computation of the main dimensions of the stator and rotor cores, the permanent magnets sizing, as well as the winding and stator slots sizing, were established.

Then, based on the results obtained in the pre-dimensioning, respectively specifications generation stages, the virtual model of the machine was built, using JMAG software package. The process started with the modelling of the stator and rotor cores, the winding, and permanent magnets, all these steps being detailed in this chapter. Subsequently to this, the processes of materials assignment, setting the simulation conditions, implementation of the machine's circuit, and definition of the mesh are presented.

The next step is represented by the execution of the electromagnetic analysis. In this regard, both the no-load and rated-load operation scenarios were considered. The simulations results are also included in this chapter. In addition, the thermal analysis of the machine was also taken into account in this chapter.

Additionally, the control strategy used to validate the model, as well as the results obtained from the simulations performed in MatLAB Simulink are highlighted here.

Chapter 5 is focused on the laboratory testing of the machine. This section includes the presentation of the experimental set-up built for the constructed prototype and the results of the measurements performed in the laboratory.

The **last chapter** presents the main conclusions of this thesis, along with the personal contributions of the author and the future perspectives in this field.

The thesis also includes the author's list of publications, lists of figures, tables, and abbreviations, and an appendix. Moreover, an extensive reference list appears at the end of each chapter, which may be valuable for any specialist who intends to study the IPMSMs development.

2. Permanent Magnet Synchronous Machine

2.1 Introduction

This chapter aims to present the main characteristics of Permanent Magnet Synchronous machines, including their particularities, some advantages and disadvantages, and their applicability in the industry.

In addition, a brief classification of PMSMs, based on different criteria, such as: the air-gap flux orientation, the stator windings distribution, the positioning of the permanent magnets on the rotor, as well as the position of the rotor against the stator.

Moreover, the constructive elements of the PMSM, and some existing constructive variants of IPMSMs, as well as the principle of operation, are highlighted.

2.2 General information

At this moment the electric machines market is led by Permanent Magnet Synchronous Machine (PMSM) [1], but this has not always been the case. It took decades for PMSMs to be used in industry and not just in laboratory experiments. The reason why the expansion of these electric machines has been so slow, is mainly due to the poor quality of the permanent magnets [2]. However, these limitations have led to progress in the industry, as many researchers in the field have dedicated their time and knowledge to develop new, more efficient and powerful permanent magnet variants to improve the characteristics of PMSMs [3]. With the discovery of the alnico magnet, which was 100 times more powerful than any other product on the market at that time, in 1930, interest in PMSMs returned [4].

With the development of electronic equipment used in control, these electric machines become more and more popular.

However, this aspect was not the only one that propelled PMSMs among the most used AC electric machines. The popularity of PMSM is,

in a large extent, due to the advantages it offers. These are mostly provided by permanent magnets and include: higher efficiency and power/torque density compared to other AC machines, a faster dynamic response, lower cost of operation and maintenance. Moreover, the constructive simplicity is another important advantage. This is due to the fact that the rotor electrical excitation is provided exclusively by the permanent magnets, automatically involving the reduction of machine`s size and the increase of its reliability [5].

Among the drawbacks, the most important are the high cost of high-quality permanent magnets and the risk of demagnetization. Furthermore, defects that arise during operation are frequently permanent and difficult to identify, making prevention nearly impossible. In addition, for structures with low saliency, high-speed operation can be crucial, putting additional strain on the inverter, which must supply extremely strong demagnetization (d-axis) currents.

In terms of applicability, the automotive sector is, by far, the largest consumer of PMSMs. The number of auxiliary motors mounted in a vehicle can range from a handful in a budget car to almost one hundred in a luxury car [6]. However, because PMSMs are used in a wide range of power and speed, it's fair to assume that they are used in a wide range of applications, including: industry, commodities, information and office equipment, transportation, aerospace industry, medical and healthcare equipment, power tools, renewable energy systems and so on.

The wide range of applications for PMSMs makes it a vital technology today, and it is deservedly regarded as one of the finest innovations in the industry [7].

2.3 Types of PMSM

According to various criteria, PMSMs can be classified into four major categories, as shown in Fig.2.1. These criteria include the air-gap flux orientation, the distribution of stator windings, the positioning of permanent magnets on the rotor, and the position of the rotor against the stator.

Regarding the classification in terms of air gap flux orientation, there are three constructive variants, namely: axial flux, radial flux, and transverse flux. The particularities of each of them will be highlighted below.

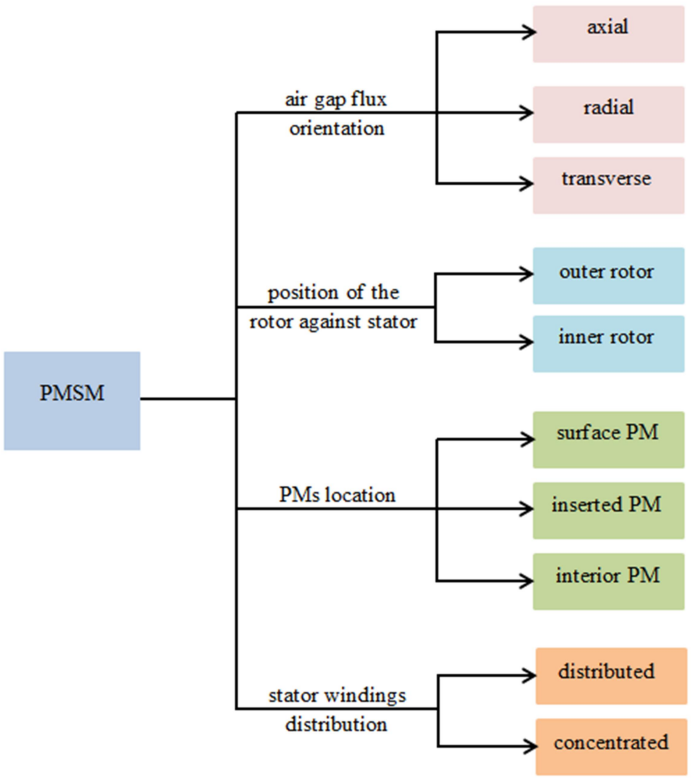

Fig.2. 1Types of PMSMs

In the case of PMSMs with axial flux, presented in Fig.2.2, the flux flows axially through the air gap, as the name suggests, whereas the current flows radially. This type of electric machine can achieve great efficiency and it has the highest torque density of all PMSMs variants. Other advantages compared to the other architectures include reduced vibrations and noise, higher power density, and better ventilation and cooling capability, due to a larger inner diameter [8]. The main drawback of this type is the very high production price. This is largely due to the fact that the stator manufacturing process in difficult.

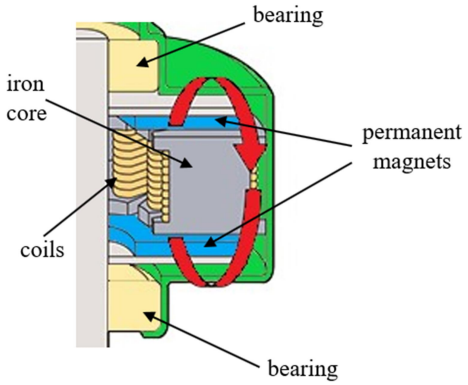

Fig.2. 2 Axial flux PMSM

The most common variant is the one with radial flux (Fig.2.3). In this case, the flux flows in a radial direction through the air gap, while the current flows in an axial direction, that is, in the same direction as the machine`s rotating axis. PMSMs with radial flux are very popular due to their simplicity and since the production cost is smaller compared to other permanent magnet machines. However, their weight and dimensions are substantially larger compared to PMSMs with axial or transverse flux [9].

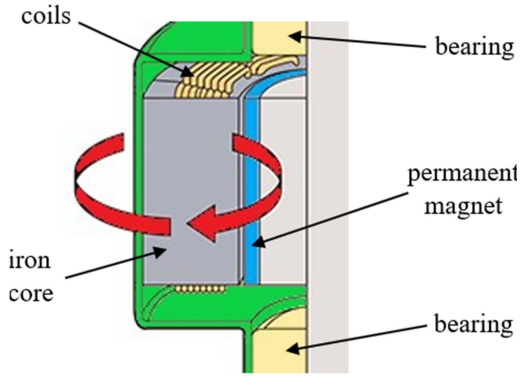

Fig.2. 3 Radial flux PMSM

The third and last option covered by this criterion is the PMSM with transverse flux (Fig.2.4). Despite the fact that it is not yet a commonly used architecture, it has several benefits worth highlighting.

This includes a high specific torque developed by the machine, which automatically involves its compactness. Among the disadvantages, the low power factor at high specific torque and the high production costs due to the complexity of the model are among the main negatives features [10].

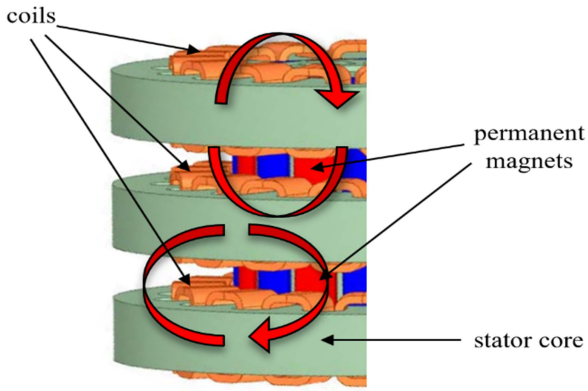

Fig.2. 4 Transverse flux PMSM

Regarding the position of the rotor against the stator criterion, there are two available options, namely: PMSM with outer rotor, respectively PMSM with inner rotor.

PMSMs with outer rotor (Fig.2.5) are electric machines with rotor situated on the outer side, while the stator is located on the inner side. This kind of machines are usually implemented in low speed applications as they have higher inertia compared to outer rotor machines. The high inertia helps the motor to overcome torque variations at low speeds, but does not allow high accelerations [11].

Among the main advantages of outer rotor machines are the shorter axial length compared to inner rotor configuration, and the production of more torque, as the torque is directly proportional to the square value of rotor diameter. In addition, the fact that shorter end turns can be used, can lead to a decrease in copper losses as well as lower inductances. Moreover, the possibility of using low energy magnets has a positive influence on the production cost of these machines.

On the other hand, one of the drawbacks of this configuration is the difficulty with cooling, as the stator and winding are on the inner side and the heat dissipation is very poor. To overcome this inconvenient, a coolant system must be considered. Other disadvantages relate to the weight and size of these machines, which are higher at comparable powers than PMSM with inner rotor, and to the iron losses, which are higher too [12].

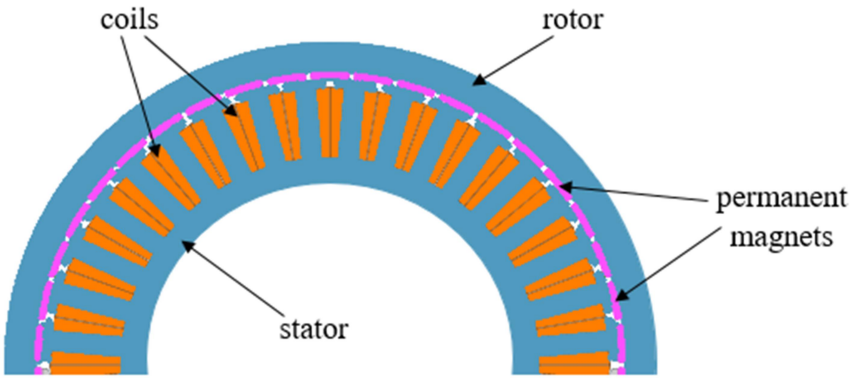

Fig.2. 5 Outer rotor PMSM

Those electric machines whose rotor is located inside, while the stator is placed on the outside are known as inner rotor machines (Fig.2.6). They are predominantly used in applications that require fast acceleration because their inertia is low and, thus, they are more sensitive to torque variation.

The main advantage of these machines is that they can be cooled much easier compared to outer rotor machines. This is due to the position of the stator, which in this case has direct contact with the outside, so that heat dissipation is much more efficient [13].

As for the disadvantages, they refer to the production costs, which are higher, compared to the outer rotor machines, because larger quantities of iron and copper are used and at the same time, it is necessary to use high-energy magnets. Moreover, the use of longer end turns leads to higher copper losses and higher inductance values [14].

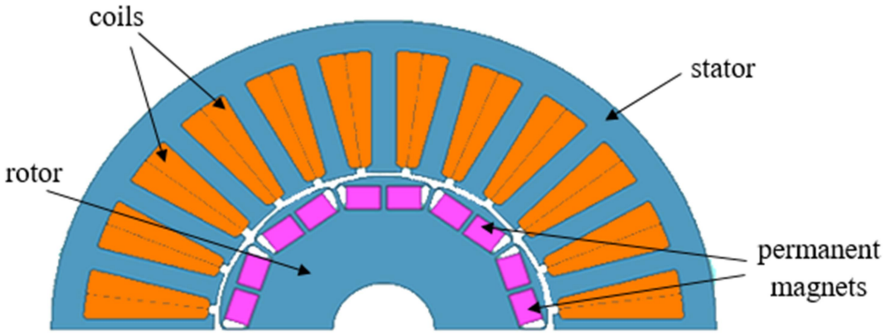

Fig.2. 6 Inner rotor PMSM

In terms of permanent magnets location, there are three constructive options, as follows: PMSMs with permanent magnets mounted on the rotor surface, PMSMs with permanent magnets inserted in the rotor, and PMSMs with interior permanent magnets, respectively.

Regarding surface permanent magnets, shown in Fig.2.7, the main advantages of this structure are its constructive simplicity and its lower production cost compared to other PMSM structures. On the other hand, the most important drawback is that the permanent magnets are extremely exposed to demagnetization. Moreover, it is not recommended to use these electric machines at high speeds, as the risk of detaching the permanent magnets from the rotor is very high in such situations [15].

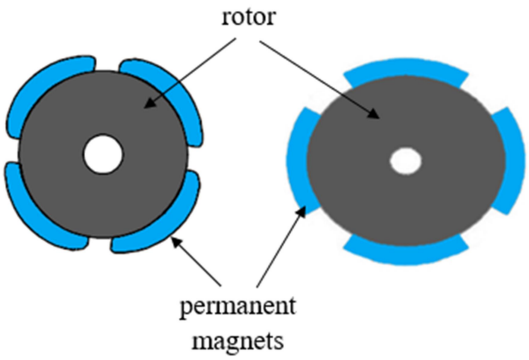

Fig.2. 7 Surface Permanent Magnet Synchronous Machine

Compared to surface permanent magnet synchronous machines, inset PMSMs (Fig.2.8) have iron inter-poles that provide a completely different structure to the machine. As a result, an inset PMSM combine the benefits of surface PMSMs with the added benefit of reluctance torque [16].

Interior or buried permanent magnets synchronous machines (IPMSMs), presented in Fig.2.9, are preferred for their high-speed performance, considering that magnets are better protected against mechanical stress than in the structures exemplified above. In addition to the alignment torque from the permanent magnets, IPMSMs produce a reluctance torque. In this scenario, the benefit is that the rotor can be designed to have a lower reluctance to winding flux than to field flux [17].

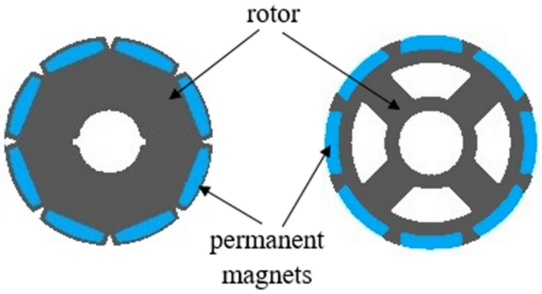

Fig.2. 8 Inset Permanent Magnet Synchronous Machine

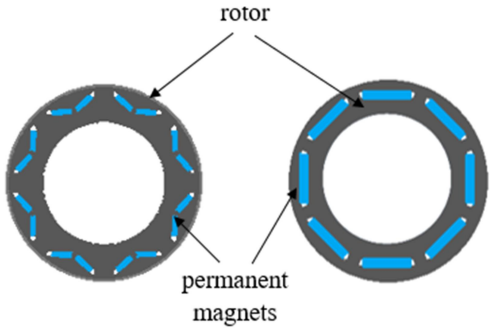

Fig.2. 9 Interior Permanent Magnet Synchronous Machine

Another advantage of this structure is that it offers the ability to concentrate the flux generated by the magnets in the rotor. In this

situation, the flux density in the air gap is higher. However, there are disadvantages too. Among the most important ones are the complicated construction and control, which automatically involve higher costs than in the case of the other two structures [18].

The last PMSM classification criterion taken into consideration refers to the classification according to the way the stator windings are distributed. Depending on the number of slots and poles, the winding can be concentrated or distributed.

PMSMs with concentrated windings, presented in Fig.2.10, are preferred in low-speed applications, considering that they can have a high number of poles and a limited number of slots. Due to the advantages that these electric machines have at the expense of electric machines with distributed windings, they could be very popular for electric vehicle propulsion systems. The only downside is that there is currently a severe lack of experience and knowledge in this area. Among the most relevant advantages of PMSMs with concentrated windings the following can be enumerated: the low value of the cogging torque, which automatically implies lower mechanical stress, lower costs in terms of manufacturing, or the fact that the back electromotive force has an almost sinusoidal shape [19].

There are also certain disadvantages such as the possibility of high variations of magnetic forces on the stator teeth, significant iron losses, the appearance of vibrations and noises, or high values of airgap magnetic flux density harmonics. Moreover, nowadays, this configuration of stator windings cannot be applied to PMSMs with surface magnets [20].

Due to its good and affordable manufacturability, but also its lower copper losses and higher power density, concentrated windings are more preferred than distributed windings (Fig.2.11). However, distributed windings have certain advantages over concentrated ones. Among them, there are higher efficiency and low eddy currents at high speeds [21]. On the other hand, the difficulty in winding automation and the long-end windings are the most relevant drawbacks [22].

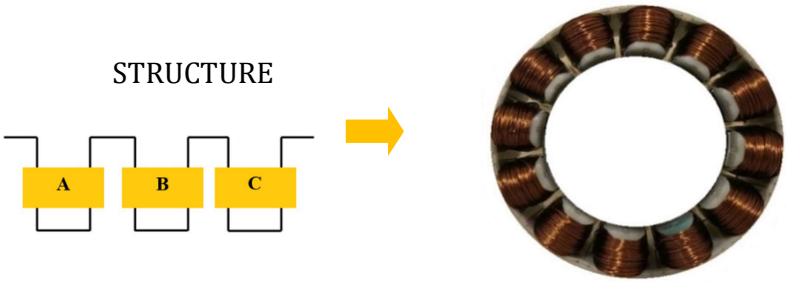

Fig.2. 10 Concentrated winding stator

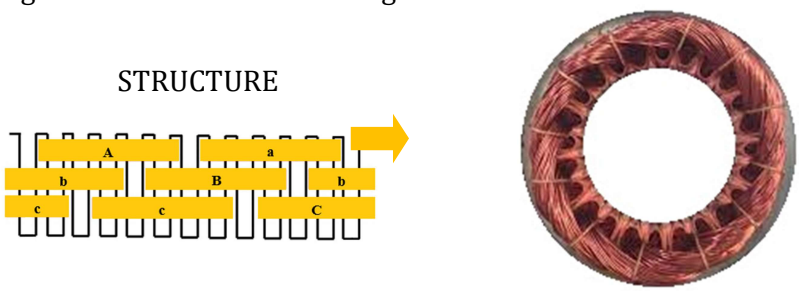

Fig.2. 11 Distributed winding stator

2.4 Constructive elements

Like any other rotating electric machine, PMSM has a stator and a rotor as major constructive parts. The stator, or the fixed part of the machine, is similar to the stator of an asynchronous machine. It is built from a ferromagnetic core and an alternative current winding, which is placed in the core notches. The ferromagnetic core is made of electrical steel sheets coated with natural oxides, organic varnish with inorganic pigments, or phenolic-based organic varnish, to insulate them from each other.

Regarding the rotor core, it is almost identical to the synchronous machine rotor core, the only differences being the lack of slip rings and rotor winding, which is replaced by the permanent magnets. Usually, the permanent magnets are made of neodymium-iron-boron or samarium-cobalt due to their high permeability and their good value for money.

2.5 Constructive variants of IPMSMs

Regarding the IPMSM, there are several constructive variants, based on the shape and arrangement of the magnets, as well as the air gap type (constant or variable).

Depending on the arrangement of the permanent magnets, there are several possibilities to design an IPMSM.

One popular rotor topology is based on lateral magnets. In this case, the magnets can be arranged either in a single layer or in two layers, as shown in Fig, 2.12a and b, respectively. The configuration with two layers of permanent magnets can reduce the torque ripples developed by the machine and, at the same time, it can improve the reluctance torque. In addition, at the same current value, the torque developed by the machine is higher compared to the PMSM with a single layer. The main disadvantage of this configuration is the increase in production costs due to the additional amount of magnetic material [23].

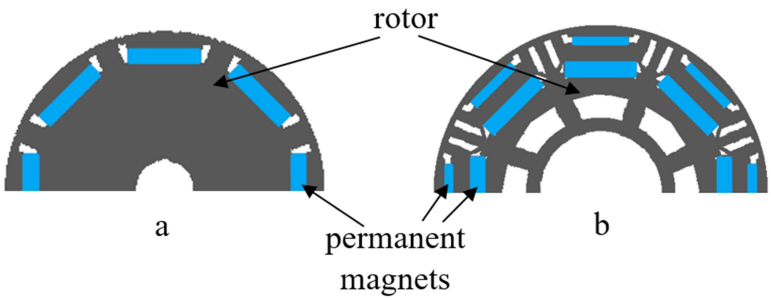

Fig.2. 12 IPMSM with lateral magnets a. single layer b. double layer

The V-shape PMSM, presented in Fig. 2.13, is another constructive solution. Compared to the model with lateral magnets, this design offers the advantage of better performances for flux weakening operation. In addition, the flux density in the airgap can be increased, while the magnetic flux leakage can be decreased. The main disadvantage of this structure is the increase of iron losses, mainly due to the airgap flux density harmonics [24].

Another popular arrangement is with the permanent magnets placed radially, in the form of spokes (Fig. 2.14). In this case, the magnets are tangentially magnetized. The use of magnets whose faces are large compared to those used in the case of machines with lateral magnets, for example, brings a very important advantage in terms of higher torque density, no matter if the machine is equipped with ferrite or rare earth magnets. This kind of machine has some downsides too, such as the possibility of irreversible permanent magnets demagnetization, limitations regarding the use of flux weakening technique when the machine operates at high speed, and waveform distortion in the back EMF [25].

Also, in order to maximize the advantages of the previously presented models, different combinations between them have been developed. Thus, different variants of IPMSMs with double layer of permanent magnets were studied. Among the most popular there are hybrid double V IPMSM, delta shape IPMSM or hybrid delta shape IPMSM.

Regarding the magnetic materials used for permanent magnets, IPMSMs producers use both rare earth permanent magnets and ferrite magnets or AlNiCo alloys. Table 2.1 presents the main properties of the magnetic materials used in the production of permanent magnets. The properties that were considered were: the remanence (B_r), the coercivity (H_c), the maximum energy product (BH_{max}) and the Curie temperature (˚C).

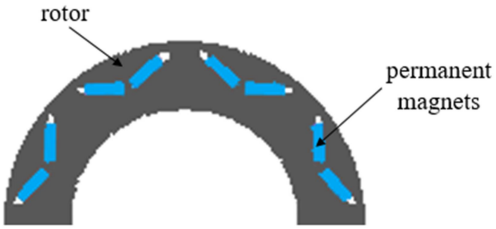

Fig.2. 13 IPMSM with V-shape magnets

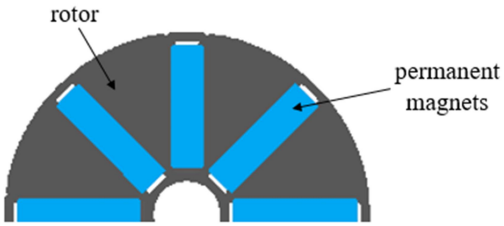

Fig.2. 14 IPMSM with spoke-shape magnets

Table 2. 1 The main properties of the magnetic materials

	NdFeB	**SmCo**	**Alnico**	**Ferrite**
B_r [T]	1.0-1.4	0.8-1.1	0.6-1.4	0.2-0.78
H_c [kA/m]	750-2000	600-2000	275	100-300
BH_{max} [kJ/m³]	200-440	120-200	10-88	10-40
T_c [°C]	310-400	720	700-860	450

In order to understand what is the impact of using a magnetic material, researchers in the field compared identical motors in terms of performance but equipped with permanent magnets made of different materials. Thus, to obtain approximately the same performance, 5 times more ferrite than NdFeB was used, respectively 2.5 times more than SmCo [26].

Another element that can be considered is the air gap. It can be either constant (Fig. 2.15 a) or variable (Fig. 2.15 b). A variable air gap allows the distribution of the field in the air gap, so that it can be more sinusoidal than in the case of a constant air gap. In this way, the magnetic flux density in the air gap harmonics are significantly reduced, which automatically implied the reduction of torque ripple. In addition, the choice of an IPMSM with variable air gap can also have a good influence in terms of stator core losses [27].

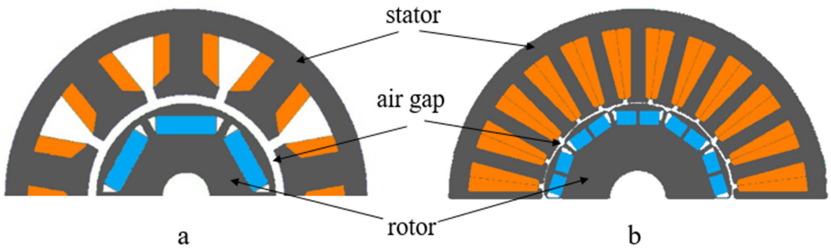

Fig.2. 15 IPMSM air gap a. constant b. variable

2.6 Principle of operation

Generally, in order to generate an electromagnetic torque, the presence of a rotor flux and a stator magnetomotive force is required. These parameters must be stationary with regard to each other, while the phase shift between them must be nonzero. The requisite rotor flux in the case of PMSMs is produced by the permanent magnets positioned in the rotor area, while the stator magnetomotive force is generated by the stator winding currents. When the magnetomotive force and the rotor flux have the same rotational speed, the relative speed between them is considered zero. The rotating stator magnetomotive force is produced due to the injection of a set of polyphase currents that are phase-shifted from each other by the same amount. Therefore, the magnetic field created by the permanent magnets placed on the rotor interacts with the stator field created by the current flowing through the stator windings, and therefore a torque is generated. The main issue of PMSMs is that the rotor poles link up with the stator's magnetic field only when the speed of the stator field is equal to the speed of the rotor. Therefore, these electric machines cannot start on their own.

There are several possibilities to overcome this drawback. Currently, three methods are used to indirectly start a PMSM. The first option is to start the PMSM with the help of an auxiliary motor (asynchronous machine or a direct current machine), connected to its shaft. Another possibility is to start the PMSM in asynchronous mode. This option is valid only if the PMSM is equipped with a damping cage. In addition to the advantage at start-up, this variant also has a very important benefit, namely, the fact that in transient mode, the cage

allows the machine to maintain its stability. However, there is a drawback regarding the impact on PMSMs weight.

The last way to start a PMSM is through a power converter. If the stator's spinning magnetic field rotates at a low enough speed, the rotor will be able to accelerate and lock in with the stator's magnetic field without difficulty. By progressively increasing the supply frequency up to its typical value, the speed of the stator magnetic field can be increased to its rated operating speed. With the development and improvement of electronic equipment, starting PMSMs in this way is very easy, the frequency is set to a value as low as possible for starting, and then it is increased to the value necessary for the optimal operation of the electric machine.

2.7 Conclusions

This chapter aims to highlight the main characteristics of IPMSMs. In this regard, the existing types of IPMSMs were described, by presenting their particularities, as well as some of their advantages and disadvantages. Then, a brief presentation of the constructive elements of this electric machine was introduced, followed by highlighting the properties of some popular constructive variants. Finally, the operating principle of PMSM, as well as the methods used to indirectly start such a machine was discussed.

As a conclusion of this chapter, the variety of PMSM types, its advantages compared to other electric machines and the multitude of fields where PMSM is used, make it an indispensable device nowadays, remaining, rightfully, one of the greatest inventions of the industry.

References

[1] Gyselinck & A.-C. Pop, ICEM, Lausanne, Switzerland, 4-7 September 2016, Tutorial: Finite-element and lumped-parameter modelling and simulation of PMSMs.

[2] Juha Pyrhonen, Tapani Jokinen, and Valeria Hrabovcova. “Design of Rotating Electrical Machines”. John Wiley & Sons, 2009. Page 200.

[3] Jacek F. Gieras, PM Motor Technology: Desing and Applications, CRC Press, Taylor and Francis Group, 2010.
[4] Peter Kelly Sokolowski, Processing and Protection of Rare Earth Permanent Magnet Particulate for Bonded Magnet Applications, ProQuest, 2007.
[5] H. Wang and J. Leng, "Summary on development of permanent magnet synchronous motor," 2018 Chinese Control And Decision Conference (CCDC), Shenyang, 2018, pp. 689-693, doi: 10.1109/CCDC.2018.8407219.
[6] Gieras, J.F. Wing, M., Permanent Magnet Motor Technology. Design and Applications, Second Edition, Revised and Expanded.
[7] **C. -A. Bilaţiu**, P. Karaisas and C. -S. Marţiş, "Electromagnetic Analysis and Experimental Validation of an Interior Permanent Magnet Synchronous Motor," 2021 12th International Symposium on Advanced Topics in Electrical Engineering (ATEE), 2021, pp. 1-6, doi: 10.1109/ATEE52255.2021.9425229.
[8] Daniel Martinez, „Design of a Permanent-Magnet Synchronous Machine with Non-Overlapping Concentrared Windings", Stockholm, Sweeden, 2012, XR-EE-E2C 2012:020.
[9] F. Meier, „Permanent Magnet Synchronous machines with no-overlapping concentrated windings for low-speed direct-drive applications", Doctoral Thesis, Royal Int. Technol., Stockholm, Sweeden, 2008.
[10] Tomasz Drabek, Piotr Kapustka, Tomasz Lerch, Jerzy Skwarczynski, „A novel Approach to Transverse Flux Machine Construction", Energies 2021,14,7690, doi:10.3390/en.14227690.
[11] Ilya Petrov, Juha Pyrhönen, "Perormance of Low-Cost Permanent Magnet Material in PM Synchronous Machines", IEEE Transactions on Industrial electronics, Vol. 60, No. 6, June 2013.
[12] Enwelum I., Mbadiwe, Erwan Bin Sulaiman, "Design and Optimization of outer-rotor permanent magnet flux switching motor using transverse segmental rotor shape for automotive applications", Ain Shams Engineering Journal, Volume 12, Issue 1, 2021, ISSN 2090-4479.

[13] Taha, Harwan, & Alnaab, Ismaeil. (2019), Designs of PMSMs with Inner and Outer Rotors for Electric Bicycles Applications, Kurdistan Journal of Applied Research, 4, 20-25, 10.24017/science.2019.1.4.

[14] Irfan Ali Soamro et al, "Overview of inner rotor radial permanent magnet machines for electric vehicles", 2020 IOP Conference, Series: Mater. Sci. Eng. 917 012005.

[15] P. Salminen, J. Pyrhönen & M. Niemelä, "A Comparison Between Surface Magnets and Embedded Magnets in Fractional Slot Wound PM Motors", Computer Engineering in Applied Electromagnetivism, 2005, ISBN: 978-1-4020-3168-7.

[16] Pang, Da-Chen & Shi, Zhen-Jia & Xie, Pei-Xuan & Huang, Hua-Chih & Bui, Thinh. (2020), "Investigation of an Inset Micro Permanent Manget Synchronous Motor Using Soft Magnetic Composite Materials", Energies, 13, 4445, 10/3390/en13174445.

[17] Eilenberger, Andreas & Schrödl, M. (2010), "Sudden short-circuit analysis of a salient permanent magnet synchronous machine with buried magnets for traction applications", 10.1109/EPEPEMC. 2010.5606596.

[18] Kolehmainen, Jere & Ikaheimo, Jouni, "Motors With Buried Magnets for Medium-Speed Applications", Energy Conversion, IEEE Transactions on. 23. 86-91, 10.1109/TEC.2007.914331.

[19] H.C.M. Mai, R. Bermard, P. Bigot, F. Dubas, D. Chamagne, and. C.Espanet, "Optimal Design of a PMSM Using Concentrared Winding for Application Urban Hybrid Vehicle", 978-1-4244-8218-4/10/$2600, 2010 IEEE.

[20] Olivier Barré, Bellemain Napane, "Concentrated Windings in Compact Permanent Magnet Synchronous Generators: Managing Efficiency", Machines 2016, 4, 2; doi: 10.3390/machines4010002.

[21] Kwon, Soon-O & Kim, Sung-Il & Zhang, Peng & Hong, J.P., (2006), "Performance comparison of IPMSM with distributed and concentrated windings", 1984-1988, 10.1109/IAS.2006.256807.

[22] Hongbo Qiu, Yong Zhang, Cunziang Yang, Ran Yi, "Performance analysis and comparison of PMSM with concentrated windings and distributed winding", Archives of Electrical Engineering, Vol

69(2), p.p. 303-317 (2020), 2019, DOI: 10.24425/aee.2020.133027.

[23] Huynh, Thanh Anh & Hsieh, Min-Fu. (2018). Performance Analysis of Permanent Magnet Motors for Electric Vehicles (EV) Traction Considering Driving Cycles. Energies. 11. 1385. 10.3390/en11061385.

[24] Lee, Kab-jae & Kim, KiChan & Kim, Sol & Ahn, Joon-Seon & Lim, SeongYeop & Lee, ju. (2005). Optimal magnet shape to improve torque characteristics of interior permanent magnet synchronous motor. Journal of Applied Physics. 97. 10Q505-10Q505. 10.1063/1.1852411.

[25] Montalvo-Ortiz, Eduardo & Foster, Shanelle & Cintron-Rivera, Jorge & Strangas, Elias. (2013). Comparison between a spoke-type PMSM and a PMASynRM using ferrite magnets. 1080-1087. 10.1109/IEMDC.2013.6556230.

[26] Sekerak, Peter & Hrabovcova, Valeria & Onufer, Matus & Kaiamen, Lukas & Rafajdus, Pavol. (2012). Synchronous motors with different PM materials. 10.1109/ELEKTRO.2012.6225646.

[27] Zhu, Shushu & Hu, Yaohua & Liu, Chuang & Jiang, Bin. (2020). Shaping of the Air-gap in a V-typed IPMSM for Compressed-Air Systems Applications. IEEE Transactions on Magnetics. PP. 1-1. 10.1109/TMAG.2020.3034152.

3. Design and Analysis of IPMSMs – Approaches and Implementation

3.1 Introduction

This chapter describes the main steps that should be followed when designing and analysing an IPMSM. Firstly, the specifications of the electric machine to be designed must be defined. The next step would be the choosing of the materials from which each component of the machine is made. Then, the pre-sizing procedure can be implemented, including the computation of the main dimensions of the machine, such as the inner/outer stator/rotor diameter or the machine's length, as well as the PMs volume, the choice of the optimal combination between the number of poles and number of stator slots, and the winding configuration. In the end, a complete analysis of the machine should be carried, both from electromagnetic, structural and thermal point of view, and, if necessary, the optimization process should be implemented.

Further, the general dynamic model of a PMSM will be presented. In this regard, the machine's equations are presented both in three-phase system and orthogonal system. In addition, some online and offline techniques for parameters estimation and computation are mentioned. Moreover, the saturation and cross-saturation impact on the machine's parameters is also discussed in this section, as well as the four levels of complexity in the PMSMs models development.

3.2 General considerations

Nowadays, the design of electrical machines is a very popular topic, especially due to the fast evolution of this industry. The demand for the most efficient and reliable electric machines is even grated. Therefore, the designers must constantly find the optimal solutions to be able to satisfy the market demand, taking into account, at the same time, the fundamental principles of design.

When the decision of designing an electric machine is made, its basic components must be known very well. In the case of rotating electric machines, such as IPMSM, the main components that should be taken into account in the design process are the physical parts of the machine (stator and rotor), the magnetic circuit, the electric circuit, the insulation and the cooling system (if applicable). The dimensioning of these elements is carried out using analytical equations.

The common problem faced by designers is that often, the situations they face may not have a single answer but rather several. They must ensure that the final product works in compliance with the given requirements, improving, as much as possible, its performance in terms of efficiency, losses or cost and at the same time, taking into account the fact that the product must be durable and reliable. Moreover, they should be open to making certain compromises, because not always the ideal design can be achieved by the manufacturer. Last but not least, national and international standards in force must be respected.

A final design can only be reached through an iterative process since the design incorporates several assumptions and limitations. The final design is obtained in large part thanks to the computer, due to the special software packages that were developed. The impact of a single parameter on the performance of the machine may be investigated using the finite element method (FEM). Furthermore, FEM enables the virtually execution of tests that aren't even physically possible in a laboratory setup.

Regarding the limitations of the design process, in addition to the limitations imposed by the client or by different standards in force, there are also some limitations given by the chosen materials and their behaviour in different scenarios. These limitations are caused mainly by the conductor’s current density, insulation properties, iron saturation, power factor or temperature changes. For example, a higher current density will increase the copper losses, even if it will reduce the volume of the needed copper, or a higher power factor, even if it is desirable, will increase the maintenance cost. Additionally, the iron saturation can

affect the core losses. Therefore, there must be a very fine balance between all these parameters, so that the final design can be as good as possible.

The design of an electrical machine is closely managed by the design of the system/application in which it will be integrated [1]. The derivation of the electrical machine specifications, which are founded on application (system and/or subsystem level) requirements, marks the beginning of the design process(Fig. 3.1). On the machine side, these requirements cover steady-state and dynamic performances, seconded by specific geometrical/dimensional/technological constraints, manufacturing costs, thermal and NVH limits, etc.

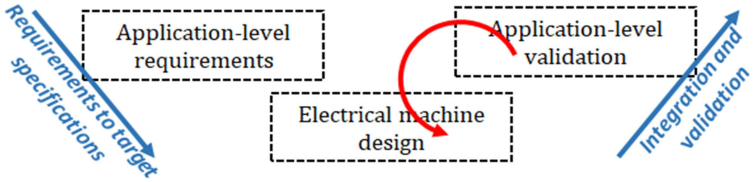

Fig.3. 1 The electrical machine design and validation flow

The specifications of the machine include the main input data both from electrical and mechanical point of view. For instance, the rated power, torque, current, and speed are considered, as well as the maximum speed of the machine or the efficiency. Moreover, the voltage value and the source type used to power the machine (AC or DC) are defined at this step. From mechanical point of view, the main geometrical parameters are established, taking into account, of course, the technological constraints. At this step, the cooling method, the thermal constraints, as well as the insulation class and the noise and vibration constraints are defined, depending on the application requirements [2]. Then, the materials used for each machine component are chosen. All of these parameters are defined based on a continuous balance between fulfilling the customer's requirements and respecting the established manufacturing cost.

After all of these specifications are clearly defined, the designer can start the electrical machine design.

The electrical machine design process is an iterative and multiphysics one (Fig. 3.2) and, once the topology chosen, it starts with the pre-sizing procedure. The generation of the main dimensions of the machine (pre-sizing), whose main objective is to gather a preliminary set of information about the machine's main dimensions, winding configuration, or the materials used in the construction of the machine, Moreover, after the sizing stage the designer will also obtain an initial evaluation of the parameters and machine's performances [3].

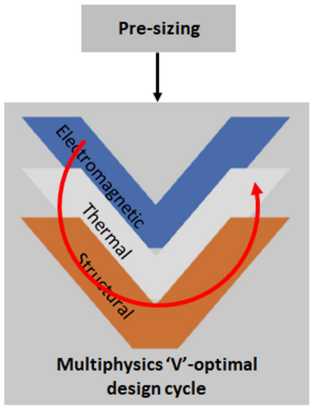

Fig.3. 2 Electrical machine design flow

In order to obtain an assessment as precise as possible in terms of machine's performances and its parameters values, data obtained in the pre-sizing stage are included in a multiphysics design analysis. If necessary, an optimization technique is implemented, at machine level too [4].

Having the output parameters of machine-level simulation available, such as machine's parameters, magnetization maps and curves, the efficiency map, the next step (application-level validation) can be performed. This step is very important in order to analyze the machine's dynamic performances and also to analyze the impact that certain control strategies or power converter topologies have on these

performances. All of these analysis scenarios are done based on the operation scenarios that have been established in the stage of defining the machine's specifications. Moreover, as in the previous stage, it may be necessary to implement an optimization loop in order to obtain an ideal design for the electric machine [5].

3.3 Electrical machine specifications generation

The engineer must translate the application-level requirements into subsystem-level specifications, which are then translated into component-level specifications, while also understanding the complex relationships between the system's various components.

The identification of the propulsion system (gearbox, electrical machine, power converter & controller, and battery) for an electric vehicle has to consider and summarize all parameters and requierements for the vehicle: type of the vehicle, characteristics of the vehicle and other requirements.

From the point of view of vehicle type, the market of the conventional vehcles is usually segmented based on vehicle size. We can identify A/B/C/D/E/F segments for respectively basic / subcompact / compact / midsize / large / large plus. Other segments include sports, MPV, SUV, Van, etc. When considering electric vehicles, we could also identify five main categories based on size, powertrain architecture, performance and cost:

- Neighbourhood Electric Vehicles (NEV)
- City Electric Vehicles (CEV)
- Extended-Range Electric Vehicles (E-REV)
- Plug-In Hybrid Electric Vehicles (PHEV)
- High Performance Electric Vehicles (HPEV)

Vehicle characteristics refer to total vehicle mass, mass distribution, tyre width, tyre height, wheel diameter, vehicle powertrain architecture (central driving, distributed driving, single or two speed transmission), as well as the vehicle performance requirements (continuous power, continuous torque, peak torque/power, maximum

speed at the wheel, voltage level, etc.). Other requirements, like dimensional constraints, cost per unit, power/torque density, etc. are also to be defined [6].

The first step in choosing the drive system (motor, gearbox, and controller) for an electric vehicle is to summarize all the drive parameters and requirements [1], [2]:

- Establishing the rated and maximum speed, the acceleration, the number of acceleration steps and the maximum torque value;
- Establishing the vehicle's mass;
- Choosing the machine that propel the vehicle;
- Establishing the transmission ratio of the gearbox.

The electrical machine's rated speed, as well as the transmission ratio of the gearbox must be chosen so that the maximum speed of the vehicle, combined with the gear ratio and the circumference of the wheels, is close to the maximum desired speed. However, the calculated value should be higher than the maximum speed to be sure that it can be reached.

As a result, choosing the rated speed and the gearbox ratio must be done all at once. The most important connection between the ideal gearbox ratio (i_{opt}) and the rated rotational speed (n_{motor}) is:

$$i_{opt} = \frac{n_{rmotor}}{n_{rroata}} = \frac{n_{rmotor} \cdot D_r \cdot \pi}{v_{max}} \tag{3.1}$$

where v_{max} is the maximum vehicle speed and D_r is the wheel diameter.

To obtain the rated torque value, the friction force, as well as the air resistance must be considered. Generally, the following equation can be used to determine the friction force:

$$F_{rr} = m \cdot g \cdot c_{rr} \tag{3.2}$$

where m is the vehicle's mass, g is the gravitational acceleration, and c_{rr} is the friction coefficient.

The air resistance force can be determined with the following equation:

$$F_w = \frac{\rho_{air} \cdot c_w \cdot A_{front} \cdot v^2}{2} \tag{3.3}$$

where ρ_{air} is the air density, which is highly dependent on temperature and altitude, c_w is an aerodynamic coefficient, A_{front} is the vehicle frontal area and v is the vehicle speed.

The torque required to overcome the resistive torques is calculated based on the required power, as follows:

$$P = \frac{(F_{rr} + F_w) \cdot v_r}{\eta_{total}} \tag{3.4}$$

$$\mathrm{T} = \frac{P}{\omega_r} = \frac{P}{2 \cdot \pi \cdot n_r} \tag{3.5}$$

The maximum required power should be determined according to the maximum ramp that the vehicle should be able to climb:

$$\alpha = \arctan(\frac{a[\%]}{100\%}) \tag{3.6}$$

$$F_{max} = m \cdot g \cdot sin\alpha \tag{3.7}$$

Based on these calculations, the rated, respectively the peak torque, can be determined:

$$M_{max} = \frac{F_{max} \cdot v_r}{2 \cdot \pi \cdot n_r \cdot \eta_{total}} \tag{3.8}$$

The following data are required in order to choose the electrical machine:

- Rated torque/power;
- Battery voltage;
- Rated speed;
- Operation scenarios;
- The choice of the gearbox.

When choosing the gearbox, the radial and axial forces that act on it should be taken into account. The maximum radial force is calculated based on the following equation:

$$F_{maxrad} = \frac{m \cdot (g + a)}{2} \tag{3.9}$$

The maximum axial force depends on the angle at which the axial force occurs:

$$F_{maxaxi} = m_g \cdot g \cdot sin\alpha \tag{3.10}$$

When choosing the battery package, the battery capacity (in Ah) should be calculated, as follows:

$$C_r = \frac{P}{V_r} \tag{3.11}$$

In addition, the maximum current that the battery package can provide must be determined, based on the relationship:

$$I_{max} = \frac{P_{max}}{V_r} \tag{3.12}$$

3.4 Electrical machine design – IPMSM specific issues

3.4.1 Materials in IPMSM

The primary material properties that are important for electrical machines are those related to insulation, conductors and ferromagnetic materials. The choice of materials is a very important step in the design process of an electric machine, considering that they have a strong influence on its performances.

3.4.1.1 Insulators

Regarding the insulating materials, they should have some properties in order to prevent the electrical activity between electric machine`s components with different potentials: a high temperature resistivity and a good thermal conductivity, a high electrical resistivity,

and dielectric strength as high as possible. Moreover, they should be flexible and should have the ability to resist to thermal oxidation, and not deteriorate due to repeated heat cycles. It is very important that the insulation resist the stresses due to the forces that appear in the machine during operation, as well as to vibrations or bending. In the case of liquid insulators, it is mandatory that they do not evaporate. It is also desirable that the insulating materials do not absorb moisture.

Insulating materials can be broadly divided in three categories depending on their state of aggregation, as follows: solid (Teflon, glass, porcelain), liquid (mineral oil, pyranols) and gas (nitrogen, mercury, fluorine). Another classification criterion is based on thermal resistivity. Table3.1 shows the main characteristics of each class of insulation, according to the international standards of insulation. The maximum operating temperature can be defined as the temperature that the insulation can reach without suffering any damage during operation and it is determined by summing the ambient temperature, the allowed value of the temperature increase and the tolerance of the winding hot spot. It is very important to take into account the insulation when designing an electrical machine considering that this element is one of the weakest against heat and it can decide the life span of the equipment. This is why the maximum operating temperature should not be exceeded. In the case of electric machines, insulation class F is usually chosen, considering that the materials from this class meet the requirements [11], [12].

Table 3. 1 Insulating materials classes and their maximum operating temperatures.

Class	**Max. operating temperature [°C]**	**Materials**
A	105	paper, wood, cotton impregnated with oils and natural resins
B	130	asbestos, glass fiber, mica
C	>180	ceramics, glass, mica quartz with resins
E	120	nylon tapes, polyvinyl epoxy resin
F	155	class B + bonding materials for higher

		thermal resistance
H	180	asbestos, glass fiber, mica with silicone resins

3.4.1.2 Conductive materials

In electrical machines industry, aluminium and copper are mostly used as conducting materials. Table 3.2 highlights the main and most relevant characteristics of these materials. Comparing the two materials, it was found that, although aluminium is much lighter and cheaper than copper, in terms of cross-sectional area, it is approximately 60% larger for the same length and resistance. From the performance point of view, copper is clearly superior [13].

Table 3. 2 Aluminium and copper properties.

	Aluminum	Copper
Resistivity [Ω·m]	2.655e-8	1.72e-8
Density [kg/m^3] (at 20°C)	2699	8960
Thermal conductivity [W/m/°K]	237	401
Specific heat [J/kg/°C]	900	380
Melting point [°C]	660	1083
Temperature coefficient [%/°C]	0.4	0.39
Coefficient of linear expansion [/°C]	2.35e-7	1.68e-7

In addition, research in the field of materials, as well as the desire to develop materials with superior properties, have led to the appearance of substitute products that have much better performance than copper or aluminum.

Therefore, copper alloys can be used, such as, copper clad aluminum (CCA), which consists of a copper layer covering 5 to 15% of the total cross section area of an aluminum rod. Combining these materials in order to obtain an alloy has several important advantages. Among these are better reliability and conductivity, compared to aluminum, but also a lower cost and lower weight, compared to pure copper.

Another new and advanced material is the carbon nanotube (CNT). This type of material has better conductivity compared to aluminum or copper, while its mass density is reduced. Moreover,

because its temperature coefficient is low, the resistance will not be very affected with the temperature increasing.

Additionally, CNT can be combined with copper. Studies have shown that by combining copper with CNT in a proportion of 55%-45%, the mass density is reduced by 40% than in the case of pure copper, while the electrical conductivity is increased by 25%. The high current carrying capacity of CNT-Cu composite is another significant benefit. For example, a combination of Cu and CNT in proportion of 35%-65% will not only reduce the weight of the conductor, but it will also increase its ampacity approximately 100 times.

Last, but not least is the high-temperature super (HTS) conductor, which is one of the most promising options for a variety of rotating electric machines. The advantages of these conductors are the high current values that can be carried by them, the winding loss reduction, as well as the great efficiency and high power density that can be achieved by using them. On the other hand, regarding the drawbacks, due to several technological problems, such as the excessive mechanical stress that causes a significant decline in the performance of the conductors, the commercialization of HTS is limited [14].

3.4.1.3 Permanent Magnet materials

The most relevant magnetic materials utilized in the industry today are depicted in Fig.3.3.

Rare earth magnets, which have exceptionally high magnetic properties compared to other permanent magnetic materials, were created in the second half of the 1960s. Neodymium iron boron (NdFeB) and samarium cobalt (SmCo) are just two examples of materials in this category.

On the other hand, strontium (Sr), barium (Ba) and iron (Fe) oxides are the primary elements of ferrite magnets. One of the biggest advantages of these materials is their low price. Additionally, as the oxides are the principal component of these materials, they provide excellent corrosion resistance and high specific resistance [15].

The strength of rare earth magnets is the primary distinction between them and ferrite magnets. Performance of permanent magnets is influenced by coercive force and magnetization intensity. Rare earth magnets have a high magnetism because they contain cobalt and iron in an oxygen-free condition. Additionally, rare earth magnets are significantly stronger magnets than ferrite because their magnetization has a strong force aligning the magnetism in one direction. Rare earth magnets are employed for strong magnetic circuits because they perform approximately ten times better than ferrite magnets in terms of total energy per volume.

In addition to being used alone, permanent magnetic materials are occasionally ground into a powder, combined with plastic or rubber, and moulded. Bonded magnets are the name for such magnets. Bonded magnets may be flexibly processed into any shape and combined with other components to make a single unit, but because there is less magnetic material overall, their magnetic force is also decreased.

One of the most important quantities characterizing the quality of a permanent magnet is the magnetic flux density (B), measured in Tesla [T]. This can be determined using equation 3.13 [16, 17].

$$B = \mu_0 H + J \tag{3.13}$$

where:

- μ_0 [H/m] is the magnetic permeability of vacuum

$$\mu_0 = 4\pi \times 10^{-7}; \tag{3.14}$$

- H [A/m] is the magnetic field;
- J [T] is the magnetization.

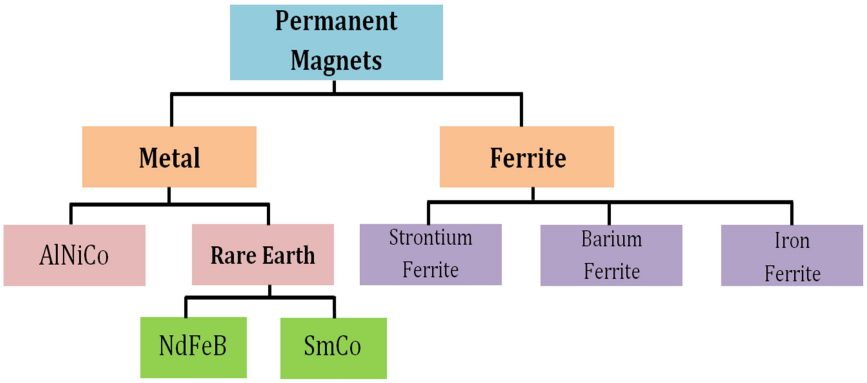

Fig.3. 3 Permanent magnets types

Speaking about the design stage of PMSMs, it is very important to mention that the hysteresis loop or the B-H curve must always be the basis of the permanent magnets design. This curve depicts the whole cycle of a magnet in a closed circuit. Fig.3.4 shows the B-H curve.

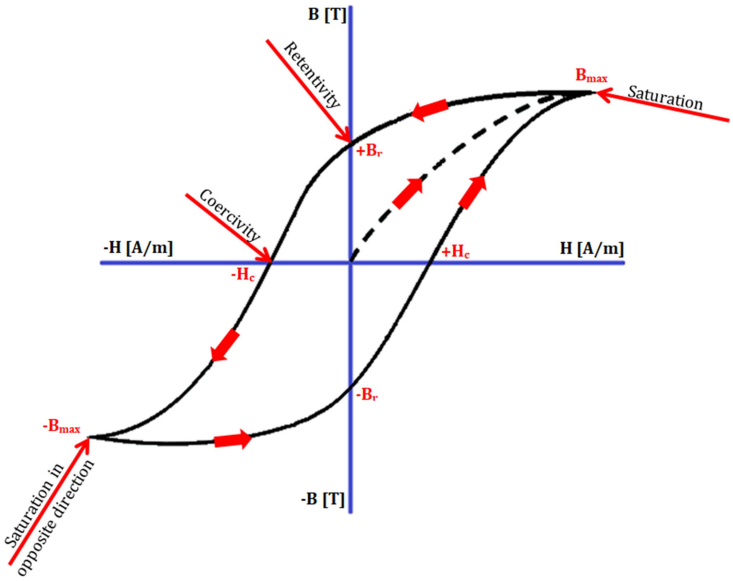

Fig.3. 4 Typical B-H curve of magnetic materials

As it can be seen, the first quadrant of the graph shows the process in which the magnet is brought to saturation, while the second one, also named the demagnetization curve quadrant, is considered the most important quadrant as the main parameters of the materials, such as, B_r and H_c are defined there. The points where the curve intersects the B (B_r) and H (H_c) axes, as well as the point where the product BH has the maximum value, are the three key features of the curve. $B_{r,}$ or the residual flux density, is the maximum flux that the magnet can generate in a closed circuit, while H_c stands for the moment when the permanent magnet starts to be demagnetized due to an external magnetic field. BH_{max} can be defined as the maximum value of the magnetic field density in the air gap around the magnet. These are three of the most important values that must be taken into account when designing the magnets, together with influence of the temperature on the hysteresis loop [18], [19].

Moreover, the stability of the magnets must be taken into account when designing an electric machine. This can be affected by several factors, such as: temperature, time, shocks and vibrations during operation or reluctance changes due to the air gap dimensions changes that may occur during operation. If in the case of modern permanent magnets the time and shocks or vibrations effects are minimal, the same cannot be said about temperature variations. These can produce more or less serious damages. For this reason, a classification of losses has been made according to their severity: reversible losses, irreversible but recoverable damages and, finally, irreversible and irreparable damages.

Damages are considered reversible when the reversible temperature coefficients, α – for B_r, respectively β – for H_c, are not exceeded. For the most relevant materials in electric machines design, α and β values, as well as Curie temperature (T_{Curie}) are shown in Table 3.3. Curie temperature is the temperature at which the magnetic material becomes fully demagnetized.

Regarding the irreversible damages, partial demagnetization is considered an irreversible, but recoverable loss because, even if the

magnet cannot recover itself with the restoring of the initial temperature, the defect can be fixed by remagnetization. On the other hand, when the operation temperature exceeds the Curie temperature (TCurie), the magnet is considered to be total demagnetized and the damage cannot be fixed by remagnetization. This is an unrecoverable loss [20].

Table 3. 3 Reversible temperature coefficients and Curie temperature.

	AlNiCo	**NdFeB**	**SmCo**	**Ferrite**
α [%/°C]	-0.02	-0.12	-0.04	-0.2
β [%/°C]	-0.01	-0.55	-0.4	0.27
T_{Curie} [°C]	860	310	750	460

3.4.1.4 Soft magnetic materials

Regarding the soft magnetic materials used in electric machines construction, their quality has increased considerably following the discoveries made by researchers in this field.

When the foundations were laid for the construction of the first electric machine, around the 1830s, simple iron cores were used. Then, in order to reduce the eddy currents losses, the iron wires were introduced. Around 1873, the iron wires were replaced by electrical isolated iron sheets, as later, in 1880, laminated sheets were used for the first time. This electric machines cores manufacturing method is still used today.

However, studies and experiments did not stop there, so that, at the end of the 19th century different iron alloys, such as nickel-iron (NiFe) and silicon-iron (SiFe) were studied, in order to be used in electric machines production industry. Their properties were clearly superior compared to laminated sheets, therefore SiFe alloy is still the most popular solution in terms of cores manufacturing.

Over time, there was a need to improve the performances and qualities of these materials, so that not only considerable improvements were made to SiFe alloys, but other materials that could

be used in this purpose were also intensively studied. Mostly, the emphasis was on soft magnetic composites (SMC), as well as on amorphous and nano-crystalline alloys [21].

Regarding the parameters taken into account when choosing the materials, these are both technical and economical. For instance, the final choice is based on elements such as: the coercivity value, the iron losses quantity, the magnetic saturation, the material permeability, or the noise. In addition, from politico-economical perspective, the prices, as well as the market availability are considered. Therefore, the chosen material should perfectly balance all these parameters, taking into account the requirements of the application too.

Refocusing to conventional materials, the following materials are the most used nowadays.

Cold-rolled motor lamination steels (CRML steels) are steels combined with carbon in a very small proportion (about 0.06%). Regarding the advantages of these materials, they provide good permeability, as well as good performances regarding the saturation flux density. Moreover, the manufacturing costs are lower compared to other alloys. Usually, they are delivered without the final annealing and they should be annealed in batches after lamination. Sometimes, after annealing they are insulated with oxide coating. Among the drawbacks, the most relevant is the low performance in terms of core losses [22].

Another material from this category and the one which is one of the most used in electric machines industry is silicon-iron (SiFe) alloy. Silicon-iron alloy is available both in grain-oriented and non-oriented states. The grain-oriented state means that the material has anisotropic properties, while in non-oriented state the material is practically isotropic [23].

The grain-oriented state SiFe is used in electrical transformers, as well as in some rotating electric machines (mostly in research studies), while the majority of rotating electric machines on the market use non-oriented state SiFe, especially for the uniformity of the magnetic properties provided [24].

In non-oriented state, the alloy is combined with aluminium (Al) and manganese (Mn) in proportion of about 1% and 0.5% respectively, while the silicon content is up to 3%.

The advantages the silicon and aluminium offer are related to the increase of electrical and mechanical resistivity, while the disadvantages brought are the decrease of the permeability and, at the same time, of the saturation magnetization. The permeability problem can be solved by increasing the manganese content, but this will lead to higher iron losses.

On the market, the SiFi is available both in semi-processed state and fully-processed state. The semi-processed state means that the material did not receive the final annealing and it have be to annealed after stamping, while the fully-processed SiFe is fully annealed and it can receive as secondary annealing, but it is not mandatory.

Willing to improve as much as possible the SiFe alloy properties, researchers developed new variants. For example, non-oriented SiFe with high content of Silicon (up to 6.5%) provides higher electrical resistivity, but unfortunately the higher amount of silicon makes the material harder and thus, it is much more difficult to work with it. Therefore, increasing the amount of silicon will increase the final production cost too.

Another relevant material in this category is cobalt-iron (CoFe) alloy. This is one of the most expensive alloys in the industry, due to the high quantity of cobalt (between 15% and 49%). Typically, CoFe alloy is combined with 2% vanadium. Due to its high price, it is used in those electric machines that have a critical ration between performances and weight. In order to reduce the overall cost, smaller amounts of cobalt may be used (between 15% and 30). Of course, performances suffer in this case, but it is an assumed compromise [25].

Last, but not least, is the nickel-iron alloy (NiFe). In this alloy, the amount of nickel is about 40-50%. A higher content of nickel will increase the relative permeability of the material on the one hand but will also increase the eddy current losses by increasing the electric

conductivity, on the other hand. The main advantages of this material are its high relative permeability and the low amount of iron losses, while the most important disadvantages are the small flux density and the low saturation. Another important aspect is that in order to obtain the best magnetic performances, the alloy must be annealed at temperatures above 1100˚C and then covered with a surface oxide layer [26].

Regarding the non-conventional materials, the focus is on amorphous alloys, mostly due to their very low losses in terms of iron. The iron losses amount is that low mainly due to the thin structure of the material. In addition, the manufacturing cost is also an important advantage. Amorphous alloys are typically made of iron, boron and silicon and are typically used in transformers and electronic equipment [27].

Another material in this category is the nano-crystalline alloy which basically is a better variant of amorphous alloy, having a microstructure with grains smaller than 50nm. Compared to amorphous alloys, nano-crystalline alloys have better soft magnetic material characteristics [28].

Soft magnetic composite (SMC) is another interesting non-conventional material used in electric machine industry. The non-conventionality of this material is due to the fact that using it, the part of the machine will no longer consist in laminated sheets, but in a single part core. Basically, this material consists in a powder made of very small iron particles that are isolated from each other. The main advantage of this material is that it can be used in order to obtain special geometries. Moreover, it is suitable for very high frequencies applications, having a very high electromagnetic resistivity. However, among the drawbacks, there are the low mechanical strength compared to other materials and the low permeability [29].

3.4.2 Pre-sizing of the IPMSM

The pre-sizing of an electrical machine has as ultimate scope the determination of the main dimensions of the machine, i.e. outer stator diameter, axial length, inner stator diameter, and outer rotor diameter.

The inner stator diameter size can be estimated depending on the required rated apparent power, the machine's constant (C), the aspect coefficient (λ), and the rated rotational speed.

The aspect coefficient (λ) generally depends on the number of poles, while the machine's constant (C), can be estimated according to the equation 3.15. In this calculation, both the total electric load (A) and the magnetic flux density in the air gap ($B_{\delta 1}$) are chosen from the specialized literature, based on the required rated power and polar pitch (N_1).

$$C = \frac{\pi^3}{2\sqrt{2}} \cdot k_{\Phi} \cdot k_w \cdot \alpha_p \cdot B_{\delta 1} \cdot A \tag{3.15}$$

where:

- k_{Φ} is the magnetic field shape coefficient;

$$k_{\Phi} = \frac{\pi^2}{8} \cdot \frac{\alpha_p}{\sin(\frac{\pi}{2} \cdot \alpha_p)} \tag{3.16}$$

- k_w is the winding factor, initially considered as a unit value;
- α_p is the polar coverage factor.

It is important to mention that during the machine's sizing process, some of the estimated parameters at the beginning for approximating a suitable constant, will be recalculated.

Generally, equation 3.17 describes an optimal inner stator diameter, which is very important in estimating the necessary length of the machine, considering that this element is mandatory in order to obtain the required permanent magnets volume for the given application.

$$D_{is} = \sqrt[3]{\frac{S_n \cdot 60}{C \cdot \lambda \cdot n_s}} \quad (3.17)$$

Usually, when sizing a permanent magnet synchronous motor, the length of the stator, rotor and permanent magnets is considered equal to the machine's length (L_i).

$$L_i = D_{is} \cdot \lambda = l_s = l_r = l_{PM} \quad (3.18)$$

The air gap length is also approximated based on the inner stator diameter, as can be seen in equation 3.19.

$$\delta_i = 0.5 \cdot 10^{-3} + \frac{D_{is}}{400} \quad (3.19)$$

Regarding the outer rotor diameter, it can be calculated using the following equation:

$$D_{er} = D_{is} - 2 \cdot \delta_i \quad (3.20)$$

The outer stator diameter can be estimated according to the k_d coefficient, which depends on the number of the machine's pole pairs, as can be seen in the following equation:

$$D_{es} = \frac{D_{er}}{k_d} \quad (3.21)$$

The shaft diameter (D_{sh}) is approximated to an average value, as follows:

$$0.2 < \frac{D_{sh}}{D_{er}} < 0.25 \quad (3.22)$$

The stator pole pitch can be calculated using:

$$\tau = \frac{\pi \cdot D_{is}}{2 \cdot p} \quad (3.23)$$

3.4.3 Permanent magnet volume computation

The total volume of permanent magnets required to produce the magnetic flux for the given application can be estimated with the following equation [30]:

$$V_{PM} = \frac{P_\delta \cdot 0.45 \cdot k_{ad} \cdot \sin\beta \cdot k_m \cdot \sigma_0}{\sqrt{2} \cdot \pi \cdot f_1 \cdot \cos\beta \cdot \zeta \cdot H_c \cdot B_r} \quad (3.24)$$

where:

- P_δ is the electromagnetic power, which is the ratio between the output power (P_2) and the efficiency of the machine (η), from which iron losses (p_{Fe}) and copper losses (p_{el}) are subtracted;

$$P_\delta = \frac{P_2}{\eta} - (p_{Fe} + p_{el}) \quad (3.25)$$

- k_{ad} is the shape coefficient of the magnetic field on d-axis;
- β is the current angle;
- k_m is the maximum armature current per unit;
- σ_0 is the flux leakage factor;
- f_1 is the input frequency;
- ζ is the permanent magnets utilization coefficient;
- B_r is the residual flux density;
- H_c is the coercive field of the magnets.

The values of current angle (β), the maximum armature current per unit (k_m), the flux leakage factor (σ_0), as well as the shape coefficient of the magnetic field on d-axis (k_{ad}), can be chosen as recommended in [31], [32], [33], as they are unknown at this stage of the procedure.

3.4.4 Number of poles - number of stator slots combination

An important aspect to take into account when designing an AC machine, and especially an IPMSM, is the slots-poles combination. This choice has a major impact on the output performances of the machine, especially regarding the torque ripples, magnetomotive force, noise and vibrations.

A smooth torque is required in many applications in order to prevent vibrations and noises. For this reason, many researchers in this field tried to find out how to diminish the torque ripples and the radial forces, which influence the electromagnetic torque, in electrical machines, to obtain more reliable and efficient products [34].

The torque ripples are mainly due to the cogging torque that appears, in absence of any current, because of the interaction between the stator teeth and the permanent magnets from the rotor. Therefore, the slots-poles combination directly influences this parameter. More explicitly, the higher the least common multiple (LCM) between the number of poles and the number of slots, the lower the cogging torque is. For example, from this point of view, it can be said that the 10 poles and 24 slots combination, whose LCM=120, is more feasible than the 8/12 (LCM=24) combination or 10/18 combination (LCM=90).

Moreover, the greatest common divider (GCD) between the poles number and slots number has a serious influence in the radial forces distribution. The higher the GCD is, the more balanced the machine is in terms of radial forces. Otherwise, if the GCD has a low value, the radial symmetry of the machine will also be poor. This can be translated into noises and vibrations during operation. Therefore, it is desirable for the GCD to have an even value, as high as possible to avoid the appearance of radial forces. For example, the 10/24 configuration, whose GCD=2 is more efficient than 4/15 configuration (GCD=1), but less efficient than 4/36 (GCD=4) or 8/48 (GCD=8) configurations from this point of view.

Another problem is the appearance of harmonics. As a result of harmonic waves, which are distortions of the fundamental wave, losses occur in the machine.

For instance, the magnetomotive force (MMF) harmonics cause iron losses, while the electromotive force (EMF) harmonics cause the main winding losses. In this regard, the optimal topology should be identified to reduce, as much as possible, the harmonic distortion. Therefore, the first harmonic should be as high as possible, while the

other ones must be as low as possible. In this way, the losses in the machine are reduced [35].

From the poles-slots combination point of view, knowing that their LCM is closely related to the 1st harmonic of the cogging torque, as previously explained, the order of the harmonics of the MMF distribution with which it may interact must be analysed. For example, a 12/4 topology, with LCM=12, has 12 slots, 4 magnetic poles and 2 pole pairs. In order to determine the MMF distribution harmonics that can generate the highest torque ripples, there is an algorithm that can be applied. For the mechanical frame, the number of pole pairs is added, respectively subtracted, to the LCM value, while for electrical frame, the mechanical frame harmonics previously obtained are divided by the number of pole pairs [36]. Therefore, for the given example (12/4 topology), 10th and 14th harmonics in the mechanical frame, and 5th and 7th harmonics in the electrical frame respectively should be reduced in order to minimize the torque ripple.

Table 3. 4 Different poles-slots topologies

Poles / Slots	4	8	10	12	14	18	20
	LCM | GCD q						
12	12 | 4 1	24 | 4 0.5	60 | 2 0.4		84 | 2 0.286		60 | 4 0.2
15	60 | 1 1.25	120 | 1 0.625	30 | 5 0.5		210 | 1 0.357		60 | 5 0.25
18	36 | 2 1.5	72 | 2 0.75	90 | 2 0.6	36 | 6 0.5	126 | 2 0.429		180 | 2 0.3
24	24 | 4 2	24 | 8 1	120 | 2 0.8		168 | 2 0.571		120 | 4 0.4
27	108 | 1 2.25	216 | 1 1.125	270 | 1 0.9	108 | 3 0.75	378 | 1 0.643	54 | 9 0.5	540 | 1 0.45
30	60 | 2 2.5	120 | 2 1.25	30 | 5 1		210 | 2 0.714		60 | 10 0.5
36	36 | 4 3	72 | 4 1.5	180 | 2 1.2	36 | 12 1	252 | 2 0.857		180 | 4 0.6
48	48 | 4 4	48 | 8 2	240 | 2 1.6		336 | 2 1.143		240 | 4 0.8
60	60 | 4 5	120 | 4 2.5	60 | 5 2		420 | 2 1.429		60 | 20 1

where: LCM – the least common multiple;
GCD – the greatest common divider;
q – number of slots per pole per phase.

3.4.5. Winding configuration

Another important parameter in electrical machines design in general, and in IPSM in particular is the winding configuration. To analyse the influence of this parameter, four winding configurations were considered. As Fig.3.5 shows, the winding arrangement has a major impact both on the electromagnetic torque value and torque ripples. Two winding configurations with 2 layers (a and b), respectively 2 winding configurations with one layer (c and d), were analysed.

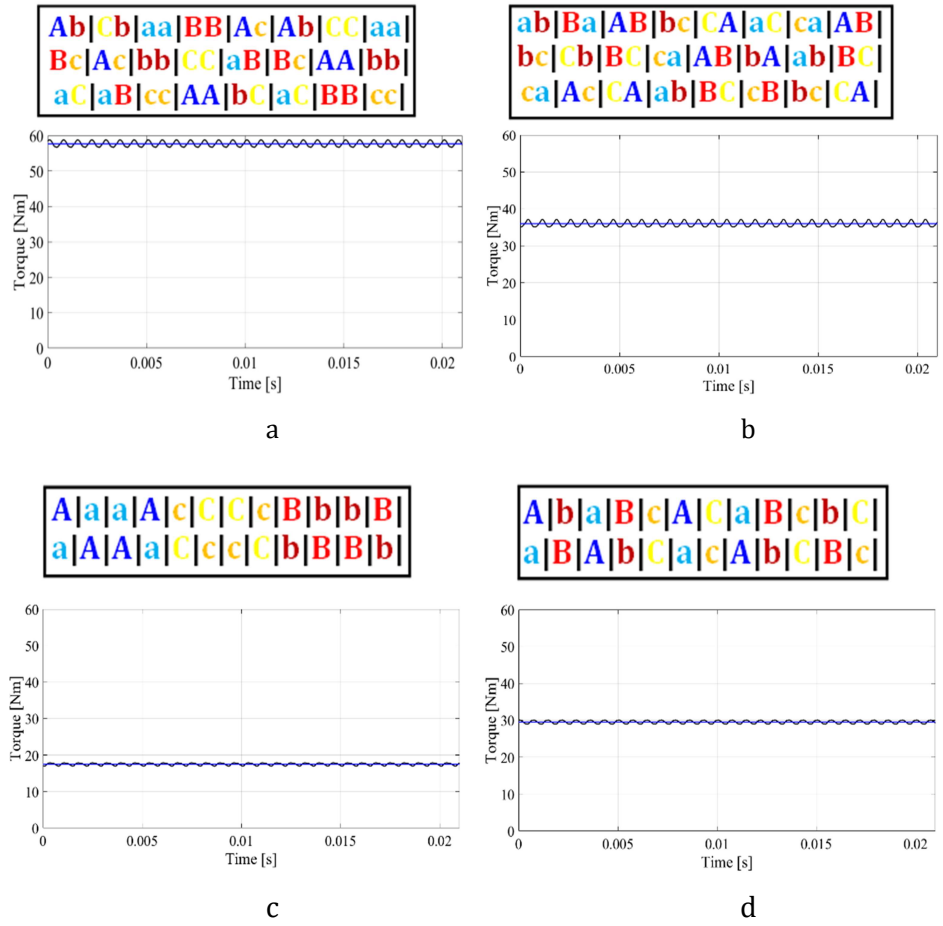

Fig.3. 5 Winding configuration influence on electromagnetic torque

As it can be noticed, option (a) provides an average torque of approximately 60Nm, while the torque ripples are relatively reduced. On the other hand, in the case of option (b), where another two layers configuration was chosen, the average value of the torque is about 36Nm. Regarding the (c) and (d) arrangement options, the torque ripples are relatively similar, but its average value is much lower than in the first case.

Table 3.5 depicts the percentage of torque ripples for each of the four cases exposed. As it can be noticed, the lowest value of torque ripple was obtained in the first case, while at the opposite pole is the second case.

In addition, researchers have demonstrated that the winding arrangement also influences the back-EMF [37]. In this regard, Fig. 3.6 presents the variation of back-EMF for all four models, previously mentioned, while Fig 3.7 shows the voltage harmonics.

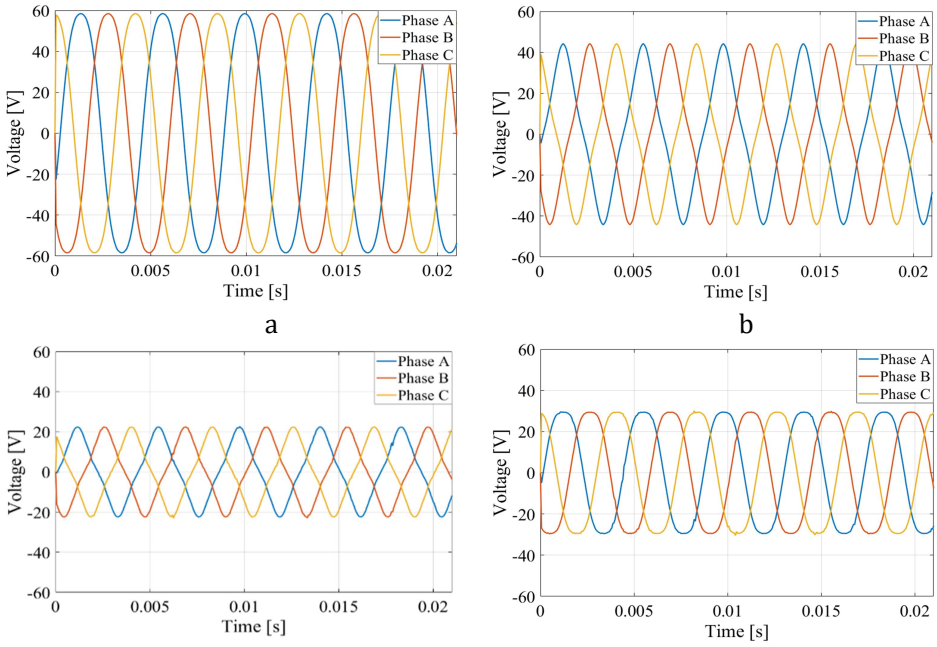

Fig.3. 6 Back-EMF for different winding distributions

Regarding the back-EMF harmonics, in all four cases, odd-order harmonics can be observed, with the third order harmonic having the largest influence. The harmonics were obtained by applying the Fourier analysis on the Back-EMF values. By comparison, the influence of harmonics is the least in the first case.

Table 3. 5 Impact of the winding distribution on the electromagnetic torque

Model	**T_{max} [Nm]**	**T_{min} [Nm]**	**T_{avg} [Nm]**	**Torque ripple [%]**
a	58.76	56.67	57.66	3.63
b	37.20	35.14	36.00	5.72
c	17.92	16.94	17.49	5.62
d	30.09	28.98	29.54	3.74

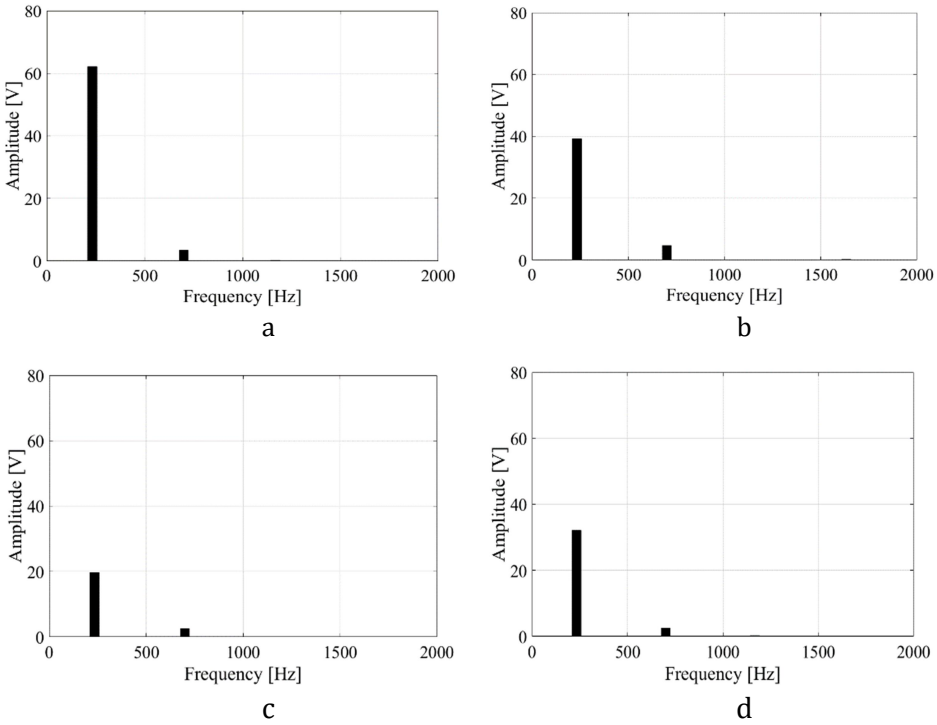

Fig.3. 7 Back-EMF harmonics

As expected, winding distribution also impacts the variation of circuit voltage during rated load operation, and implicitly, its harmonics. To carry out this study, a three-phase power supply was used, and the simulations were performed at a current of 180A. The obtained results are shown in Fig.3.8 and Fig.3.9, respectively.

In this case too, the observations made for no-load operation scenario are valid. Therefore, regarding the first model, it can be noticed that the sinusoidal shape of the voltage variation is maintained, while its amplitude reaches approximately 80V. On the other hand, case (b) shows distortions of the waveform and a considerable decrease in amplitude, while in cases (c) and (d) the sinusoidal shape is relatively conserved, but the amplitude is strongly affected, compared to case (a). Moreover, similar to no-load analysis, the voltage harmonics are from odd order, the third one having the biggest influence. In this case as well, the second model has the highest harmonics, but this was to be expected, considering the voltage distortion.

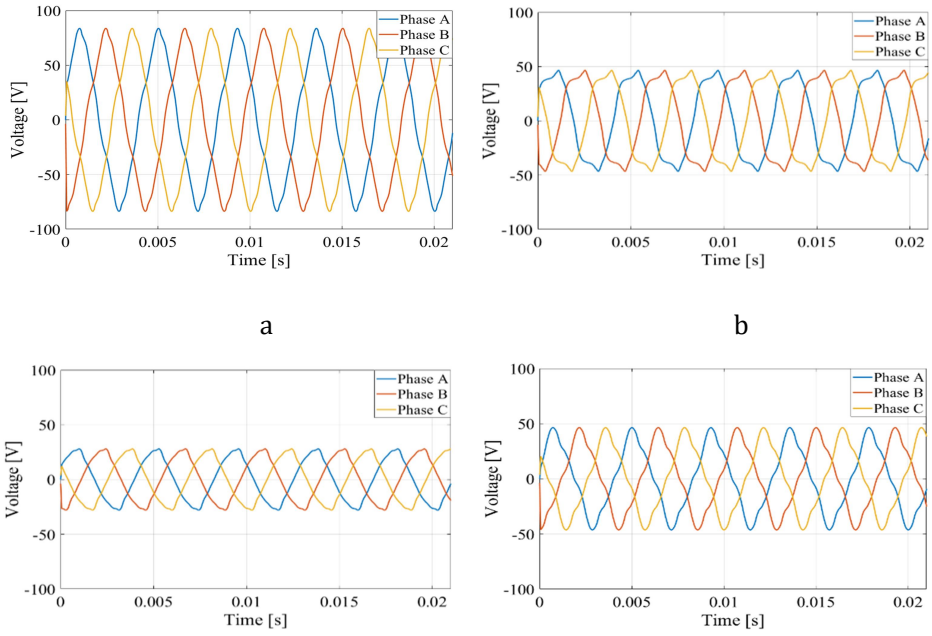

Fig.3. 8 Variation of circuit voltage at rated operation

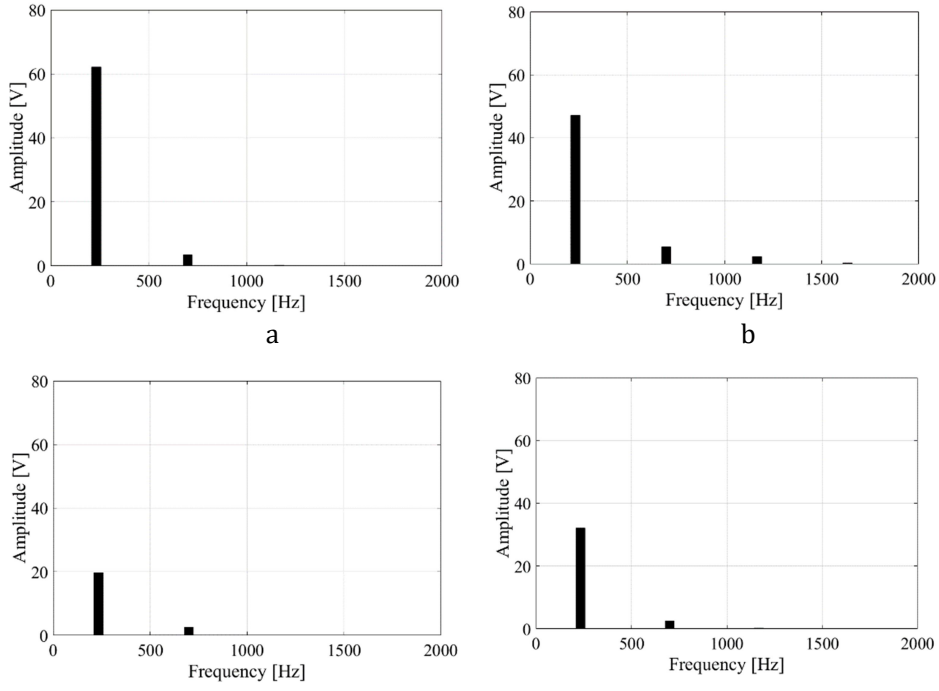

Fig.3. 9 Voltage harmonics at rated operation

3.5. Electrical machine analysis

Although the generation of the electromagnetic field is the basis of the operation of electric machines, an analysis that only includes the understanding of the electromagnetic behaviour of the machine is not enough. A complete analysis must be seen as a multi-physical analysis, containing, in addition to the electromagnetic analysis, a thermal analysis and a mechanical one.

The purpose of the thermal analysis is, on one hand, to determine the parameters necessary for sizing the cooling system, if such system is required, and to provide the information about the heat distribution inside the machine, as well as about the critical point from this point of view. Regarding the mechanical analysis, its importance is to highlight the possible structural problems that may occur during operation, but also to analyse the noise and vibrations.

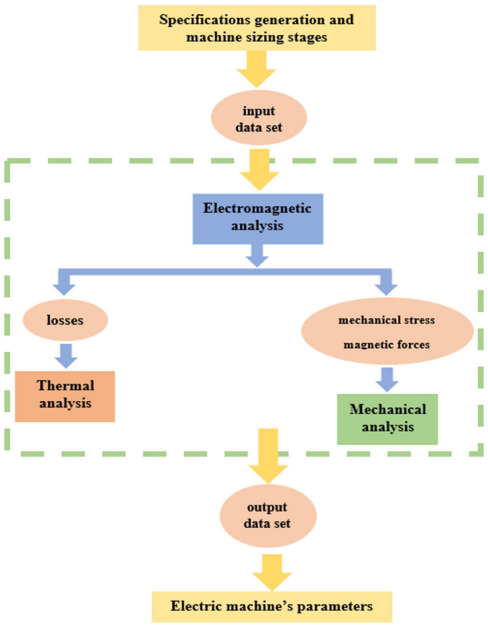

Fig.3. 10 Electrical machine analysis process

3.5.1. Electromagnetic analysis

Although possible, an electromagnetic analysis carried out by analytical methods is difficult to achieve, because it requires the use of advanced mathematics, not very accurate and quite time-consuming. However, if desired, one of the most used methods in this case is the equivalent magnetic circuit analysis [38].

On the other hand, the use of dedicated software packages that have implemented finite element analysis (FEA) as computation method can considerably ease the work of the designer, as well as reduce the time required for the entire analysis and increase its accuracy.

Therefore, over the years various software packages suitable for this kind of analysis have been developed. Among them there are: JMAG Designer, ANSYS Maxwell, Flux 2D/3D, etc.

In order to compute a simulation in one of the previously mentioned software packages, first of all, the machine's model must be either imported from a CAD file, or directly created in the software's interface. Then, the analysis type (static or transient) should be established. The next step is to choose the materials for each component of the machine, to define the winding configuration as well as the electrical circuit and its properties, and to implement all the conditions and limitations decided in the sizing stage of the machine. Then, the mesh can be generated either automatically or manually. After all of these parameters are well defined, the analysis can be run. Regarding the obtained results, they are easy to be processed and analyzed. Fig. 3.11 shows the steps that have to be completed before running an electromagnetic analysis, in a specialized software package.

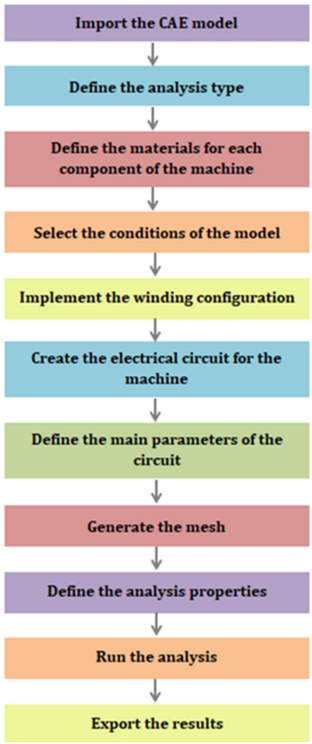

Fig.3. 11 Electromagnetic analysis flowchart

3.5.2. Thermal analysis

The electrical machines thermal analysis can be performed both by analytical and numerical methods. One of the most used analytical methods is the lumped parameter thermal network, also known as LPTN [39]. Using the finite difference method, it estimates the thermal performances of the electrical machine under test. However, a thermal analysis performed just by LPTN method is insufficient to accurately anticipate the temperature distribution in the electric machine. In this regard, various numerical methods were developed. Among them, there are finite element analysis (FEA) and computational fluid dynamics (CFD). The main benefit of using FEA for thermal modelling is its ability to predict conductive heat transfer accurately. This is especially true when electromagnetic FEA models are combined, which allows for an accurate loss determination and the creation of thermal solutions for solid regions with high temperature gradients, like windings. Convective boundaries, however, require an adaptation of convective heat transfer correlations. On the other hand, when the thermal analysis of the machine from the point of view of velocity distribution, flow rate, or pressure decreasing along the cooling system is desired, CFD method is the most appropriate. Moreover, by combining convection and conduction heat transfer, conjugate heat transfer simulations can be performed in order to predict the distribution of temperature and the heat transfer rate at convective boundaries [40], [41].

In addition, researchers in this field demonstrated that the analytical and numerical methods can be combined in order to obtain more accurate results. Therefore, on high complexity models, CFD and LPTN methods were combined and the results were much more accurate than in the case of using a single method.

The thermal analysis is very important, since exceeding critical temperatures can produce irreversible defects for the machine. In order to increase the life of the electromagnetic device, the thermal analysis must provide information about the time, duration, and areas where dangerous temperatures occur in the machine. Therefore, it can be said

that a thermal analysis provides a clear and accurate image of the heat distribution in the machine, during its operation.

Moreover, the thermal analysis is useful for cooling system sizing, if necessary, considering that a correct interpretation of the obtained results can provide the necessary data set for the cooling system dimensioning.

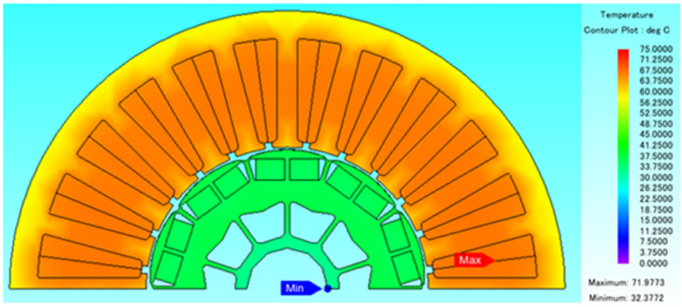

Fig.3. 12 Thermal analysis performed in JMAG Designer

3.5.3. Mechanical analysis

Considering the electric machine itself as a very complex device, the mechanical analysis is required in order to obtain a complete image of the machine's behaviour. It can be broadly divided into two closely related categories, as follows: the structural analysis and the vibroacoustic analysis. Carrying out such an analysis is very important considering that, during the operation of the machine, certain forces are developed, usually with a negative impact on the stability, performances, and life span of both the machine and the system in which the machine operates.

The noise and vibration analysis can be also performed using either analytical or numerical methods. The analytical approach can offer a quicker, more computationally effective solution. However, the numerical approach is considered more accurate because the structural details of the model can be taken into account when the simulation is run [42].

Therefore, a well done mechanical analysis can provide information about the influence, intensity, and critical points regarding the magnetic forces that may occur during the machine's operation, as well about the deformations of the stator core that appear when the radial magnetic force's frequencies are quite close to the stator core's natural frequencies.

3.6. Electrical machines optimization process

The optimization process of electric machines has become, at least in recent years, interesting for the developers of new electric machines, primarily due to the fierce competition on the market, but also to the increase in the price of electricity or the pressure regarding the conservation of these devices. The goals of the optimization process are the reduction of the machine's cost, as well as increasing its performances [43].

Sometimes, the specifications of the electric machine that should be designed, such as maximizing the torque or power density while minimizing the losses or the machine's weight, are contradictory. Due to a large number of parameters that influence the machine's performances, finding an optimal solution from the first attempt can be difficult or even impossible. For this reason, it is necessary to establish a systematic approach based on an iterative process so that the optimal solution can be obtained gradually [44].

Generally, the optimization process can be implemented at the machine-level or at the entire drive-system in which it works, as shown in Fig. 3.13.

Speaking about the optimization process, there are three approaches that should be considered, as follows: robust, deterministic and reliability. However, in electrical machines industry robust models are preferred.

There are two categories of optimization algorithms: classic and modern intelligent algorithms. Among the most popular optimization algorithms used in this industry, there are: conjugate gradient, estimation of distribution (EDA), particle swarm optimization (PSO),

ant colony, immune algorithm, evolutionary algorithms, muti-objective genetic algorithms (MOGA), non-dominated sorting genetic algorithm (NSGA), etc [45]

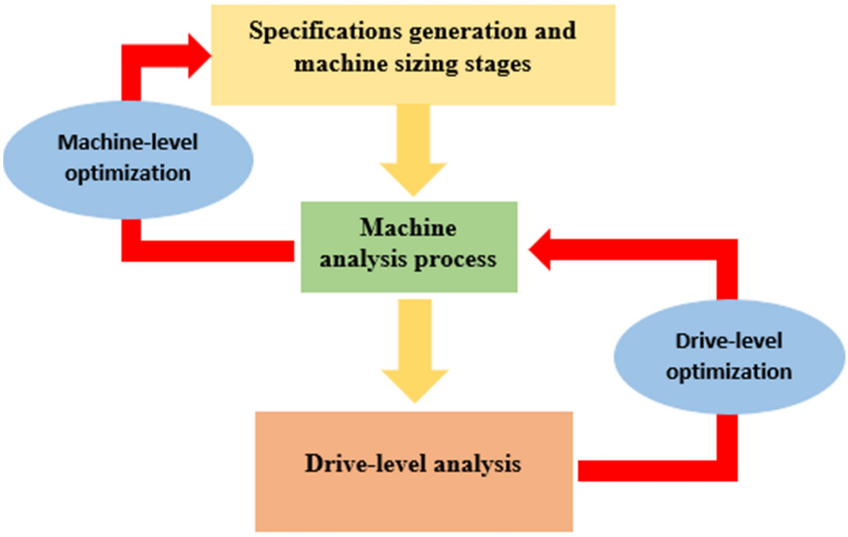

Fig.3. 13 Optimization process of an electric machine

3.7. PMSM Dynamic model

In order to describe the dynamic behavior of a PMSM, the mathematical model should be developed. For a better understanding of it, its starts from the main laws of physics regarding the equilibrium of electrical systems.

To represent the voltages of the three phase windings of a PMSM, the equations can be expressed, as follows:

$$\begin{aligned} u_A &= R_s i_A + \frac{d}{dt}\Psi_A \\ u_B &= R_s i_B + \frac{d}{dt}\Psi_B \\ u_C &= R_s i_C + \frac{d}{dt}\Psi_C \end{aligned} \tag{3.26}$$

where R_s is the stator resistance, while Ψ_A, Ψ_B, Ψ_C are the total flux linkages in each phase. Their values can be determined using the following expression:

The relation between electro-mechanical characteristics indicated by the equation of equilibrium regarding the torque (3.27) completes the mathematical model of the PMSM.

$$J\frac{d\Omega_r}{dt} = T_e - T_L \tag{3.27}$$

where:

- J is the moment of load inertia;
- Ω_r is the mechanical rotor speed;
- T_e is the electromagnetic torque;
- T_L is the load torque.

$$T_e = \frac{P_{output}}{\Omega_r} \tag{3.28}$$

where P_{output} is the output power of the machine and Ω_r can be defined as the ratio between the electrical rotor speed (ω_r) and the number of pole pairs (p). Therefore, (3.28) can be written as:

$$T_e = \frac{p \cdot P_{output}}{\omega_r} \tag{3.29}$$

Regarding the load torque, it can be defined as follows:

$$T_L = B\Omega_r + T_{LE} = B\frac{\omega_r}{p} + T_{LE} \tag{3.30}$$

where:

- B is the viscous coefficient of the load;
- T_{LE} is the extra load torque input.

It is important to mention that these values are all derived from the law of energy conservation.

The three-phase model of an AC machine is usually transformed in a two-phase model based on:

$$\begin{bmatrix} d \\ q \\ 0 \end{bmatrix} = \begin{bmatrix} \sin\theta & \sin(\theta - \frac{2\pi}{3}) & \sin(\theta + \frac{2\pi}{3}) \\ \cos\theta & \cos(\theta - \frac{2\pi}{3}) & \cos(\theta + \frac{2\pi}{3}) \\ \frac{1}{2} & \frac{1}{2} & \frac{1}{2} \end{bmatrix} \begin{bmatrix} A \\ B \\ C \end{bmatrix} \tag{3.31}$$

where:

- θ is the angle between the A and d-axis (for the d-axis alignment), and θ=ωt;
- ω is the rotational speed of the d-q reference;
- d, q are the components of the two-axis system in the rotating reference frame;
- 0 is the zero component of the two-axis system in the stationary reference frame;
- A, B, C are the components of the three-phase system in the abc reference frame.

Park's transformation is usually implemented in two steps. The three-phase system is converted into an orthogonal fixed two-phase (α-β) system. The general form of the transformation equation is presented in (3.32). The d-q system is then obtained by rotating the resultant system by θ degrees [46]. Fig. 3.14. illustrates the transformation flow.

$$\begin{bmatrix} \alpha \\ \beta \end{bmatrix} = \frac{2}{3} \begin{bmatrix} 1 & -\frac{1}{2} & -\frac{1}{2} \\ 0 & -\frac{\sqrt{3}}{2} & -\frac{\sqrt{3}}{2} \end{bmatrix} \begin{bmatrix} A \\ B \\ C \end{bmatrix} \tag{3.32}$$

$$\begin{bmatrix} d \\ q \end{bmatrix} = \begin{bmatrix} \cos\theta & \sin\theta \\ -\sin\theta & \cos\theta \end{bmatrix} \begin{bmatrix} \alpha \\ \beta \end{bmatrix} \tag{3.33}$$

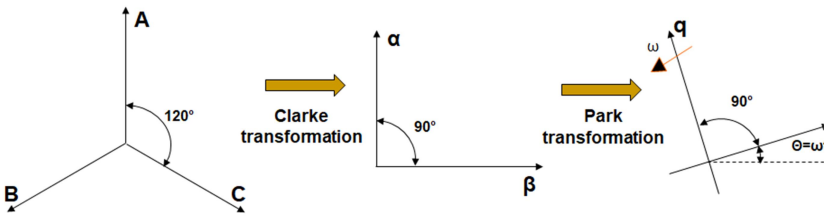

Fig.3. 14 Three-phase rotating system to d-q system transformation flow

The advantage of using the orthogonal system over the three-phase one is that the mathematical model is greatly simplified, which brings a gain both in terms of the model implementation time and the computation time [47].

The d-q machine model results as:

$$u_{sd} = R_s i_{sd} + \frac{d\Psi_{sd}}{dt} - \omega\Psi_{sq} \tag{3.34}$$

$$u_{sq} = R_s i_{sq} + \frac{d\Psi_{sq}}{dt} + \omega\Psi_{sd} \tag{3.35}$$

$$J\frac{d\Omega_r}{dt} = T_e - B\omega_e - T_L \tag{3.36}$$

The electromagnetic torque of an IPMSM is highlighted in (3.37).

$$T_e = \frac{3}{2}p(\Psi_d i_q - \Psi_q i_d) \tag{3.37}$$

For a PMSM Ψ_d and Ψ_q are the direct and quadrature flux linkages defined by:

$$\Psi_d = L_d i_d + \Psi_{PM} \tag{3.38}$$

$$\Psi_q = L_q i_q \tag{3.39}$$

where L_d and L_q are the direct and quadrature inductances.

Therefore, taking into account (3.38) and (3.39), equation (3.37) can be written as:

$$T_e = \frac{3}{2} p[\Psi_{PM} i_q + (L_d - L_q) i_d i_q] \quad (3.40)$$

It is important to mention that the electromagnetic torque consists of two components: (i) synchronous torque generated by the interaction between the quadrature current and the permanent magnet flux; and (ii) reluctant torque, produced due to the rotor core's anisotropy. Although for surface PMSMs the reluctance component of the electromagnetic torque can be neglected, in the case of IPMSMs it makes its presence felt, and it can be controlled by adjusting the current on d and q axes.

3.8. Machine's electrical parameters

Different PMSM control strategies heavily depend on electrical parameters, phase resistance and direct and quadrature inductances. Determining the electrical parameters as accurate as possible is required in EV and HEV applications, for instance, in order to identify the optimal current trajectories when maximum torque per voltage or maximum torque per ampere control strategies are implemented [48],[49]. Moreover, accurate parameters determination is critical in order to improve the efficiency of the machine, as well as to ensure the system stability or to improve the dynamic response when direct torque control (DTC), field-oriented control (FOC) or model predictive control (MPC) strategies are used [50],[51],[52].

The techniques for parameters estimation and computation have been developed in the last years and, as a consequence, both offline and online methods can be implemented. On one hand, offline estimation methods have been studied and used on both electrical machine and controller design. On the other hand, the online approach is suitable for real time acquisition of the machine parameters [53].

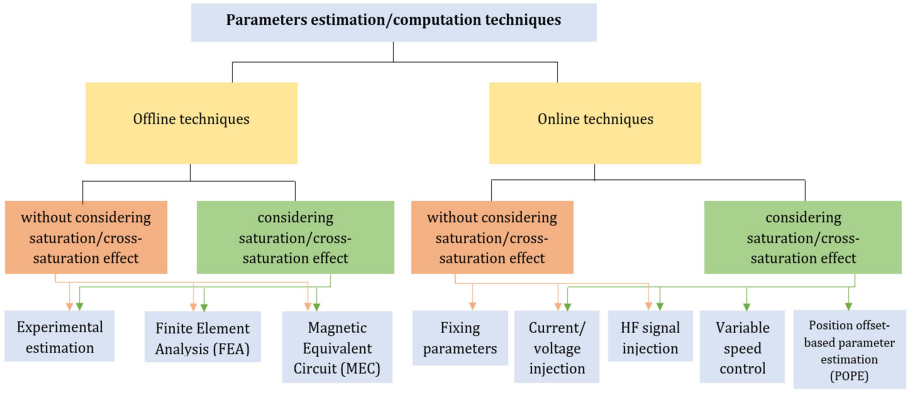

Fig.3. 15 Parameters estimation and computation techniques

Fig. 3.15 highlights the main parameters estimation and computation techniques used these days. Both offline and online methods were considered.

Regarding the offline estimation techniques, FEA is the most used. This method is a very accurate one, but it requires a detailed knowledge of the geometry, dimensions and materials used in the construction of the machine [54]. FEA method can be implemented both taking into account the saturation and cross-saturation effects, as well as neglecting them. Of course, the first variant will provide more accurate results. As for the limitations of the FEA method, they mainly arise from the lack of complete information regarding the characteristics of the materials used [55] and from the high computation time.

Another method used to determine the machine's parameters, especially when the saturation and cross-saturation phenomena are considered, is based on the magnetic equivalent circuit (MEC) of the machine. At the end of 50s, several scientists in the field, including Fiennes, Slemon and Ostrovic, introduced this method [56].

Despite that at the beginning the method was exclusively used for the analysis of the machines in saturated state, it has been proven that it is also effective for the study of steady state and transient

regimes. Shortly, using this method, the machine is no longer characterized as a complicated magnetic circuit, but rather as a resistive electrical network, which greatly simplifies any analysis.

Compared to FEA method, MEC has a lower computation time and a lower accuracy, mainly because in this case there are much fewer elements to be analyzed (between 30 and 100, compare to 10000 in the case of FEA). In this moment, it is not clear if this compromise between the accuracy and computational time is worth it, taking into account that in the last years the computational speed has been considerably improved.

In order to improve the entire process, many experimental methods were developed in the last decades. Among them, there are: DC-step voltage excitation, dq-axis voltage pulse injection, AC signal excitation, Fast Fourier transform analysis or estimation under constant or variable speed techniques [57],[58],[59],[60],[61],[62].

Regarding the online parameter estimation and computation techniques, they use high levels of computational efficiency. Algorithms based on artificial intelligence were developed and applied in the analysis of PMSM [63].

One of the used methods for online parameters estimation is by injecting current or voltage. Based on this idea, various algorithms have been developed, such as recursive least squares (RLS), artificial neutral network (ANN) or evolutionary algorithm (EA) [64],[65]. In addition, by injecting a non-zero current on d-axis and implementing a self-learning, respectively co-evolutionary particle swarm optimization (PSO) algorithm, satisfactory results were obtained regarding the estimation of parameters such as L_d, L_q, Ψ_{PM}, etc., as shown in [66] and [67]. Another efficient tested method is using the position offset-based parameter estimation (POPE) [68].

Last, but not least, is the high frequency (HF) injection technique. It can be used in sensorless control strategies, to estimate the machine's inductances, as well as the permanent magnets temperature or the electromagnetic torque [69][70][71].

Therefore, with the development of PMSMs, many strategies used to determine their parameters, both offline and online, were developed. The use of specialized software packages, complex algorithms, but also artificial intelligence in the development of new techniques for estimating and computation of parameters led to obtaining more accurate models and more efficient control strategies implementations.

3.8.1. Saturation and cross-saturation and their impact on the machine's parameters

Most of the time, the d-q model is based on certain assumptions, one of which is that the materials used in the machine's construction have linear characteristics, meaning that the flux linkage on d and q axis have a linear dependence on the d axis current, and q-axis current, respectively.

Therefore, in the classical d-q model of a PMSM, that neglects the saturation and cross-saturation phenomena, the flux can be defined according to Equations (3.38) and (3.39), where L_d and L_q are constant [72]. In this case the direct and quadrature axes are assumed to be completely decoupled, meaning that q-axis has no influence on d-axis and vice versa. This approach works when the electric machine is operating at constant speed.

In the case of propulsion of an electric vehicle, for example, when the speed varies a lot, the assumption of constant d and q inductances can generate large discrepancies between the real and simulated models. The non-linear behavior of the materials, reflected by the BH curve, will have an important impact on the d and q inductances. The non-linearity due to the saturation phenomenon have to be taken into account. In this case, the d and q axes fluxes have a non-linear behavior versus the d and q axes currents, respectively. The d and q axes fluxes are decoupled, meaning that d-axis flux depends only on d-axis current and q-axis flux depends only on q-axis current. The d- and q-axis inductances will not be constant anymore and they can be computed using:

$$L_d(i_d) = \frac{\Psi_d(i_d)}{i_d}|_{\Psi_{PM}=0} \tag{3.41}$$

$$L_q(i_q) = \frac{\Psi_q(i_q)}{i_q} \tag{3.42}$$

Therefore, the d-axis inductance will only depend on the d-axis current, while the q-axis inductance will only depend on the q-axis current.

However, d and q fluxes share the same magnetic circuit, and consequently the fluxes, and implicitly the inductances on d and q axes simultaneously depend on i_d and i_q (cross-saturation), as [73]:

$$\begin{cases} \Psi_d = f(i_d, i_q)|_{\Psi_{PM}=0} \\ \Psi_q = f(i_d, i_q) \end{cases} \tag{3.43}$$

$$\begin{cases} L_d = f(i_d, i_q)|_{\Psi_{PM}=0} \\ L_q = f(i_d, i_q) \end{cases} \tag{3.44}$$

The idea of saturation is clearly defined in specialized literature, while according to the articles that were published over the time, the concept of cross-saturation was defined in two distinct ways. According to the publications, cross-saturation is a phenomenon that results from saturation. The problem arises when attempting to define these two phenomena from a mathematical point of view. On one hand, some studies define the cross-saturation as a mutual inductance caused by the saturation produced on a magnetic circuit region associated with an axis by the current on the other axis [74][75]. On the other hand, in other articles the cross-saturation phenomenon is defined starting from the hypothesis that axes d and q respectively can saturate each other, therefore, the current on axis d will affect the value of inductance on axis q and vice versa [76][77].

Numerous scientific studies highlight the significance of taking into account the saturation and cross-saturation effects and even provide significant examples. These effects directly affect the outcomes of the electromagnetic and performance analyses, as well as the

identification of the machine's parameters. In addition, these have an important impact on the development of control strategies, especially when advanced control strategies are chosen, such as sensorless control [78],[79],[80].

Regarding the errors that may occur when the saturation and cross-saturation are not taken into account, they mainly refer to the determination of the rotor position. Studies have shown that errors can reach tenths of degrees, depending, of course, on the degree of the machine's loading. In this case, not taking into account these two phenomena, will impact in a negative way the true image of the machine's behavior [81].

In this regard, for a more accurate model, the inductances should be defined in differential form, depending on the flux linkages changes ($\partial\Psi_{d,q}$) due to direct, respectively quadrature currents modifications ($\partial i_{d,q}$) [82].

Based on Equations (3.43) and (3.44), the derivative of d- and q-axis fluxes in (3.34) and (3.35) can be written as:

$$\frac{d\Psi_d(i_d,i_q)}{dt}|_{\Psi_{PM}=0} = \frac{\Psi_d(i_d,i_q)}{i_d}\frac{di_d}{dt} + \frac{\Psi_d(i_d,i_q)}{i_q}\frac{di_q}{dt} \tag{3.45}$$

$$\frac{d\Psi_q(i_d,i_q)}{dt} = \frac{\Psi_q(i_d,i_q)}{i_d}\frac{di_d}{dt} + \frac{\Psi_q(i_d,i_q)}{i_q}\frac{di_q}{dt} \tag{3.46}$$

Fig. 3.16 and Fig. 3.17 show some examples from literature on how saturation impacts the machine's parameters, such as the flux leakages on d-, respectively q-axis, as well as the d- and q-axis inductivities.

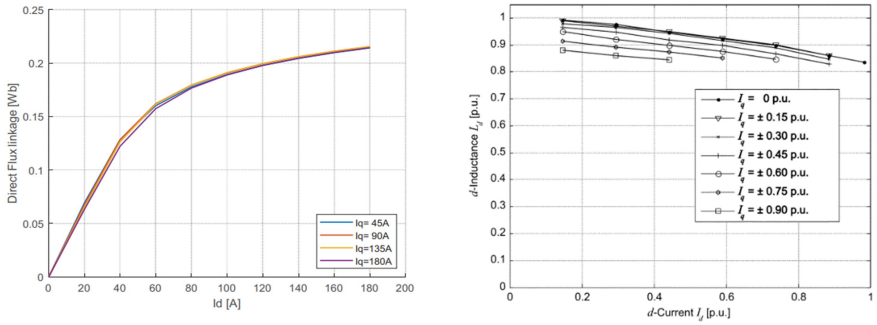

a b

Fig.3. 16 Saturation impact on machine's parameters on d-axis (a) flux leakages [82], (b) inductivities [83]

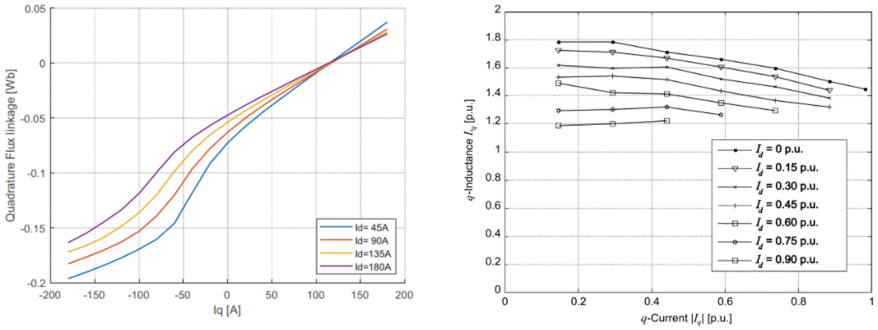

a b

Fig.3. 17 Saturation impact on machine's parameters on q-axis (a) flux leakages [82], (b) inductivities [83]

When the cross-saturation is defined as a mutual inductance caused by the saturation produced on a magnetic circuit region associated with an axis by the current on the other axis (3.45) and (3.46) become:

$$\frac{d\Psi_d(i_d,i_q)}{dt}|_{\Psi_{PM}=0} = L_d\frac{di_d}{dt} + L_{dq}\frac{di_q}{dt} \tag{3.47}$$

$$\frac{d\Psi_q(i_d,i_q)}{dt} = L_q\frac{di_q}{dt} + L_{qd}\frac{di_d}{dt} \tag{3.48}$$

where:

$$L_d = \frac{\Psi_d(i_d, i_q)}{i_d}|_{\substack{\Psi_{PM}=0 \\ i_q=cst}} \; L_{dq} = \frac{\Psi_d(i_d, i_q)}{i_q}|_{\substack{\Psi_{PM}=0 \\ i_d=cst}} \tag{3.49}$$

$$L_q = \frac{\Psi_q(i_d, i_q)}{i_q}|_{\substack{\Psi_{PM}=0 \\ i_d=cst}} \; L_{qd} = \frac{\Psi_q(i_d, i_q)}{i_d}|_{\substack{\Psi_{PM}=0 \\ i_q=cst}} \tag{3.50}$$

When the cross-saturation phenomenon is defined starting from the hypothesis that axes d and q respectively can saturate each other, therefore, the current on axis d will affect the value of inductance on axis q and vice versa, (3.45) and (3.46) become:

$$\frac{d\Psi_d(i_d, i_q)}{dt} = L_d(i_d, i_{q)} \frac{di_d}{dt} \tag{3.51}$$

$$\frac{d\Psi_q(i_d, i_q)}{dt} = L_q(i_d, i_{q)} \frac{di_q}{dt} \tag{3.52}$$

As in the case of the saturation phenomenon, the figures below (Fig. 3.18, Fig. 3.19) present some examples that highlight the impact that the cross-saturation phenomenon has on the machine parameters. As in the previous case, the parameters considered were the flux leakages and the inductivities on the d-, respectively q-axis.

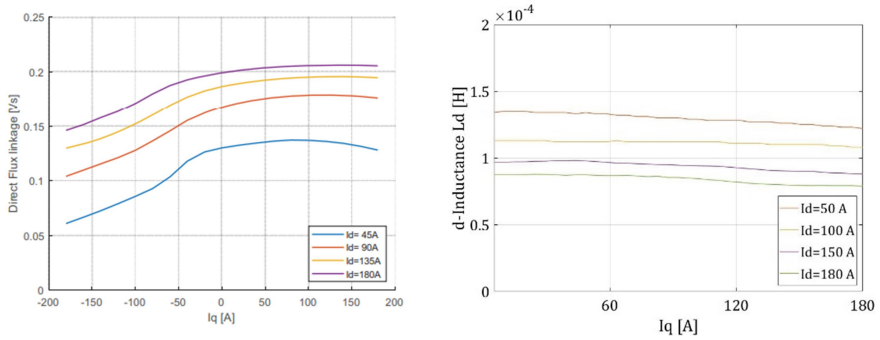

a b

Fig.3. 18 Cross-saturation impact on machine's parameters on d-axis (a) flux leakages [82], (b) inductivities

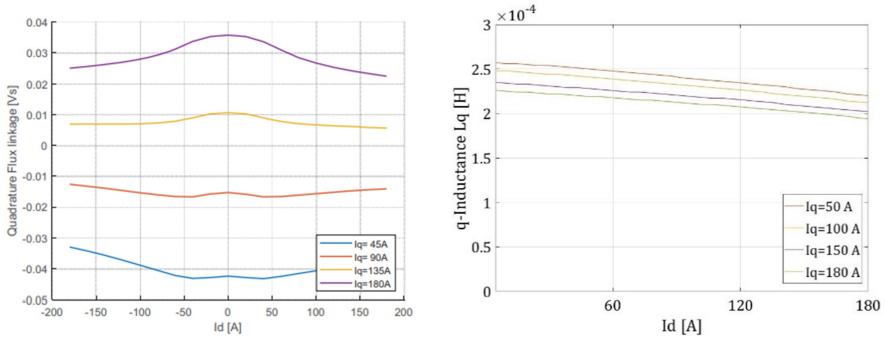

a b

Fig.3. 19 Cross-saturation impact on machine's parameters on q-axis (a) flux leakages [82], (b) inductivities

In order to analyze the impact of saturation and cross-saturation and to compute the inductances, Finite Element Analysis (FEA) can be used. It is very popular technique nowadays, due to the fact that it is a simple and very accurate method. This method is used in order to analyze the machine's behavior from an electromagnetic point of view, at different values of currents on d and q axes respectively, as well as at different rotor positions [84].

The simulation of the machine model implemented in a FE-based software package is done for different rotor positions and different values of i_d and i_q currents. Then, using the frozen permeability technique, and replacing the permanent magnet in the model by air, the simulations are done again for the same rotor positions and i_d and i_q currents. The flux linkages Ψ_d and Ψ_q are extracted. By deriving the flux linkage values with respect i_d and i_q, the inductances are determined as family curves, depending on rotor position and i_d and i_q currents [85]:

$$L_d = \frac{d\Psi_d}{\mathrm{d}i_d}\Big|_{\substack{i_q=constant \\ \Psi_{PM}=0}} \cong \frac{\Delta\Psi_d}{\Delta i_d}\Big|_{\substack{i_q=constant \\ \Psi_{PM}=0}} \tag{3.53}$$

$$L_q = \frac{d\Psi_q}{\mathrm{d}i_q}\Big|_{\substack{i_d=constant \\ \Psi_{PM}=0}} \cong \frac{\Delta\Psi_q}{\Delta q}\Big|_{\substack{i_d=constant \\ \Psi_{PM}=0}} \tag{3.54}$$

$$L_{dq} = \frac{d\Psi_d(i_d, i_q)}{di_q}\Big|_{\substack{i_d=constant \\ \Psi_{PM}=0}} \cong \frac{\Delta\Psi_d(i_d, i_q)}{\Delta i_q}\Big|_{\substack{i_q=constant \\ \Psi_{PM}=0}} \quad (3.55)$$

$$L_{qd} = \frac{d\Psi_q(i_d, i_q)}{di_d}\Big|_{\substack{i_q=constant \\ \Psi_{PM}=0}} \cong \frac{\Delta\Psi_q(i_d, i_q)}{\Delta i_d}\Big|_{\substack{i_q=constant \\ \Psi_{PM}=0}} \quad (3.56)$$

3.8.2. Complexity levels in the development of PMSM models

Based on the complexity of the phenomena taken into account for the estimation/computation of the machine parameters, four levels of complexity can be defined for the electrical machine, as they are presented in Figure 3.20.

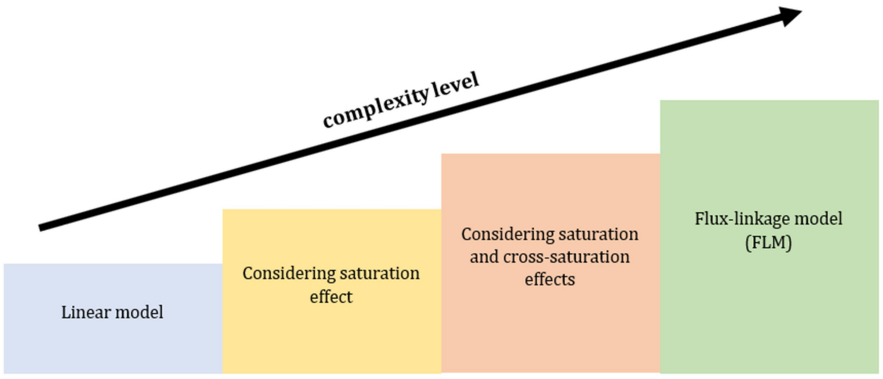

Fig.3. 20 Complexity levels in the development of an electrical machine model using knowledge models

The first complexity level, also known as the linear model, is thus the one corresponding to constant values for L_d and L_q, and it is described by Equations (3.34) to (3.39). This model can be applied, for instance, when the machine's operating point is below the point when the saturation phenomenon becomes relevant, so that, the variation of the machine's inductances is not relevant [86]. The second complexity

level of the machine is described by the Equations (3.34) to (3.37), with direct and quadrature axis inductances defined either as function of the same axis currents, or as a table of the inductances at specific current values, for each axis. This model takes into account only the saturation level, considering the two axis fluxes independent. The third complexity level takes into account both saturation and cross-saturation phenomena, and is described by Equations (3.34) to (3.37), (3.45) and (3.46). When implemented in a software package to perform the simulation, the inductances are estimated at each simulation step using look-up tables based on the rotor position and currents feedback.

The main drawback of the last two models is linked to the errors introduced by the flux derivation process used to compute the inductances. Therefore, in order to eliminate these errors, a fourth complexity level model is defined, based on the computation of the fluxes. The model is described by Equations (3.34) to (3.37) with:

$$\begin{cases} \Psi_d = f(i_d, i_q, \theta) \\ \Psi_q = f(i_d, i_q, \theta) \end{cases} \tag{3.57}$$

The flux-based developed model describes more accurately the real machine, as it includes all the phenomena in the machine (saturation, cross-saturation, leakage, etc.). Thus, (3.34) and (3.35) become:

$$u_d = R_s i_d + \frac{d\Psi_d(i_d, i_q, \theta)}{dt} - \omega \Psi_q(i_d, i_q, \theta) \tag{3.58}$$

$$u_q = R_s i_q + \frac{d\Psi_q(i_d, i_q, \theta)}{dt} + \omega \Psi_d(i_d, i_q, \theta) \tag{3.59}$$

which can be written as:

$$\frac{d\Psi_d(i_d, i_q, \theta)}{dt} = u_d - R_s i_d + \omega \Psi_q(i_d, i_q, \theta) \tag{3.60}$$

$$\frac{d\Psi_q(i_d, i_q, \theta)}{dt} = u_q = R_s i_q - \omega \Psi_d(i_d, i_q, \theta) \tag{3.61}$$

The direct and quadrature axis fluxes are computed using FE-based simulations for a set of values for direct & quadrature axis currents, and rotor positions. The values are saved as 3D look-up tables, which need to be transformed to define the current-flux relation in order to implement the model in a simulation environment.

In order to implement the state equations, the currents-fluxes-rotor position relation should be defined as follows:

$$i_{d,q} = g(\Psi_d, \Psi_q, \theta) \tag{3.62}$$

The new flux-linkages maps can be obtained by interpolating the original flux-linkages maps and cutting them into a predetermined number of contour isolines. Each of these lines codify all possible (i_d, i_q) combinations for a flux-linkage level. In order to determine an intersection between Ψ_d and Ψ_q curves for all stator flux linkage combinations, the intersection algorithm is used.

References

[1] M. Cheng, L. Sun, G. Buja, L. Song, "Advanced electrical machines and machine-based systems for electric and hybrid vehicles," Energies, vol. 8, no. 9, pp. 9541-9564, 2015

[2] F. Pop Piglesan, R. Marţiş, C. Marţiş, C. Faria, F. Chauvicourt, "Electromagnetic and NVH study for low power synchronous reluctance machine," in Proceedings of the 2018 AEIT International Annual Conference, Bari (Italy), 2018.

[3] Soong WL. Sizing of electrical machines. Power Eng Brief Note Ser. 2008;9:17–8.

[4] Marius Rosu, Dingsheng Lin, Ping Zhou, Dan M. Ionel, David Staton, Frede Blaabjerg, Mircea Popescu, Vandana Rallabandi, "Multiphysics Simulation by Design for Electrical Machines, Power Electronics and Drives", IEEE Press series on power engineerin, vol. 66, Wiley, 2018, ISBN: 1119103460, 9781119103462

[5] Bo Ma, "Advanced Design and Optimization Techniques for Electrical Machines", University of Technology Sydney Faculty of Engineering and Information Technology February, 2020

[6] "Selection and gearing of electrical drives," Heinzmann GmbH & Co. KG, Schönau (Germany), 2013.

[7] Vasilis Pagonis, David Guerra, Sean Chauduri, Brian Hornbecker, Nathan Smith: “Effects of air resistance”, Western Maryland College, Physics Department, Westminster, MD 21157

[8] Umut Aktas, Kristian Abdallah, "Aerodynamics Concept Study of Electric Vehicles, Drag Reduction and Range Increase" , Master’s Thesis in Automotive Engineering, Department of Applied Mechanics, CHALMERS UNIVERSITY OF TECHNOLOGY, Gothenburg, Sweden 2017

[9] **Bilatiu, Cristina** & Cosman, Sorin & Martis, Radu-Andrei & Martis, Claudia & Morariu, Silvan. (2019). Identification and Evaluation of Electric and Hybrid Vehicles Propulsion Systems. 1-5. 10.1109/EV.2019.8892965.

[10] Boran Pikula, Elmedin Mesic, Elmedin Mesic, M. Hodzic „Determination of air drag coefficient of vehicle models”, Conference: International Congress Motor Vehicles & Motors 2008 - MVM 2008, „Sustainable Development of Automotive Industry“

[11] W.T. Shugg, "Handbook of Electrical andd Electronic Insulating Materials", Van Nostrande Reinhold Co., New York, 1986

[12] M. Clark, "Insulating Materials for Design and Engineering Practice", John Wiley and Sons, New York, 1962

[13] F. R. Fickett, "Electrical Properties of Materials and Their Measurement at Low Temperatures", Electromagnetic Technology Division, National Engineering Laboratory, National Bureau of Standards, Boulder, Colorado 80303, March 1982

[14] Selema, A.; Ibrahim, M.N.; Sergeant, P. Electrical Machines Winding Technology: Latest Advancements for Transportation

Electrification. Machines 2022, 10, 563. https://doi.org/10.3390/machines10070563

[15] Campbell, Peter. “Permanent Magnet Materials and their Application.”, Cambridge University Press, 1994.

[16] Jimenez-Villacorta, F. & Lewis, Laura, “Advanced Permanent Magnetic Materials”, 2014

[17] A. E. Fitzgerald, C. Kingslay, and S. Umans, Electric Machinery. New Delhi: Tata McGraw Hill, 2002.

[18] Ketheeswaren, Sivapackiyanathan. (2005). Magnetic properties of Materials: A Study.

[19] I. Petrov, D. Egorov, J. Link, R. Stern, S. Ruoho and J. Pyrhönen, "Hysteresis Losses in Different Types of Permanent Magnets Used in PMSMs," in IEEE Transactions on Industrial Electronics, vol. 64, no. 3, pp. 2502-2510, March 2017, doi: 10.1109/TIE.2016.2548440.

[20] Sara Hamidizadeh, "Study of Magnetic Properties and Demagnetization Models of Permanent Magnets for Electric Vehicles Application", Department of Mining and Materials Engineering, Faculty of Engineering, McGill University, Montréal, Québec, Canada, April 2016

[21] A. Krings, A. Boglietti, A. Cavagnino and S. Sprague, "Soft Magnetic Material Status and Trends in Electric Machines," in IEEE Transactions on Industrial Electronics, vol. 64, no. 3, pp. 2405-2414, March 2017, doi: 10.1109/TIE.2016.2613844.

[22] “ASTM A726-05: Standard Specification for Cold-Rolled Magnetic Lamination Quality Steel, Semiprocessed Types,” ASTM International, West Conshohocken, Pennsylvania, USA, 2010.

[23] K. Chwastek, “Anisotropic properties of non-oriented steel sheets,” IET Electric Power Applications, vol. 7, no. 7, pp. 575–579, Aug. 2013.

[24] R. Cardoso, L. Brandao, and M. Cunha, “Influence of grain size and additions of Al and Mn on the magnetic properties of non-

oriented electrical steels with 3 wt. (%) Si," Materials Research, vol. 11, no. 1, pp. 51–55, Mar. 2008

[25] B. C. Mecrow, J. W. Bennett, A. G. Jack, D. J. Atkinson, and A. J. Freeman, "Drive Topologies for Solar-Powered Aircraft," IEEE Trans. Ind. Electron., vol. 57, no. 1, pp. 457–464, Jan. 2010.

[26] R. Brand and J. Nunn, "Material developments," Magnetics Technology International - Showcase, 2012.

[27] T. Meydan, "Application of amorphous materials to sensors," J. Magn. Magn. Mater., vol. 133, no. 1–3, pp. 525–532, May. 1994.

[28] M. E. McHenry, M. A. Willard, and D. E. Laughlin, "Amorphous and nanocrystalline materials for applications as soft magnets," Progress in Materials Science, vol. 44, no. 4, pp. 291–433, Oct. 1999.

[29] A. Boehm and I. Hahn, "Comparison of soft magnetic composites (SMCs) and electrical steel," in 2nd International Electric Drives Production Conference (EDPC), Oct. 2012.

[30] Stoev, Bozhidar & Todorov, George. (2015). Analytical Model for Sizing the Magnets of Permanent Magnet Synchronous Machines. Journal of Electrical Engineering. 3. 134-141. 10.17265/2328-2223/2015.03.004.

[31] Gieras, Jacek F, and Mitchell Wing. Permanent Magnet Motor Technology : Design and Applications. 2nd ed., rev. and expanded New York (N.Y.): Dekker, 2002.

[32] C. C. Mi, "Analytical design of permanent-magnet traction-drive motors," in IEEE Transactions on Magnetics, vol. 42, no. 7, pp. 1861-1866, July 2006, doi: 10.1109/TMAG.2006.874511.

[33] Balagurov, V. A., Galtieev, F. F., and Larionov, A. N. "Permanent Magnet Electrical Machines", Moscow, Russia, 1964.

[34] Verez, Guillaume & Barakat, Georges & Amara, Yacine & Hoblos, Ghaleb. (2015). Impact of Pole and Slot Combination on Vibrations and Noise of Electromagnetic Origins in Permanent

Magnet Synchronous Motors. Magnetics, IEEE Transactions on. 51. 1-4. 10.1109/TMAG.2014.2354019.

[35] Wolnik, T.; Styskala, V.; Mlcak, T. Study on the Selection of the Number of Magnetic Poles and the Slot-Pole Combinations in Fractional Slot PMSM Motor with a High Power Density. Energies 2022, 15, 215. https://doi.org/10.3390/en15010215

[36] Guo, L.; Wang, H. Research on Stator Slot and Rotor Pole Combination and Pole Arc Coefficient in a Surface-Mounted Permanent Magnet Machine by the Finite Element Method. World Electr. Veh. J. 2021, 12, 26. https://doi.org/10.3390/wevj12010026

[37] Urresty, Julio & Riba, Jordi-Roger & Romeral, Luis. (2013). Influence of the Stator Windings Configuration in the Currents and Zero-Sequence Voltage Harmonics in Permanent Magnet Synchronous Motors With Demagnetization Faults. Magnetics, IEEE Transactions on. 49. 4885-4893. 10.1109/TMAG.2013.2247046.

[38] J. Pyrhonen, T. Jokinen, V. Hrabovcova, Design of Rotating Electrical Machines. Chichester (UK): John Wiley & Sons, 2013.

[39] A. Boglietti, A. Cavagnino, D. Staton, M. Shanel, M. Mueller, C. Mejuto, "Evolution and modern approaches for thermal analysis of electrical machines," IEEE Transactions on Industrial Electronics, vol. 56, no. 3, pp. 871-882, 2009.

[40] Chong, Yew Chuan. (2015). Thermal analysis and air flow modelling of electrical machines.

[41] Chirilă, Aurel & Ghita, C. & Craciunescu, Aurelian & Deaconu, I.D. & Navrapescu, Valentin & Catrinoiu, M.. (2011). Rotating electric machine thermal study. Renewable Energy and Power Quality Journal. 1089-1093. 10.24084/repqj09.552.

[42] D. Fodorean, M.M. Sarrazin, C.S. Marţiş, J. Anthonis, H. Van der Auweraer, "Electromagnetic and structural analysis for a surface-mounted PMSM used for light-EV," IEEE Transactions on Industry Applications, vol. 52, no. 4, pp. 2892-2899, 2016.

[43] Lei, Gang & Zhu, Jianguo & Guo, Youguang & Liu, Chengcheng & Ma, Bo. (2017). A Review of Design Optimization Methods for Electrical Machines. Energies. 10. 1962. 10.3390/en10121962.

[44] S. Stipetic, W. Miebach and D. Zarko, "Optimization in design of electric machines: Methodology and workflow," 2015 Intl Aegean Conference on Electrical Machines & Power Electronics (ACEMP), 2015 Intl Conference on Optimization of Electrical & Electronic Equipment (OPTIM) & 2015 Intl Symposium on Advanced Electromechanical Motion Systems (ELECTROMOTION), 2015, pp. 441-448, doi: 10.1109/OPTIM.2015.7427030.

[45] G. Lei, T. Wang, J. Zhu, Y. Guo and S. Wang, "System-Level Design Optimization Method for Electrical Drive Systems—Robust Approach," in IEEE Transactions on Industrial Electronics, vol. 62, no. 8, pp. 4702-4713, Aug. 2015, doi: 10.1109/TIE.2015.2404305.

[46] Ali Abdul Razzaq Altahir, "Park and Clark Transformations: A Short Review", Electrical and Electronic Engineering Dept., University of Kerbala, Karbala, 56001, Iraq.

[47] Belda, Květoslav. "Mathematical Modelling and Predictive Control of Permanent Magnet Synchronous Motor Drives." (2013).

[48] M. Khayamy and H. Chaoui, ''Current sensorless MTPA operation of interior PMSM drives for vehicular applications,'' IEEE Trans. Veh. Technol., vol. 67, no. 8, pp. 6872–6881, Aug. 2018.

[49] L.-J. Cheng and M.-C. Tsai, ''Robust scalar control of synchronous reluctance motor with optimal efficiency by MTPA control,'' IEEE Access, vol. 9, pp. 32599–32612, 2021.

[50] L. Zhong, M. F. Rahman, W. Y. Hu, and K. W. Lim, ''Analysis of direct torque control in permanent magnet synchronous motor drives,'' IEEE Trans. Power Electron., vol. 12, no. 3, pp. 528–536, May 1997.

[51] Y. Xu, N. Parspour, and U. Vollmer, ‘‘Torque ripple minimization using online estimation of the stator resistances with consideration of magnetic saturation,’’ IEEE Trans. Ind. Electron., vol. 61, no. 9, pp. 5105–5114, Sep. 2014.

[52] M. Siami, D. A. Khaburi, and J. Rodriguez, ‘‘Simplified finite control setmodel predictive control for matrix converter-fed PMSM drives,’’ IEEE Trans. Power Electron., vol. 33, no. 3, pp. 2438–2446, Mar. 2018.

[53] M. S. Rafaq and J.-W. Jung, ‘‘A comprehensive review of state-of-theart parameter estimation techniques for permanent magnet synchronous motors in wide speed range,’’ IEEE Trans. Ind. Informat., vol. 16, no. 7, pp. 4747–4758, Jul. 2020.

[54] N. A. Demerdash, T. M. Hijazi, and A. A. Arkadan, ‘‘Computation of winding inductances of permanent magnet brushless DC motors with damper windings by energy perturbation,’’ IEEE Trans. Energy Convers., vol. EC-3, no. 3, pp. 705–713, Sep. 1988.

[55] T. W. Nehl, F. A. Fouad, and N. A. Demerdash, ‘‘Determination of saturated values of rotating machinery incremental and apparent inductances by an energy perturbation method,’’ IEEE Power Eng. Rev., vol. PER-2, no. 12, pp. 28–29, Dec. 1982.

[56] H. W. Derbas, J. M. Williams, A. C. Koenig, and S. D. Pekarek, “A comparison of nodal- and mesh-based magnetic equivalent circuit models A Comparison of Nodal- and Mesh-Based Magnetic Equivalent Circuit Models,” IEEE Trans. Energy Convers., vol. 24, no. 2, pp. 388–396, 2009.

[57] Y. S. Chen, ‘‘Motor topologies and control strategies for permanent magnet brushless AC drives,’’ Ph.D. dissertation, Univ. Sheffield, Sheffield, U.K., 1999.

[58] B. Stumberger, G. Stumberger, D. Dolinar, A. Hamler, and M. Trlep, ‘‘Evaluation of saturation and cross-magnetization effects in interior permanent-magnet synchronous motor,’’ IEEE Trans. Ind. Appl., vol. 39, no. 5, pp. 1264–1271, Sep./Oct. 2003.

[59] B. Stumberger, B. Kreca, and B. Hribernik, ‘‘Determination of parameters of synchronous motor with permanent magnets

from measurement of load conditions,'' IEEE Trans. Energy Convers., vol. 14, no. 4, pp. 1413–1416, Dec. 1999.

[60] K. M. Rahman and S. Hiti, ''Identification of machine parameters of a synchronous motor,'' IEEE Trans. Ind. Appl., vol. 41, no. 2, pp. 557–565, Mar. 2005.

[61] E. Armando, R. I. Bojoi, P. Guglielmi, G. Pellegrino, and M. Pastorelli, ''Experimental identification of the magnetic model of synchronous machines,'' IEEE Trans. Ind. Appl., vol. 49, no. 5, pp. 2116–2125, Sep. 2013.

[62] K. Liu, J. Feng, S. Guo, L. Xiao, and Z.-Q. Zhu, ''Identification of flux linkage map of permanent magnet synchronous machines under uncertain circuit resistance and inverter nonlinearity,'' IEEE Trans. Ind. Informat., vol. 14, no. 2, pp. 556–568, Feb. 2018.

[63] M. A. Mazzoletti, G. R. Bossio, C. H. De Angelo, and D. R. Espinoza-Trejo, ''A model-based strategy for interturn shortcircuit fault diagnosis in PMSM,'' IEEE Trans. Ind. Electron., vol. 64, no. 9, pp. 7218–7228, Sep. 2017.

[64] G. Feng, C. Lai, and N. C. Kar, ''A novel current injection-based online parameter estimation method for PMSMs considering magnetic saturation,'' IEEE Trans. Magn., vol. 52, no. 7, pp. 1–4, Jul. 2016.

[65] K. Liu, Q. Zhang, J. Chen, Z. Q. Zhu, and J. Zhang, ''Online multiparameter estimation of nonsalient-pole PM synchronous machines with temperature variation tracking,'' IEEE Trans. Ind. Electron., vol. 58, no. 5, pp. 1776–1788, May 2011.

[66] Z.-H. Liu, H.-L. Wei, X.-H. Li, K. Liu, and Q.-C. Zhong, ''Global identification of electrical and mechanical parameters in PMSM drive based on dynamic self-learning PSO,'' IEEE Trans. Power Electron., vol. 33, no. 12, pp. 10858–10871, Dec. 2018.

[67] Z.-H. Liu, X.-H. Li, L.-H. Wu, S.-W. Zhou, and K. Liu, ''GPU-accelerated parallel coevolutionary algorithm for parameters identification and temperature monitoring in permanent magnet synchronous machines,'' IEEE Trans. Ind. Informat., vol. 11, no. 5, pp. 1220–1230, Oct. 2015.

[68] K. Liu and Z. Q. Zhu, ‘‘Position-offset-based parameter estimation using the Adaline NN for condition monitoring of permanent-magnet synchronous machines,’’ IEEE Trans. Ind. Electron., vol. 62, no. 4, pp. 2372–2383, Apr. 2015.

[69] D. D. Reigosa, P. Garcia, F. Briz, D. Raca, and R. D. Lorenz, ‘‘Modeling and adaptive decoupling of high-frequency resistance and temperature effects in carrier-based sensorless control of PM synchronous machines,’’ IEEE Trans. Ind. Appl., vol. 46, no. 1, pp. 139–149, Jul. 2010.

[70] D. Reigosa, D. Fernández, M. Martínez, J. M. Guerrero, A. B. Diez, and F. Briz, ‘‘Magnet temperature estimation in permanent magnet synchronous machines using the high frequency inductance,’’ IEEE Trans. Ind. Appl., vol. 55, no. 3, pp. 2750–2757, May 2019.

[71] W. Xu and R. D. Lorenz, ‘‘High-frequency injection-based stator flux linkage and torque estimation for DB-DTFC implementation on IPMSMs considering cross-saturation effects,’’ IEEE Trans. Ind. Appl., vol. 50, no. 6, pp. 3805–3815, Nov./Dec. 2014.

[72] A. Wang, H. Li, and C. T. Liu, “Assessments of magnetic cross-coupling impacts on interior permanent magnet machine controls for electric vehicles,” Proc. Int. Conf. Power Electron. Drive Syst., vol. 200714001, pp. 1435–1438, 2009.

[73] T. J. E. Miller, M. Popescu, C. Cossar and M. McGilp, "Performance estimation of interior permanent-magnet brushless motors using the voltage-driven flux-MMF diagram," in IEEE Transactions on Magnetics, vol. 42, no. 7, pp. 1867-1872, July 2006, doi: 10.1109/TMAG.2006.874512.

[74] P. Guglielmi, M. Pastorelli, and A. Vagati, “Cross-saturation effects in IPM motors and related impact on sensorless control,” IEEE Trans. Ind. Appl., vol. 42, no. 6, pp. 1516–1522, 2006.

[75] D. Mingardi, M. Morandin, S. Bolognani, and N. Bianchi, “On the Proprieties of the Differential Cross-Saturation Inductance in Synchronous Machines,” IEEE Trans. Ind. Appl., vol. 53, no. 2, pp. 991–1000, 2017.

[76] K. J. Meessen, P. Thelin, J. Soulard, and E. A. Lomonova, “Inductance calculations of permanent-magnet synchronous machines including flux change and self- and cross-saturations,” IEEE Trans. Magn., vol. 44, no. 10, pp. 2324–2331, 2008.

[77] S. Wiedemann, R. M. Kennel, S. Hall, M. Alak, and R. Ole, “Dynamic Testing Characterization of a Synchronous Reluctance Machine,” 2016.

[78] L. Chedot and G. Friedrich, “A Cross Saturation Model for Interior Permanent Magnet Synchronous Machine. Application to a StarterGenerator,” IEEE Industry Application Society Annual Meeting, Oct. 3-7, 2004, Seattle, Washington, pp. 64–70.

[79] T. Jahns et al., “Design and Experimental Verification of a 50 kW Interior Permanent Magnet Synchronous Machine,” Conf. Rec. 2006 IEEE Ind. Appl. Conf. Forty-First IAS Annu. Meet., vol. 4, pp. 1941–1948, 2006.

[80] L. Chedot and G. Friedrich, “A cross saturation model for interior permanent magnet synchronous machine. Application to a starter-generator,” Conf. Rec. 2004 IEEE Ind. Appl. Conf. 2004. 39th IAS Annu. Meet., vol. 1, no. C, pp. 64–70, 2004.

[81] Z. Q. Zhu, Y. Li, D. Howe, C. M. Bingham and D. Stone, "Influence of Machine Topology and Cross-Coupling Magnetic Saturation on Rotor Position Estimation Accuracy in Extended Back-EMF Based Sensorless PM Brushless AC Drives," 2007 IEEE Industry Applications Annual Meeting, New Orleans, LA, USA, 2007, pp. 2378-2385, doi: 10.1109/07IAS.2007.359.

[82] Nasui-Zah, Ioana & Tamas, Anton-Horatiu & Martis, Claudia-Steluta. (2019). Impact of saturation and cross-saturation on SynRM's dynamic model. 145-148. 10.1109/EMES.2019.8795173.

[83] Meessen, Koen & Thelin, P. & Soulard, Juliette & Lomonova, E.A.. (2008). Inductance Calculations of Permanent-Magnet Synchronous Machines Including Flux Change and Self- and Cross-Saturations. Magnetics, IEEE Transactions on. 44. 2324 - 2331. 10.1109/TMAG.2008.2001419.

[84] S. T. Lee, T. A. Burress, and L. M. Tolbert, “Power-factor and torque calculation with consideration of cross saturation of the interior permanent magnet synchronous motor with brushless field excitation,” 2009 IEEE Int. Electr. Mach. Drives Conf. IEMDC ’09, pp. 317–322, 2009.

[85] Patrick Seibt and André Fischer, “Description of the Cross Saturation in an IPMSM for Electric Vehicles Using Bicubic Splines”, Springer International Publishing Switzerland 2015, L. Gołębiowski and D. Mazur (eds.), Analysis and Simulation of Electrical and Computer Systems, Lecture Notes in Electrical Engineering 324, DOI 10.1007/978-3-319-11248-0_31.

[86] B. Stumberger, G. Stumberger, D. Dolinar, A. Hamler and M. Trlep, "Evaluation of saturation and cross-magnetization effects in interior permanent-magnet synchronous motor," in IEEE Transactions on Industry Applications, vol. 39, no. 5, pp. 1264-1271, Sept.-Oct. 2003, doi: 10.1109/TIA.2003.816538.

4. Design and Analysis of an IPMSM for Propulsion System

4.1 Introduction

The present chapter addresses the design of an IPMSM for the propulsion system of an electrical VAN.

The design process follows the steps and aspects described in Chapter 3. Thus, the specifications of the electrical machine are derived based on the vehicle characteristics and requirements. The specifications are used for the preliminary design phase, after which the main dimensions of the machine are computed.

Firstly, based on the vehicle's main geometrical characteristics, as well as on the given requirements, the specifications of the machine to be design can be defined. These include the main electrical parameters of the machine, such as the required/maximum torque/power, the phase voltage and the rated/maximum phase currents. Then, the electrical machine's preliminary design can be performed. At this stage, the machine's type is chosen. Moreover, its main geometrical characteristics, such as the inner/outer rotor/stator diameter, the machine's length, the PMs, windings, and stator slots dimensions are determined at this step.

The machine's component-level model is built based on the pre-sizing results, using a commercially available software, namely JMAG Designer. Electromagnetic performances and machine's parameters are computed and analyzed, by considering both no-load and rated load operation scenarios.

The Field Oriented Control (FOC) method, combined with MTPA strategy, is chosen to be implemented for the machine under test. The implementation is performed by using MatLAB Simulink software package. In addition, the main particularities of the implementation are discussed too, and the simulation results are highlighted.

4.2 Specifications generation based on application

Nowadays, electric vehicles have become more and more popular and, as a consequence it is estimated that in the next few years, they will replace vehicles with internal combustion engine (ICE). The popularity of electric vehicles is, on one hand, due to the need to reduce the gas emissions without negatively impacting the transportation sector, and, on the other hand, due to their simplicity, both in terms of construction and operation.

Therefore, the given application involves the design of the electric machine used to propel a vehicle. The imposed vehicle is a minivan, whose geometric characteristics are presented in the Table 4.1. Moreover, the electrical machine's main requirements are highlighted in Table 4.2. Based on this data, the specifications of the electrical machine can be defined.

Table 4. 1 Main geometrical characteristics of the vehicle.

Characteristic	**Abbreviation**	**Value**	**Unit**
Length	L	4363	mm
Wheelbase	W_b	1751	mm
Height	H	1814	mm
Mass	m	2000	kg
Wheel diameter	D_{wheel}	800	mm

Table 4. 2Main requirements of the electrical machine.

	Value	Unit
Shaft diameter	60	mm
Rated power	17	kW
Rated speed	2800	rpm
DC Voltage	96	V
Phase number	3	-
Maximum torque ripple content	4-6	%
Rated efficiency	0.9	-
Rated power factor	0.9	-

Firstly, the rated rotational speed of the electrical machine, as well as the gearbox ratio must be selected [1]. The choice of these parameters in made by taking into account that the vehicle's maximum speed combined with the gearbox ratio and wheel diameter is close to the required maximum speed. To guarantee that the maximum speed can be reached, the estimated value should be bigger than the maximum planned speed.

As a result, choosing the gearbox ratio and the rated rotational speed must be done all at once. The following equation illustrates the relationship between the ideal gearbox ratio and the rated rotational speed:

$$i = \frac{n_N D_{wheel} \pi}{v_{max}} \tag{4.1}$$

where n_N is the rated rotational speed of the electrical machine and v_{max} is the maximum speed of the vehicle.

Therefore, considering that the maximum speed of the vehicle is imposed by the application to 100km/h and the rated speed of the electrical machine is 2800rpm, the gearbox ratio will be:

$$i = 8.4947$$

Then, in order to determine the required power, the friction, respectively the drag forces should be calculated [2]. The friction force can be defined as the product of the rolling resistance coefficient, the gravitational constant, and the mass of the vehicle, as shown in the following equation.

$$F_{fr} = \mu_{rr}\, mg \tag{4.2}$$

For this particular case, the rolling resistance coefficient was chosen to be 0.047. Therefore, the friction force is:

$$F_{fr} = 0.047 \cdot 2000 \cdot 9.81 = 922.14\ N \tag{4.3}$$

The drag force depends on the air density, air resistance coefficient, maximum frontal area and vehicle speed, as defined in subsection 3.3. The air resistance coefficient for the minivan under study was chosen to be 0.5. In order to determine the maximum frontal area of the vehicle, equation (4.4) can be used. Considering that the vehicle mainly operates inside the cities, the speed was chosen to be 50 km/h, which is equal to 13.8 m/s.

$$A_f = W_b\, H = 1751 \cdot 1814 = 3.17 \text{ m}^2 \tag{4.4}$$

Therefore, the drag force resulted:

$$R_a = \frac{1}{2} \cdot 1.293 \cdot 0.5 \cdot 3.15 \cdot 13.8 = 193.91\ N \tag{4.5}$$

Knowing these parameters, the required power can be computed using:

$$P = \frac{(F_{fr} + R_a)v}{\eta} = \frac{(922.14 + 193.91) \cdot 13.8}{0.9} = 16.9 \text{ kW} \tag{4.6}$$

where η=0.91 is the performance of the electrical machine.

Next, the required torque can be computed using the following equation:

$$T = \frac{P}{\Omega_N} \tag{4.7}$$

where Ω_N is the angular speed of the machine and it can be determined upon the following equation:

$$\Omega_N = 2\pi n_N \tag{4.8}$$

For this case, the rated speed of the machine (n_N) is 2800 rpm. Therefore, the required torque is equal to:

$$T = \frac{16.9 \cdot 10^3}{293.15} = 57.65 \text{ Nm} \tag{4.9}$$

In order to calculate the maximum required power and torque respectively, the maximum force required for the vehicle to climb a 10% ramp is determined.

$$F_{max} = mg \sin \alpha \tag{4.10}$$

where $\alpha = \tan^{-1}(\frac{ramp}{100})$.

In this case, $F_{max} = 2000 \cdot 9.81 \cdot 0.1 = 1950.28$ N.

Therefore, the maximum required power will be:

$$P_{max} = \frac{F_{max} v}{\eta} = \frac{1950.28 \cdot 13.8}{0.9} = 29.6 \text{ kW} \tag{4.11}$$

while the maximum required torque can be determined with the following equation:

$$T_{max} = \frac{P_{max}}{\Omega_N} = \frac{29.6 \cdot 10^3}{293.15} = 100.97 \text{ Nm} \tag{4.12}$$

Next, the phase voltage can be computed, as follows, considering that the machine has 3 phases:

$$U_{ph} = \frac{U_{DC}}{\sqrt{3}\sqrt{2}} = \frac{96}{\sqrt{3}\sqrt{2}} = 39.2 \text{ V} \tag{4.13}$$

Moreover, the rated torque was determined by analytical approach upon the following equation:

$$T_N = \frac{P_N}{\Omega_N} = \frac{17 \cdot 10^3}{293.15} = 57.97 \text{ Nm} \tag{4.14}$$

Between the machine's main dimensions and the apparent power there is a direct connection, reason why, the apparent power was computed:

$$S_N = \frac{P_N}{\eta \cos \varphi} = \frac{17}{0.9 \cdot 0.9} = 20.99 \text{ kVA} \tag{4.15}$$

Next, the phase, respectively the maximum currents are determined:

$$I_{ph} = \frac{S_N}{mU_{ph}} = \frac{20.99 \cdot 10^3}{3 \cdot 39.2} = 178.5 \text{ A} \tag{4.16}$$

$$I_{max} = \sqrt{2} I_{ph} = \sqrt{2} \cdot 178.5 = 252.43 \text{ A} \tag{4.17}$$

In addition, Fig. 4.1 presents the machine's requirements regarding the electromagnetic torque variation with speed, respectively the mechanical power variation with speed. As it can be noticed, the electromagnetic torque has a constant value up to the speed of 2800 rpm. After that, it decreases in order to keep the mechanical power at a constant value of 17 kW.

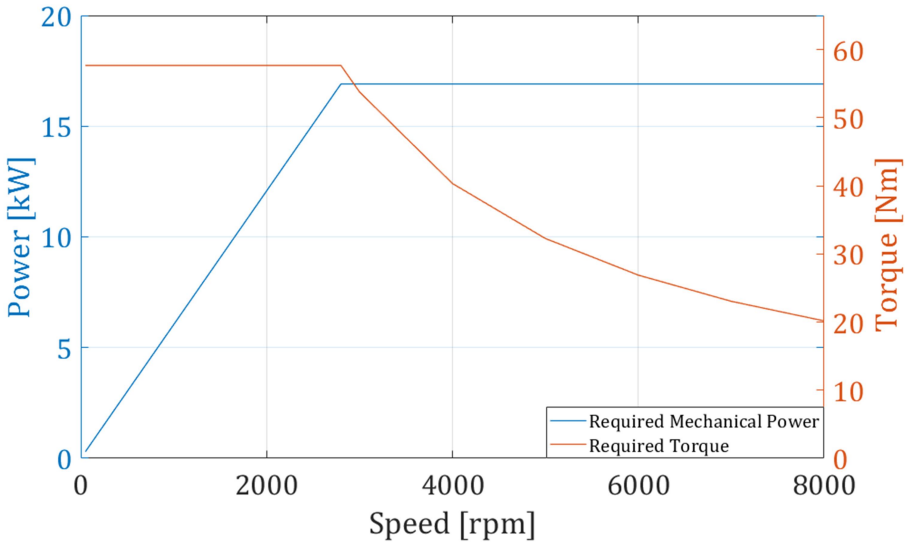

Fig. 4. 1 Required mechanical power and electromagnetic torque variation vs speed

Therefore, the main requirements of the electrical machine were determined, based on the characteristics of the vehicle that should be propelled and the limitations imposed by it.

4.3 Electrical machine preliminary design

Regarding the type of the electrical machine used to propel the vehicle, it was decided that the Permanent Magnet Synchronous Machine (PMSM) is the best option for this application. The choice was based on the advantages that these electrical machines offer compared to other. Among them, there are the high-power density, high efficiency, as well as the robustness and constructive simplicity. Moreover, regarding the constructive option it was decided to mount the permanent magnets inside the rotor. The justification of this decision is also based on the advantages that this constructive option has, compare to other available options. These advantages are presented in detail in subchapter 2.2.

From the poles/slots combination point of view, the 10 poles/24 slots combination was chosen. For this choice, two factors were considered. On one hand, the torque ripple content, as well as the radial forces were taken into account. As explained in subsection 3.5, the higher the least common multiple (LCM) between the number of poles and number of slots, the lower the cogging torque is. This is applicable for the radial forces too. The higher and even the greatest common divider (GCD) is, the more balanced the machine is. On the other hand, the manufacturing company offers the possibility to choose only certain topologies. Thus, by analysing each available topology in the manufacturer's portfolio, it was found out that the optimal topology for the given application is the one with 10 poles and 24 slots.

Moreover, considering the geometrical limitations that were imposed, the main dimensions of the machine were established too.

The next step in the design of the electrical machine is the choice of the materials used in the construction of its main components. Therefore, in order to minimize the iron losses as much as possible, for the construction of the stator core, electrical steel sheets were used, while the rotor core is made of solid electrical steel.

Regarding the permanent magnets, sintered Neodymium-Iron-Boron was chosen.

Considering that it is preferred for the machine to be as light as possible, for the stator windings, copper was chosen because it offers superior performances compared to aluminium. Section 3.4.2 highlights a brief comparison between copper and aluminium.

In addition, all the materials used in the construction of each electrical machine's components [3] are summarized in the table 4.3.

Table 4. 3 Materials used in the construction of the electrical machine.

Component	Material
Stator core	Electrical steel sheets
Rotor core	Electrical steel
Coil	Copper
Permanent magnet	Sintered Neodymium-Iron-Boron (NdFeB)

4.3.1 Stator and rotor core sizing

Therefore, in order to determine the interior stator diameter [4], the following equation was used:

$$D_{i\_s} = \sqrt[3]{\frac{2p}{\pi\lambda}\frac{60S_N}{C \cdot n_N}} \tag{4.18}$$

where C is the Esson's coefficient or the electromagnetic utilization coefficient [5]. It was estimated from specific tables, depending on the machine's apparent power and number of poles. In this case, C=750 J/dm^3.

Moreover, λ which is the aspect coefficient and can be defined as the ratio between the machine's active length and the airgap diameter. In many scientific papers, the airgap diameter is replaced by the interior stator diameter in the equation for defining the aspect factor. In addition, this value can be chosen based on the pole pairs number from specific diagrams. In this case, λ=0.8.

Therefore, the interior stator diameter for the electrical machine that should be designed will be:

$$D_{i\_s} = \sqrt[3]{\frac{2 \cdot 5}{\pi \cdot 0.8} \frac{60 \cdot 20.99 \cdot 10^3}{750 \cdot 10^3 \cdot 2800}} = 130 \text{ mm} \quad (4.19)$$

Then, based on the aspect factor and interior stator diameter, the active length of the machine is determined:

$$\lambda = \frac{L}{D_{ag}} \cong \frac{L}{D_{i_s}} => L \cong \lambda \cdot D_{i_s} = 0.8 \cdot 130 = 104 \text{ mm} \quad (4.20)$$

As in the producer catalogue the inner stator diameter value was not available, it was chosen the nearest option, i.e., D_{i_s}=122 mm, while the machine's length was approximated to L=100 mm.

Based on the ratio between the inner and outer stator diameters [6], highlighted in equation 4.21, the outer stator diameter (D_{o_s}) was computed.

$$k_D = \frac{D_{i\_s}}{D_{o\_s}} \quad (4.21)$$

Considering k_D=0.5, the outer stator diameter was approximated to 240mm.

The airgap length is a critical parameter of the electrical machines, having an important influence on its performances. The machine will return better performances the smaller the airgap length [7]. However, not always the manufacturer can ensure a very small airgap, considering that, from the constructive point of view, there are some limitations. In order to calculate the optimal airgap length, the following equation can be employed:

$$\delta = 0.2 + 0.003 \cdot \sqrt[3]{P_N} \quad (4.22)$$

The resulted value, δ=0.97mm, was approximated to δ=1 mm.

Next, the outer rotor diameter can be determined, as follows:

$$D_{o_r} = D_{i\_s} - 2\delta = 122 - 2 \cdot 1 = 120 \text{ mm} \quad (4.23)$$

Therefore, Table 4.4, highlights the main geometrical characteristics of the designed electrical machine [8].

Table 4. 4 Main geometrical characteristics of the electrical machine.

Characteristic	Value	Unit
Number of slots	24	-
Number of poles	10	-
Outer stator diameter	240	mm
Inner stator diameter	122	mm
Outer rotor diameter	120	mm
Machine's length	100	mm

4.3.2 Permanent magnets sizing

In order to determine the main dimensions of the permanent magnets mounted inside the rotor, the total required permanent magnets volume should be determined [9]. This value depends on the characteristics of the magnetic material, the volume coefficient (C_v), as well as on the rated power of the machine and its frequency, as equation 4.24 shows.

$$V_{PM\_tot} = C_v \frac{P_N}{f_N B_r H_c} \tag{4.24}$$

As previously mentioned, the material used for the permanent magnets, sintered NdFeB was chosen. Fig 4.2 highlights the magnetization curve of this material, while Table 4.5 highlights its main properties.

Table 4. 5 NdFeB main characteristics.

Characteristic	Value	Unit
Magnetic field density	1.2	T
Coercive force	907	kA/m
Maximum operating temperature	150	˚C
Curie temperature	320	%/˚C
Density	7.5	g/cm^3

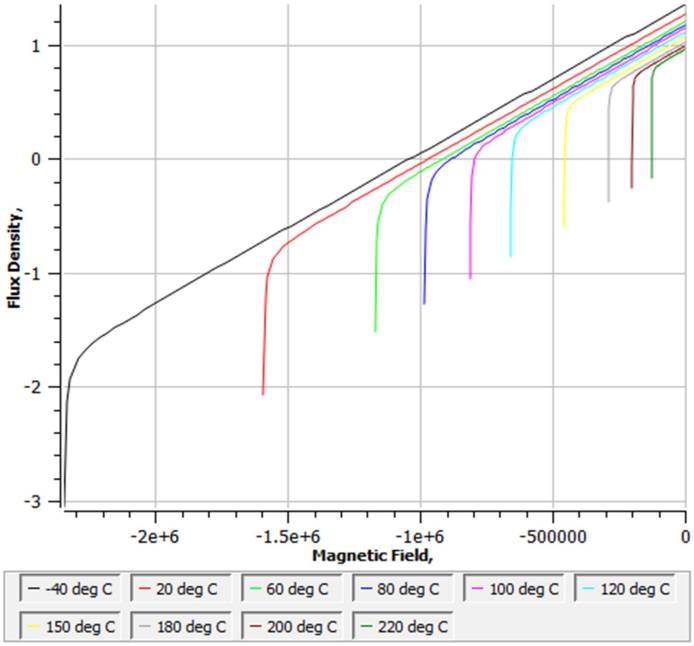

Fig. 4. 2 Magnetization curve of sintered NdFeB

Machine's frequency can be computed using:

$$f_N = \frac{pn_N}{60} = \frac{5 \cdot 2800}{60} = 233.33 \text{ Hz} \tag{4.25}$$

The volume coefficient can take any value between 0.54 and 3.1. In this case, the maximum possible value was chosen.

Therefore, the total required permanent magnets volume will be:

$$V_{PM\_tot} = 3.1 \frac{17 \cdot 10^3}{233.33 \cdot 1.2 \cdot 907 \cdot 10^3} = 0.00021 \text{ m}^3 \tag{4.26}$$

Then, the total mass of the permanent magnets should be determined by the following equation:

$$m_{PM\_tot} = \rho_{PM} \cdot V_{PM_{tot}} = 1.575 \text{ kg} \tag{4.27}$$

where ρ_{PM}=7500kg/m^3 is the density of the material from which the permanent magnet is made, as highlighted in Table 4.5.

The next step is to calculate the total required permanent magnets surface, using:

$$S_{PM\_tot} = \frac{V_{PM\_tot}}{L} = \frac{21 \cdot 10^4}{100} = 2100 \text{ mm}^2 \quad (4.28)$$

Therefore, the surface of a single permanent magnet will be:

$$S_{PM} = \frac{S_{PM\_tot}}{2p} = \frac{2100}{10} = 210 \text{ mm}^2 \quad (4.29)$$

To determine the width and height of the permanent magnet, its angular opening (α_{PM}) should be computed, as follows:

$$\alpha_{PM} = \frac{360}{2p} k_{ao} = 22.3° \quad (4.30)$$

where k_{ao}=0.62, is the angular opening coefficient.

The permanent magnet width is given by:

$$b_{PM} = D_r \sin\frac{\alpha_{PM}}{2} = 23.597 \text{ mm} \quad (4.31)$$

while its height can be computed using:

$$h_{PM} = \frac{S_{PM}}{b_{PM}} = 8.89 \text{ mm} \quad (4.32)$$

Based on these requirements, all that remains is to choose the shape and final dimensions of the permanent magnets. Due to the fact that for the permanent magnets shape it was necessary to choose one of the options from the manufacturer's catalogue, rectangular shape was chosen. Also, to comply with the catalogue offer in terms of permanent magnets dimensions, two magnets, having each 12.5 mm width and 9 mm height, were used for one rotor pole, as shown in Fig. 4.3.

Moreover, it can be observed that the rotor core has some carvings near the permanent magnets. This solution was adopted in order to reduce the machine's overall mass, and to increase its performances in terms of electromagnetic torque [10].

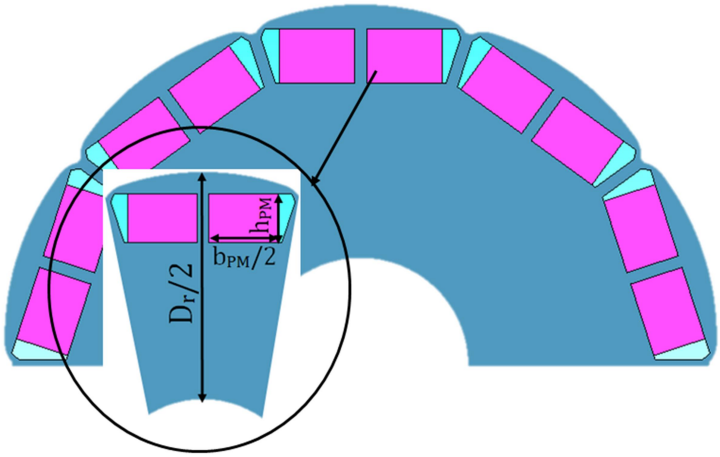

Fig. 4. 3 Permanent magnets arrangement in the electrical machine

4.3.3 Winding sizing

Next, the winding configuration was determined. As explained in subchapter 3.6, the winding configuration has a strong influence on the electromagnetic torque value, as well as on the variation of back-EMF and circuit voltage respectively. In addition, voltage harmonics can be affected by the winding configuration. Regarding the connection, the star connection was chosen, considering that it is cheaper and easier to be obtained. Moreover, this connection is preferred over the delta connection in this kind of electrical machines because in the case of delta connection cyclic currents appear. These currents can introduce copper losses and amplify the torque ripples. As for the way the stator windings are distributed, based on the arguments presented in subsection 2.2, distributed winding was chosen.

Therefore, a two layers, three phase distributed winding was chosen. The distance between the ingoing slot and outgoing slot, also known as pole pitch [11], is given by:

$$y = \frac{Z_s}{2p} \tag{4.33}$$

where Z_s is the number of slots, Z_s=24, in this case. In consequence, y=2.4.

The number of coils per phase can be determined by:

$$n_c = \frac{Z_s}{m} \tag{4.34}$$

while the number of slots per pole per phase is given by:

$$q = \frac{Z_s}{2p \cdot m} \tag{4.35}$$

Regarding the winding factor, it mainly depends on the number of slots and poles and also on the winding characteristics, such as: the number of layers and the winding type.

Thus, Fig. 4.4 shows the winding configuration of the machine, while Table 4.6 shows the main parameters of the winding.

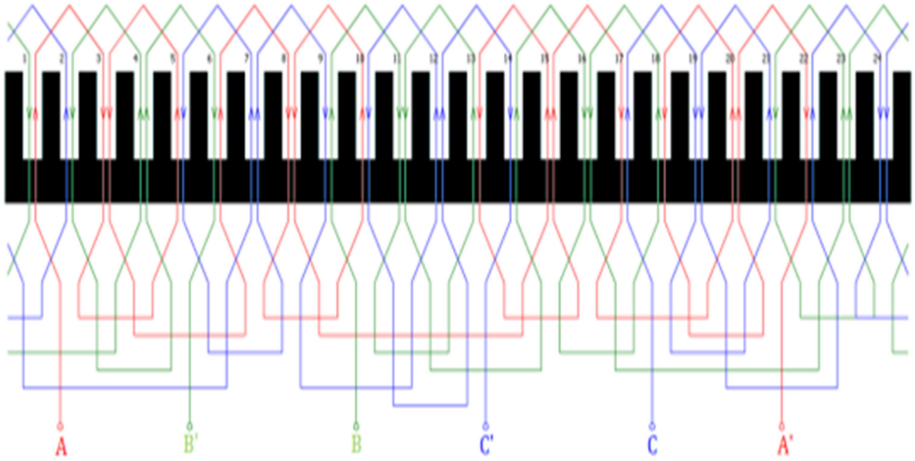

Fig. 4. 4 Electrical machine's winding configuration

Table 4. 6 Winding main characteristics.

Characteristic	Value
Number of slots	24
Number of poles	10
Number of coils per phase	8
Coil throw	2.4
Maximum winding factor	0.925
Pole pitch	2.4
Number of turns per coil	3

4.3.4 Slots sizing

To determine the main geometrical dimensions of the stator slot, the slot's shape should be chosen. In this case, the trapezoidal shape was selected. Then, the tooth pitches, both at the slot and airgap levels should be calculated. These sizes will be useful in computation of the tooth, respectively slot width.

Therefore, the tooth pitch on the slot side can be determined with:

$$\tau_s = \frac{\pi(D_{s_i} + 2h_{tt})}{2p \cdot m} = 16.22 \text{ mm} \tag{4.36}$$

while the tooth pitch on the airgap side is given by:

$$\tau_{ag} = \frac{\pi D_{s_i}}{2p \cdot m} = 15.97 \text{ mm} \tag{4.37}$$

where h_{tt}=2.5 is the height of the pole shoe, chosen based on [4].

Once these parameters are established, the minimum width of the tooth, respectively the minimum width of the slot can be determined with the following equations [12]:

$$b_{t\_min} = \frac{B_{ag}}{k_{i\_Fe} \cdot B_t} \tau_{ag} \tag{4.38}$$

where: - B_{ag}=0.9T, is the airgap magnetic field density;

- B_t=1.8T, is the tooth's magnetic field density;

- k_{i_Fe}=0.96, is the lamination insulation coefficient.

All of these values were chosen based on the machine's parameters, according to [13].

$$b_{s\_min} = \tau_{ag} - b_{t\_min} \tag{4.39}$$

Thus, the minimum tooth width b_{t_min}=8.22mm, while the minimum slot width b_{s_min}=8.4mm.

Next, the yoke height should be determined, following the equation:

$$h_y = \frac{B_{ag}}{k_{i\_Fe} \cdot B_y} \tau_{ag} = 12.47 \text{ mm} \tag{4.40}$$

where B_y=1.2T, is the magnetic flux density of the stator yoke.

Now, the slots height can be calculated, using the formula:

$$h_s = \frac{D_{o\_s}}{2} - \frac{D_{i_s}}{2} - h_{tt} - h_y = 44.03 \text{ mm} \tag{4.41}$$

Then, in order to determine the maximum slot width, the required slot surface should be estimated. Based on the possibilities of the prototype manufacturer, and also on the constraints imposed by the materials, the conductors surface, including the insulation, was approximated at S_t=80mm^2. Therefore, the required slot surface is:

$$S_{s\_req} = \frac{2S_t}{0.9k_f} = 592.59 \text{ mm}^2 \tag{4.42}$$

where k_f=0.3, is the slot fill factor.

The slot surface can also be defined as:

$$S_s = \frac{(b_{s\_max} + b_{s\_min})}{2} h_s \tag{4.43}$$

Thus, from (5.39), the maximum slot width was determined:

$$b_{s\_max} = \frac{2S_s}{h_s} - b_{s\_min} = 18.51 \text{ mm} \qquad (4.44)$$

Finally, taking into account the previously obtained results, but also the possibilities and recommendations of the manufacturer, the optimal slots dimensions were established and presented in Table 4.7, while Fig. 4.5 shows the stator configuration, including the main dimensions of the teeth and slots.

Table 4. 7 Stator slots main characteristics.

Characteristic	Value	Unit
Minimum slot width	8	mm
Maximum slot width	19	mm
Slot height	44.5	mm
Slot surface	596.12	mm^2
Pole shoe height	2.55	mm
Slot opening	3.2	mm

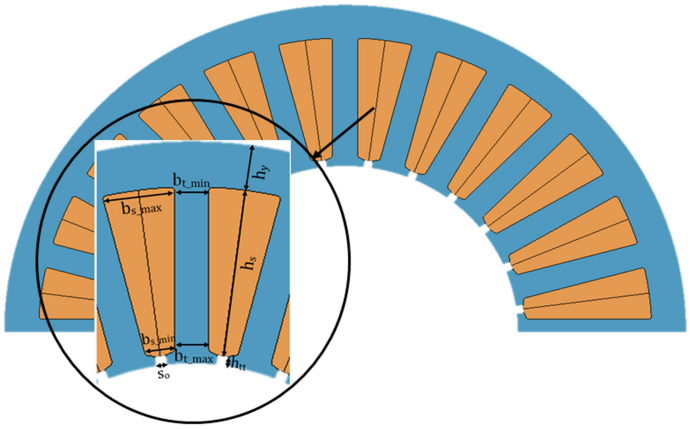

Fig. 4. 5 Permanent magnets arrangement in the electrical machine

Therefore, starting from the requirements of the application and taking into account the limitations and constraints imposed by both the manufacturer and the application itself, the topology of the machine was determined, as well as the materials from which each component is made.

4.4 IPMSM modelling

Based on the results obtained in the specifications generation stage, as well as in the machine pre-sizing stage, both detailed earlier, the model of the electrical machine that makes the subject of this thesis was built, using JMAG software package.

JMAG is a software package, created in 1983, used in the design and analysis of electric devices. It realistically simulates different phenomena in a variety of devices in order to evaluate their behavior in different operating scenarios. JMAG software includes four packages as follows: Designer, Express, RT and RT Viewer.

The heart of JMAG is Designer, a high speed and high precision Finite Element Analysis (FEA) tool. This tool includes a modelling technology combined with an intuitive interface that helps the user to reach the expected results. It offers the possibility of implementing a varied number of models and designs. Moreover, the user can easily adjust their shapes, materials properties or operating conditions.

Additionally, for a faster analysis of the machine, JMAG developers designed Express tool. This tool works based on pre-set models, which can be customized according to the user's needs, or by importing an already existing design. Thus, it instantly calculates variables such as: torque, efficiency, losses or machine power, to provide preliminary information about the chosen design.

Using JMAG-RT tool, a highly accurate plant model can be generated, based on the results from the Finite Element Model (FEM). The obtained model is very useful in system-level simulations for a more realistic portrayal of the device. Therefore, it can be implemented in Hardware in the Loop (HIL) analysis by connecting the virtual machine to a real ECU.

The last tool, but not the last, is RT Viewer. It offers the possibility to improve the usability of the models developed in JMAG-RT.

Therefore, JMAG is suitable for a large number of designs, from different DC and AC machines to transformers, in the field of electric machines. As mentioned before, the model can be customized from the existing models from the software's library or it can be imported as CAD model. Moreover, JMAG Designer has a restoring CAD geometry tool that can be used to modify the geometry imported models. This tool is useful when the user wants to analyze how some changes can affect the device behavior in different situations.

Companies in this field have been including multiphysics models in their studies as processing capability has increased. JMAG started their new era in 1994, with the magnetic field analysis coupled with thermal facilities. Since then, multiphysics capability has seen a significant degree of progress. Therefore, JMAG works together with CAE suppliers to provide a user-friendly platform from which to start a multiphysics modelling. Nowadays, in addition to electromagnetic and thermal analysis, users have the possibilities to run structural analysis in order to determine the influence of noises and vibrations.

Moreover, JMAG models can be parameterized, so that, the user can very easily obtains new models starting from the initial one. In this way, the influence of each variable in the model can be better understood and, at the same time, the entire model can be improved.

Regarding the improvement of the models, JMAG provides a variety of features that offer powerful support for design optimization. As the analysis and optimization functions are integrated, it is simple to perform factor analysis and optimization, enabling the efficient assessment of a huge number of design ideas.

In addition, the software allows different types of analysis, depending on the user needs. Among the possibilities there are: magnetic, axisymmetric and structural. Regarding the materials, JMAG formed partnerships with material manufacturers in order to provide the best data for their database. For instance, along with iron loss parameters, magnetic characteristics or mechanical properties, JMAG developers permanently try to supply the data required so that users can perform advanced and accurate analysis [14].

4.4.1. Rotor and stator cores modelling

As mentioned before, starting from the main geometrical data of the machine, highlighted in Table 4.8, respectively Table 4.9, the geometry was built step by step, using the Geometry Editor tool, available in JMAG-Designer. The modelling procedure started with the construction of the rotor core. Based on the shaft diameter, as well as on the outer rotor diameter and the permanent magnets dimensions, a half rotor pole was built. Considering that the rotor poles are symmetrical, it was possible to design just a half pole, which was later mirrored to obtain the entire rotor pole. Moreover, taking into account the machine's symmetry, to build the model used for the subsequent analyses, it is sufficient to design only one part of the machine, provided that this is specified when the analyses setup is done, as Fig. 4.6 shows.

Table 4. 8 Main geometrical characteristics of the electrical machine's rotor.

Characteristic	Value	Unit
Outer rotor diameter	120	mm
Shaft diameter	60	mm
Number of poles	10	-
PM width	12.5	mm
PM height	9	mm
Machine's length	100	mm

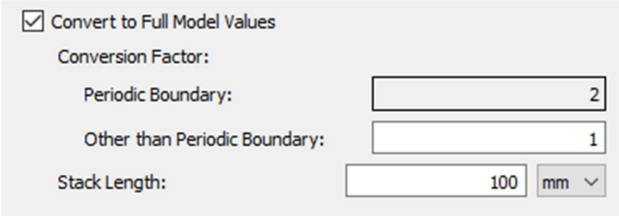

Fig. 4. 6 Partial to full model conversion dialog box (JMAG-Designer)

Halved model was chosen to perform the analysis for the study case. In this way, the simulation time will be reduced, without any negative impact on the results' accuracy. Therefore, Fig. 4.7 illustrates the rotor construction process. Following the same steps, the stator core was also designed, as shown in Fig. 4.8.

After all these steps were completed, the electrical machine's geometry was obtained, including the rotor core, the PMs, as well as the stator core, as shown in Fig. 4.9.

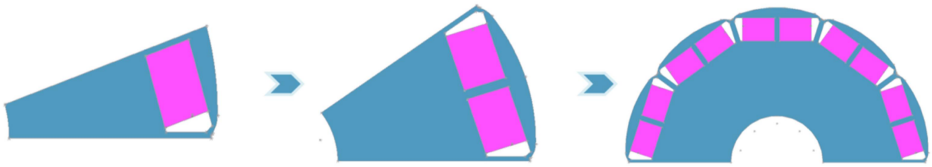

Fig. 4. 7 Rotor core construction algorithm

Table 4. 9 Main geometrical characteristics of the electrical machine's stator.

Characteristic	Value	Unit
Outer stator diameter	240	mm
Inner stator diameter	122	mm
Number of slots	24	-
Maximum slot width	19	mm
Minimum slot width	8	mm
Slot height	44.5	mm
Slot opening	3.2	mm
Pole shoe height	2.55	mm
Machine's length	100	mm

Fig. 4. 8 Stator core construction algorithm

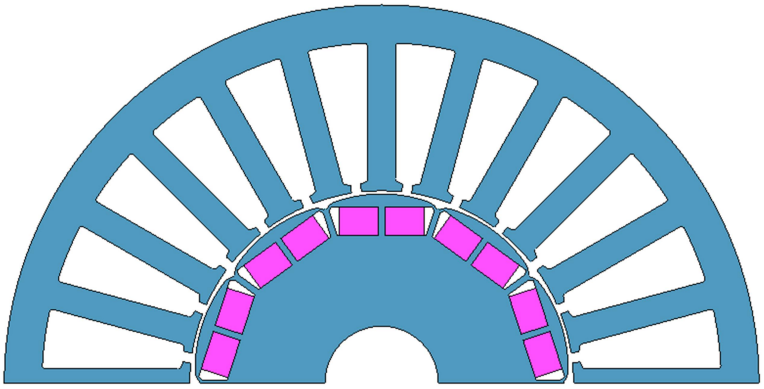

Fig. 4. 9 Electrical machine's geometry

4.4.2. Windings modelling

As previously explained, the winding configuration has a huge impact on the electromagnetic torque and torque ripples. In order to obtain the best performances of the machine, four different winding configurations were compared. The results are highlighted in Subsection 3.6. The results of the comparison, corroborated with the data obtained after performing the sizing stage, led to the optimal winding configuration, provided in Fig. 4.10. In this case, the winding scheme was manually implemented, but the software also allows automatic implementation, based on the main characteristics of the winding.

After the configuration of the winding is done, from *Conditions* panel, the corresponding coils must be assigned to each phase, taking into account the direction of the current in the coil (upward/downward). This is essential because when the electric circuit of the machine is defined, each coil in the model must be connected to its corresponding coil component in the circuit. In addition, when the electrical circuit is defined, the winding properties must be defined, such as:

- number of turns: 3;
- phase resistance: 0.0235 Ω.

The other parameters are automatically assimilated based on the chosen configuration.

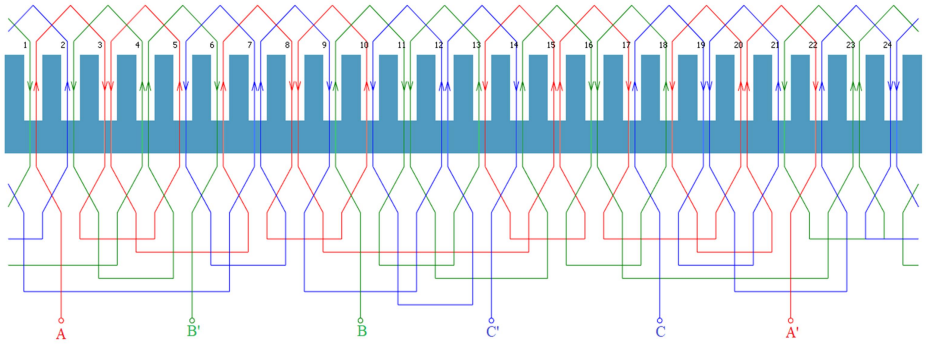

(a) slot view

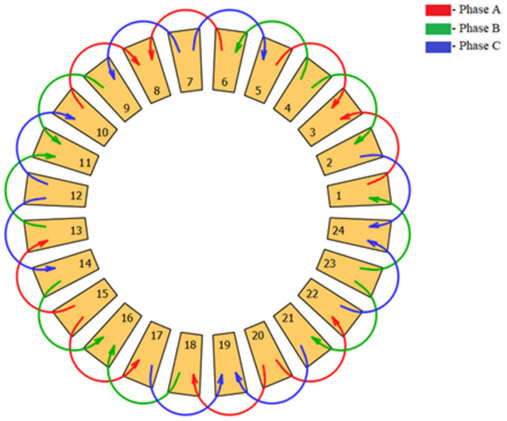

(b) model view

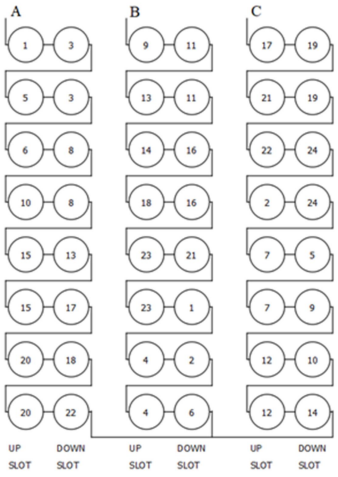

(c) winding view

Fig. 4. 10 Winding configuration

4.4.3. Choosing the materials

The next step in machine's modelling procedure is the selection of the materials of each component. The materials were chosen based on the considerations previously exposed, from the materials list

provided by JMAG-Designer library and considering their availability at the manufacturer.

Fig. 4.11 presents the materials that were used in the construction of the main components of the machine. As it can be noticed, N38SH was selected for the permanent magnets, which is a Sintered NdFeB permanent magnet material with good properties for the given application. For the stator and iron cores, M330-50A electrical steel, with 0.5mm thickness, manufactured by ArcelorMittal was selected, while the machine's windings are made of copper.

In Fig. 4.12, the main properties of the selected materials are highlighted. Regarding the machine's cores, in order to reduce the iron losses, it was decided that the stator core will be made of laminated sheets, while the rotor core will be built from solid material. As for the permanent magnets magnetization, parallel pattern in circular outward direction was selected, as shown.

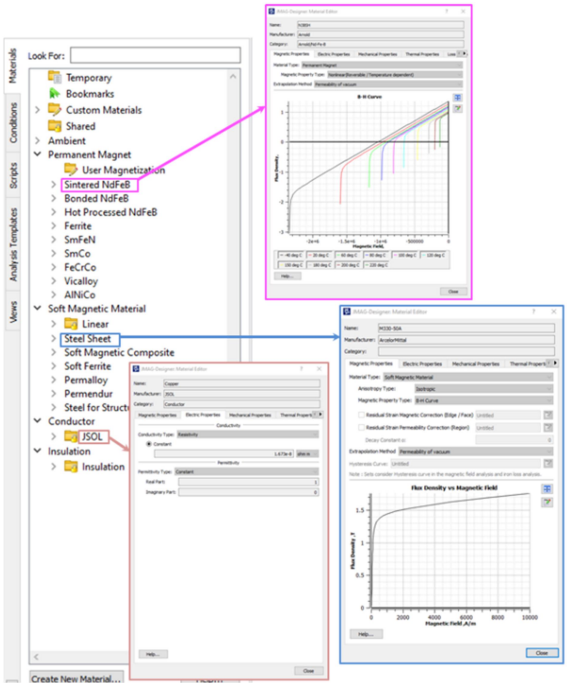

Fig. 4. 11 Materials used in the construction of the machine

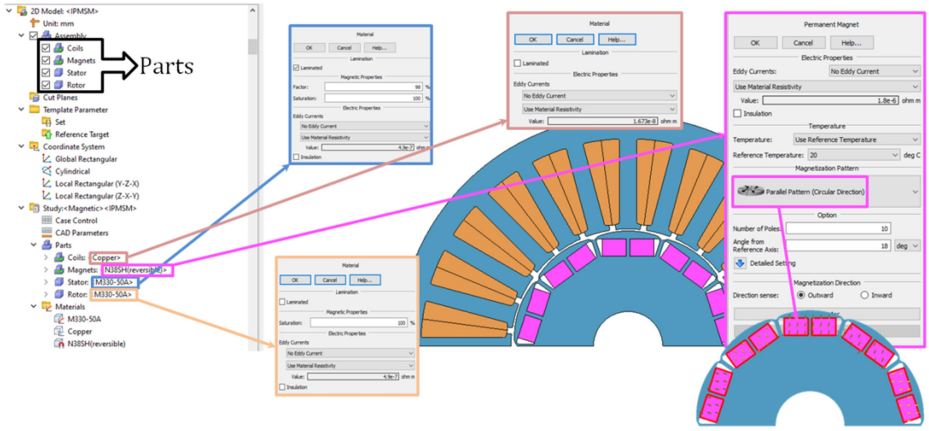

Fig. 4. 12 Selection of the materials and their properties

4.4.4. Setting the conditions of the analyses

First of all, to perform a model analysis, from an electromagnetic point of view, for example, the properties of the study must be established. In this regard, the type of the study (static, transient, etc.) must be chosen. Moreover, the *timing parameters* necessary for the analysis should be determined, as JMAG perform each analysis step by step. Among them, there are:

- number of steps for the calculation;
- step interval definition type;
- unit;
- start time;
- end time;
- divisions.

Therefore, in order to track as well as possible when certain changes appear during the analysis, these parameters must be carefully determined. For example, in this case, for one complete rotation of the machine (360 degrees), 361 steps were required for the calculation. Regarding the step interval definition type, regular interval was chosen. The number of divisions is usually 1 less than the number of steps. When regular interval is chosen, the start time is automatically pre-set to 0, while the end time can be determined according to the angular speed with the following equation:

$$end_{time} = \frac{2 \cdot \pi}{\Omega} = \frac{2 \cdot \pi}{\frac{\pi \cdot 2800}{30}} = \frac{3}{140} \tag{4.45}$$

Next, the *boundary* conditions should be set. As the machine under study is a rotating electrical machine and the implemented model is a partial one, rotation periodic boundary must be chosen from JMAG-Designer conditions list.

First of all, the model's edges on which the periodicity condition applies must be determined. Then, the periodicity of the model, as well as the periodic angle – which is the angle at which the same pattern repeats -, and the rotation axis that specifies the direction of the rotation axis, should be set. Regarding the periodicity, the software offers two options, as follows:

- periodic – meaning that the magnetic flux pattern repeats every cycle;
- antiperiodic – meaning that the magnetic flux pattern repeats in opposite direction for every cycle.

The *symmetry boundaries,* as well as the *slide* conditions are automatically set after the model's mesh is created.

In order to set the *motion* condition, the parts on which the movement acts must be determined (in this case, the rotor and permanent magnets), as well as the rated speed of the machine and the initial position of the rotor (if applicable). Moreover, the method by which the machine's *torque* is calculated must be chosen. In this regard, in JMAG-Designer there are three available options: by Nodal force, by Lorentz force and by Surface force.

Fig. 4.13 presents the conditions list, as implemented in JMAG-Designer, as well as the timing parameters setting window.

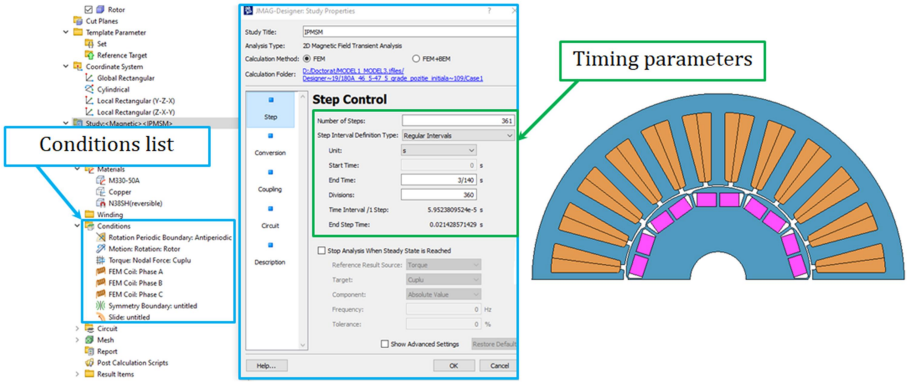

Fig. 4. 13 Conditions implemented in JMAG-Designer

4.4.5. Implementing the machine's circuit

The electrical machine's circuit can be implemented in the Circuit Editor window. The circuit can be either imported or directly created in the interface. In this case, the circuit was created from scratch. The Circuit Editor tool offers all the necessary components both for electromagnetic and thermal studies. Fig. 4.14 shows the electrical circuits implemented for no-load analysis (a), respectively for rated-load analysis (b).

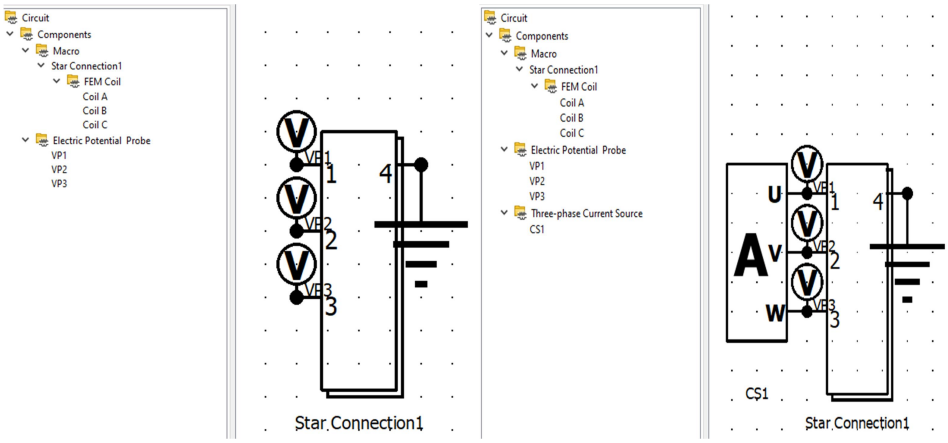

(a) no-load analysis (b) rated-load analysis

Fig. 4. 14 IPMSM circuit implementation

4.4.6. Setting the mesh

In order to use the finite element method, the model must be divided into discrete elements, so that the machine's equations can be solved. The process of dividing the model into discrete elements, also known as meshing, is crucial in electrical machines analysis considering that a high quality mesh ensures accurate results. The mesh's quality is determined both by its size and the cells form. The accuracy of the results will be impacted by any variation from the ideal shape. In this regard, the mesh should be defined taking into account that the smaller cells are employed for fine geometric details and high solution gradients, and larger cells, elsewhere.

Therefore, as it can be seen in Fig. 4.15, in the main important regions, such as the air-gap, the mesh is finer, while in the coil or stator core, the mesh is coarser. This solution was adopted in order to decrease the calculation time, without affecting the accuracy of the results.

Regarding the properties of the mesh, they can be set in the Mesh Properties tab. These include: basic settings, setting the elements size, slide division and adaptive mesh control properties.

For this model, the following settings were implemented:

- mesh type: slide mesh;
- air region scale: set for each direction;
- model length in radial direction for air region: 1.25;
- element size of parts: automatically;
- element size of air region: 5 mm;
- radial divisions: 3;
- circumferential divisions: 360.

Thus, while setting the optimal mesh for a given model, it is important to keep in mind that it should have just the right number of elements to properly represent a field solution while not using up all of the available processing resources.

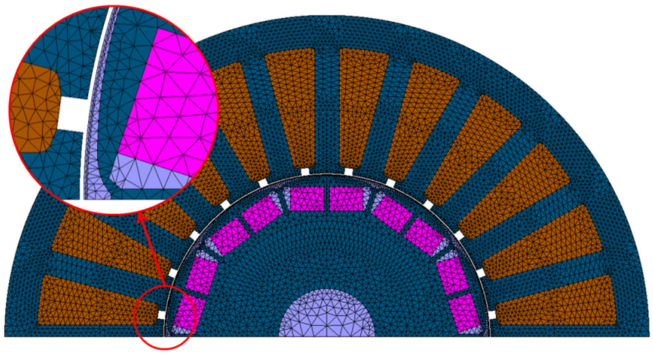

Fig. 4. 15 Machine's mesh

4.5 Electromagnetic analysis of the machine

Once the geometrical model of the machine is complete and its parameters, including materials, winding configuration and the implementation of the mesh have been defined, it is possible to continue with the electromagnetic analysis.

Firstly, a generator operation no-load analysis will be conducted. Then, the rated motor operation load analysis will be performed.

4.5.1. No-load analysis

As previously mentioned, the no-load analysis implies the generator operation of the machine with zero current in the stator windings (no-load). This means that the magnetic field developed by the electric machine is totally created by the permanent magnets mounted in the rotor.

In order to obtain a complete analysis, some parameters should be considered. These parameters include:

- magnetic flux density distribution;
- magnetic flux lines map;
- cogging torque;
- induced electromagnetic force and its harmonics;
- magnetic flux density in the airgap and other different points of the machine and their harmonics.

The permanent magnets of the machine are parallel and alternatively magnetized, as explained earlier, in this chapter. Therefore, the flux lines pass through the pole of a magnet and enter in the opposite pole of the nearest magnet, as Fig. 4.16 illustrates. The alternating magnetic field is generated once the machine rotates. It depends on the machine's speed, its frequency, as well as on the number of pole pairs. As can be observed, the magnetic flux lines appear as closed curves.

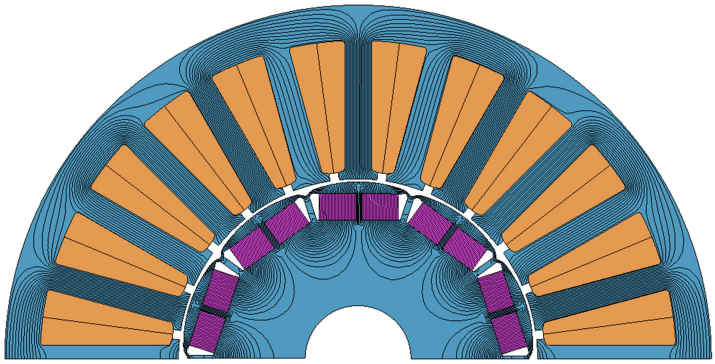

Fig. 4. 16 Magnetic flux lines

Regarding the magnetic flux distribution in the machine at no-load operation, the distribution map is presented in Fig. 4.17. As it can be observed, the maximum value is about 2.3 T and it is reached in isolated points in the rotor core, near the air-gap.

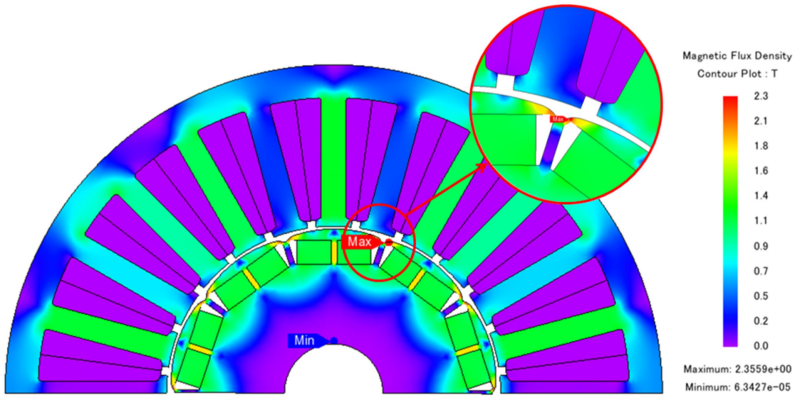

Fig. 4. 17Magnetic flux distribution map

The induced electromagnetic force, also known as the back-EMF, can be defined as the force that acts in the opposite direction to the applied voltage [15]. Basically, this force helps the machine to spin in the first move. Moreover, it reduces the current flowing through the machine's coils. Regarding its value, it is important to mention that it has to be lower than the applied voltage, but still very close to it. The back-EMF of the machine under study is depicted in Fig. 4.18. As can be seen, its amplitude is close to 60V, while the phase shift corresponds to a three phase machine (each phase is offset from the others with 120°).

By applying the Fourier transform to the back-EMF, using JMAG-Designer Calculation tool, the voltage harmonics were obtained. As can be noticed in Fig. 4.19, the voltage harmonics are of odd order. Moreover, the most influent one is the 3rd order harmonic, corresponding to a frequency of almost 700 Hz.

In addition, based on the harmonics analysis, the Total Harmonic Distortion (THD) can be determined. THD highlights the signal distortion compared to the sinusoidal shape and it can be computed using the following equation:

$$THD = \frac{\sqrt{\sum_{h=2}^{n} V_h^2}}{V_1} \cdot 100\ [\%] \tag{4.46}$$

where: - V_1 is the RMS value of the fundamental harmonic;
- V_h is the RMS value of the h^{th} harmonic.

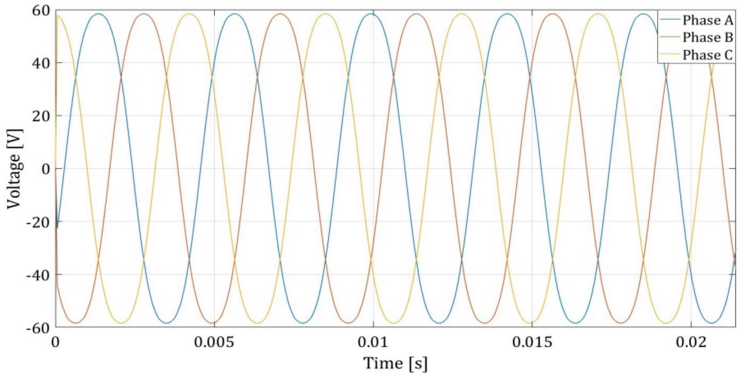

Fig. 4. 18 Back-EMF

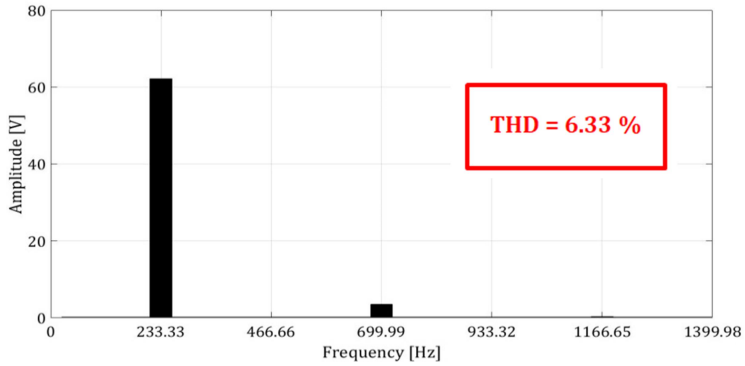

Fig. 4. 19 Back-EMF harmonics

The cogging torque describes the interaction between the permanent magnets, mounted in the rotor core, and the stator teeth [16], [17]. This torque appears because the tendency of the rotor is to line up with the stator. Another important aspect regarding the cogging torque is that it appears independent of any current.

It is well known that the cogging torque may be very harmful for the machine, reason why many studies were performed on the sensitivity of the cogging torque versus different geometrical and numerical parameters. In addition, over the time, researchers have developed different methods of cogging torque reduction, with the aim of minimizing, as much as possible, its negative influence on the machine's behavior.

Usually, the cogging torque has a very small value compared to the electromagnetic torque produced by the machine. Fig. 4.20 illustrates the cogging torque of the machine under study. Particularly for this machine, the cogging torque is very low (almost 0.05 Nm from peak to peak), while, as it will be seen in the next subsection, the electromagnetic torque reaches a value close to 58 Nm. This means that the cogging torque represents less than 0.1% of the electromagnetic torque.

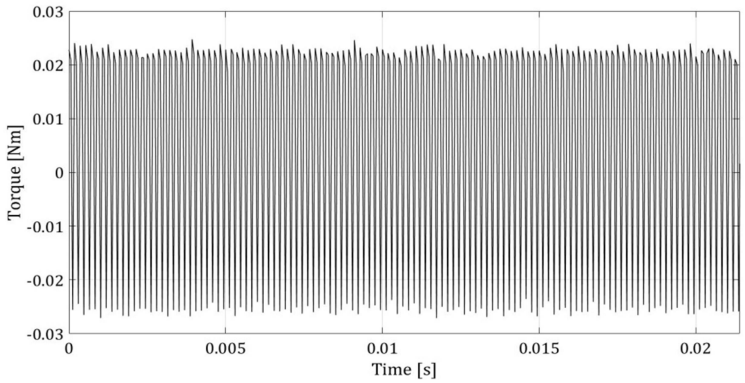

Fig. 4. 20 Cogging torque

The magnetic flux density in the air-gap was also considered. The importance of studying this parameter is closely related to the fact that it has a relevant influence regarding the output torque developed by the machine. Regarding the factors that may affect the air-gap magnetic flux density, there are the PMs parameters, such as their thickness, or the number of poles, as well as the inner and outer rotor diameter [18], [19].

The magnetic flux density in the air-gap versus time is depicted in Fig. 4.21. It can be observed that its RMS value is approximately 0.55 T, and its waveform tends to be sinusoidal. The waveform distortion appears as a consequence of the harmonics content which was calculated by Fourier transform and is presented in Fig. 4.22.

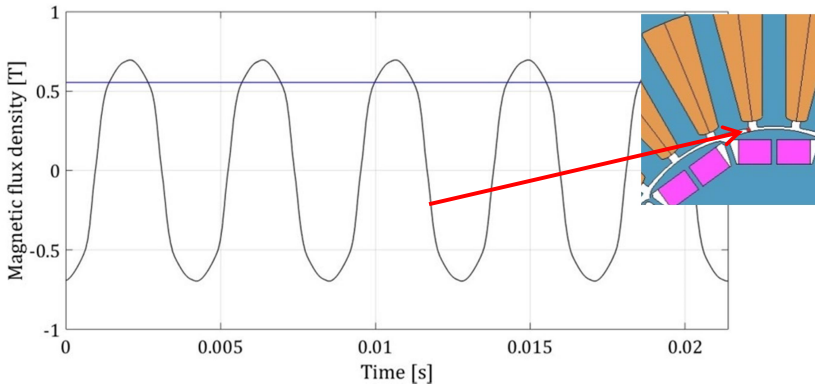

Fig. 4. 21 Magnetic flux density in the air-gap

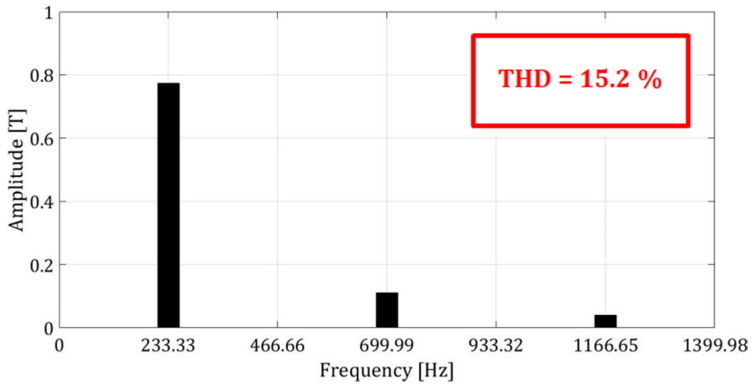

Fig. 4. 22 Magnetic flux density in the air-gap harmonics

In order to fully understand the magnetic flux properties of the machine, the magnetic flux density in different regions of the stator, such as the stator yoke and the stator tooth, was taken into account too. The analysis results are highlighted in Fig. 4.23. Compared to the magnetic flux density of the stator yoke which has the RMS=0.4 T, the magnetic flux density of the stator tooth is larger, having a RMS value of about 0.9 T. Moreover, due to the chosen topology [20], the magnetic flux density waveform in the stator yoke suffers some distortions from the ideal sinusoidal shape, compared to the stator tooth case. This observation is also reinforced by the harmonics analysis presented in Fig. 4.24. It can be observed that in the case of stator yoke, the 3th (corresponding to 700 Hz), respectively the 5th (corresponding to 1167 Hz) order harmonics have the greatest influence, while in the second case, the 3rd order harmonic is the most influent.

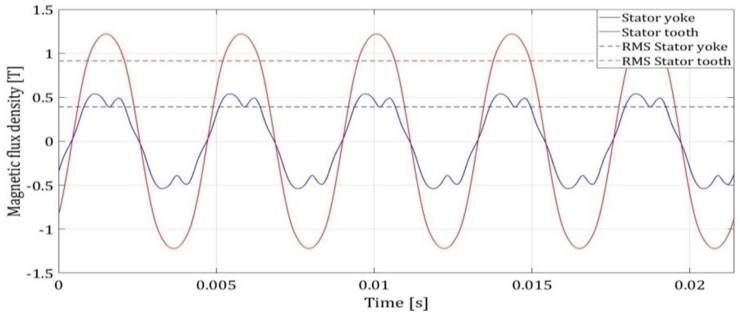

Fig. 4. 23 Magnetic flux density in the stator core

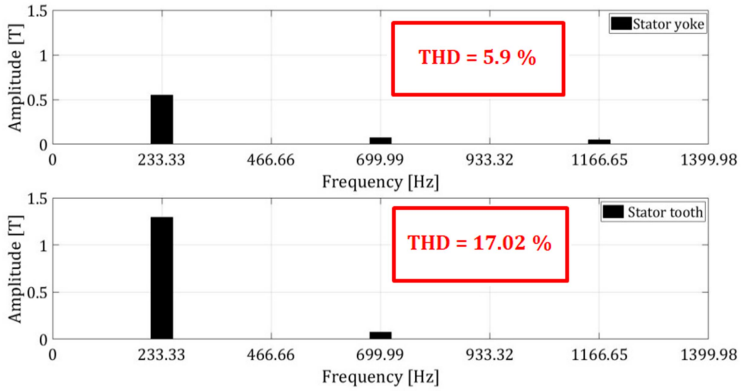

Fig. 4. 24 Magnetic flux density in the stator core harmonics

4.5.2. Rated load analysis

To understand the machine's behavior when a load is coupled on its shaft, a three-phase current source was implemented in the Circuit Editor tool.

The currents for each phase were assigned considering the following expressions:

$$\begin{aligned} I_A &= I \cdot \sin(2\pi \cdot f \cdot t + \theta) \\ I_B &= I \cdot \sin\left(2\pi \cdot f \cdot t + \theta + \frac{2\pi}{3}\right) \\ I_C &= I \cdot \sin(2\pi \cdot f \cdot t + \theta - \frac{2\pi}{3}) \end{aligned} \tag{4.47}$$

where: - I=180 A, is the current amplitude;

- f=233.33 Hz, is the current frequency;

- t, is the time, measured in seconds;

- θ=0 rad, is the phase angle.

The choice of the current phase angle θ=0 rad is explained later in this chapter.

Fig. 4.25 highlights the input currents variation. As it can be observed, the root mean square current is slightly over 127 A, while the

peak-to-peak value is 180 A on each phase. This observation was made to prove that the settings implemented in the Circuit Editor tool were respected and can be found in the analysis results.

Therefore, the simulation was performed with the same timing parameters as no-load analysis. In this case, the following parameters were considered:

- magnetic flux density distribution;
- magnetic flux lines map;
- circuit voltage and its harmonics;
- electromagnetic torque and its components;
- magnetic flux density in the airgap and other different points of the machine and their harmonics;
- d- and q-axis inductivities.

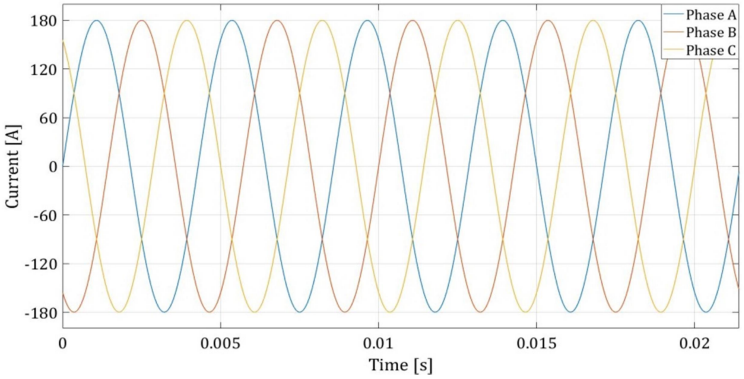

Fig. 4. 25 Circuit current variation

Fig. 4.26 illustrates the magnetic flux lines obtained under rated load conditions. As in the case of no-load analysis, the flux lines are presented as closed curves that enter in a magnetic pole after passing through the opposite pole of the nearest permanent magnet.

The magnetic flux distribution in the machine is highlighted in Fig. 4.27. As it can be noticed, the values slightly exceed the maximum values obtained at no-load computation. However, as the higher values appear only in the usual critical points, there is no risk for the permanent magnets demagnetizing prematurely.

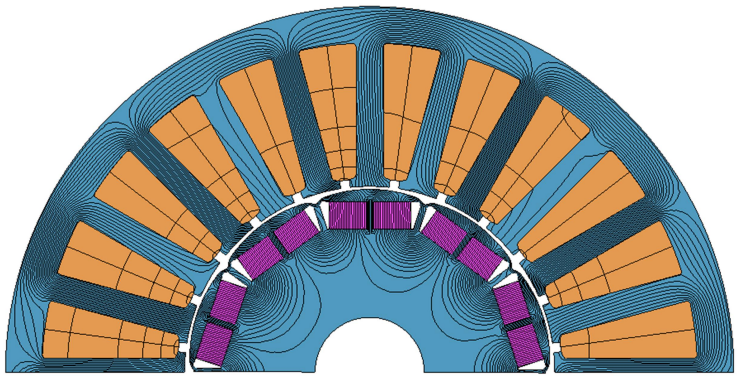

Fig. 4. 26 Magnetic flux lines

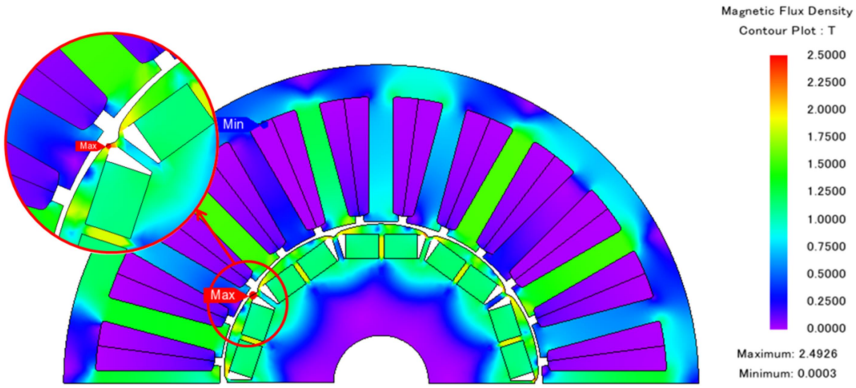

Fig. 4. 27 Magnetic flux distribution map

Regarding the circuit voltage, the observations made for no-load operation scenario on back-EMF are valid, meaning that the sinusoidal shape of the curves is preserved, but more distorted from the ideal shape, due to the armature reaction. This distortion will also be visible when performing the Fourier analysis in order to obtain the voltage harmonic. As can be observed in Fig. 4.28, the voltage amplitude is about 80 V.

In addition, similar to no-load simulation, the harmonics are from odd order, the third one being the most influent, as shown in Fig.

4.29. The difference, in this case, is the more obvious appearance of the 5th order harmonic.

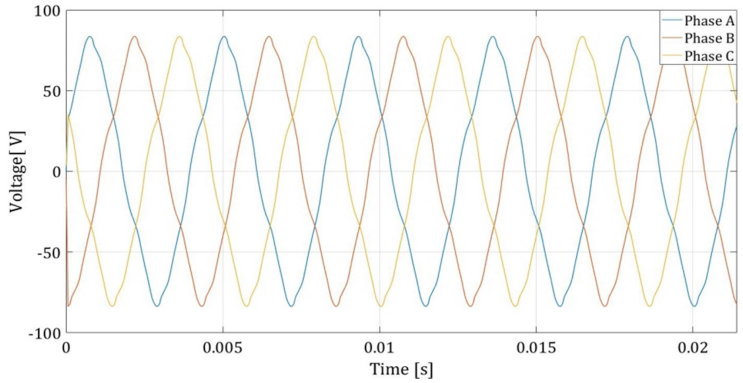

Fig. 4. 28 Circuit voltage variation

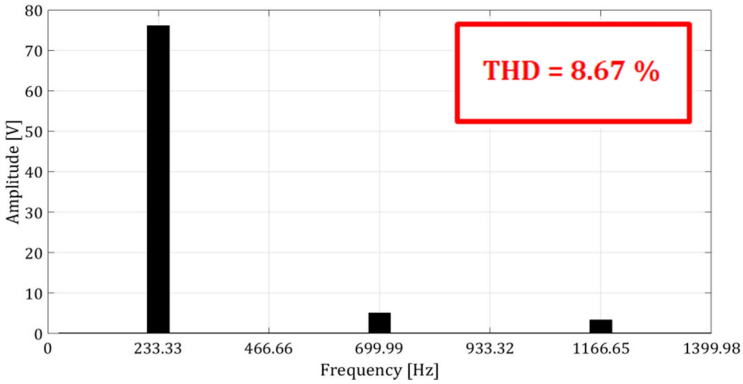

Fig. 4. 29 Circuit voltage harmonics

The electromagnetic torque developed by the machine versus time is presented in Fig. 4.30. As it can be noticed, its instantaneous value varies from 56.67 Nm and 58.76 Nm, having a peak-to-peak ripple of about 2 Nm. Moreover, the average value is 57.66 Nm.

Based on the maximum, minimum and average values, the torque ripple relative value can be computed with the following equation [3]:

$$T_{ripple} = \frac{T_{max} - T_{min}}{T_{avg}} \cdot 100 = \frac{58.76 - 56.67}{57.66} \cdot 100 = 3.63\ \% \qquad (4.48)$$

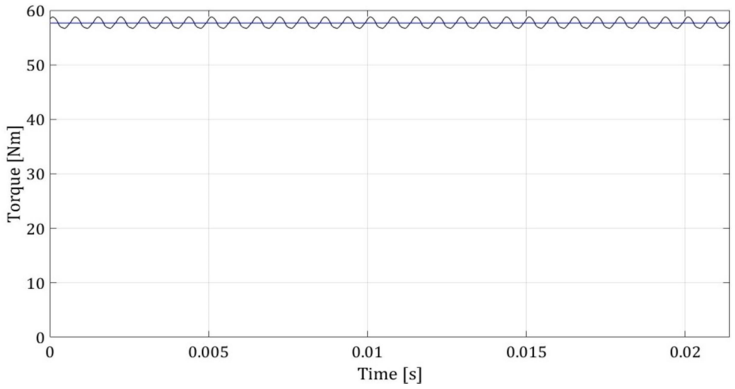

Fig. 4. 30 Electromagnetic torque

Besides the torque ripple content, it is also important to analyze the electromagnetic torque components. In the case of PMSMs with salient rotor, the total torque is composed of the reluctance torque and the torque developed as a result of the interaction between the magnetic field of the permanent magnets and the magnetic field of the stator, hereinafter referred to as the magnet torque [21], [22].

When designing a PMSM, it is mandatory to synchronize the magnetic flux of the PMs with the magnetic flux of the stator, in order to maximize the machine's performances. A complete synchronization requires, in addition to adjusting the frequency, also adjusting the stator currents phase angle (θ).

Fig. 4.31 depicts the torque components, as well as the total torque of the machine versus current phase angle. As it can be seen, the machine's capacity to produce reluctance torque depends on the current phase angle, because this angle highly influences the permanent magnets flux linkage. The maximum torque is obtained for a current phase angle of 0 degree. As a consequence, when defining the current source component properties, in the Circuit Editor tool, the current phase angle (θ) was chosen to be 0 degree.

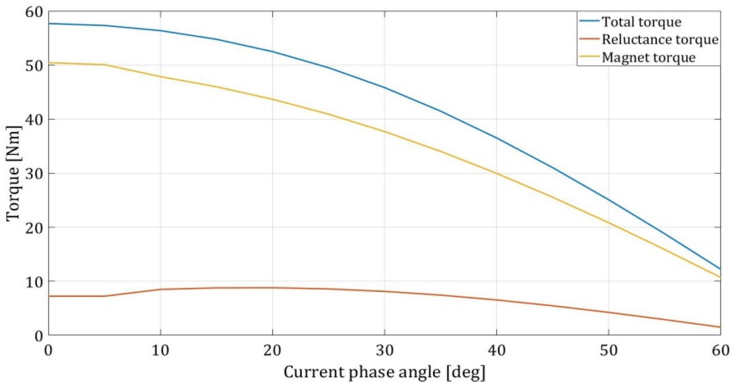

Fig. 4. 31 Electromagnetic torque components

Therefore, in order to be able to do the torque separation, frozen permeability method was implemented. For each current phase angle value, the average value of each torque component was calculated and represented on the graph. The torque separation into components is based on the electromagnetic torque equation, highlighted below.

$$T_e = \frac{3}{2} \cdot p \cdot [\Psi_{PM} \cdot i_q + (L_d - L_q) i_d \cdot i_q] \tag{4.49}$$

The first component, which plays the most important role, is the synchronous torque, while the second component is the reluctance torque, developed by the variation of the machine's air-gap reluctance with the rotor position.

Regarding the magnetic flux density in the air-gap at rated load operation, the observations made for no-load scenario are still valid, specifying that, in this case, its amplitude is a little bit higher, as expected, with a RMS value equal to 0.79 T, as shown in Fig. 4.32. Moreover, its waveform suffers certain distortions from the ideal shape too, the harmonics analysis being presented in Fig. 4.33.

The same can be said in the case of magnetic flux density in the stator core. As in the case of no-load analysis, two key points were chosen, one in the stator yoke and the other one in the stator tooth, on which the analysis were performed. In the case of stator yoke, the RMS

value remains equal to the one obtained at no-load analysis, while, in the case of stator tooth, a slight increase can be observed (RMS=1.05 T). The stator core magnetic flux density versus time is represented in Fig. 4.34.

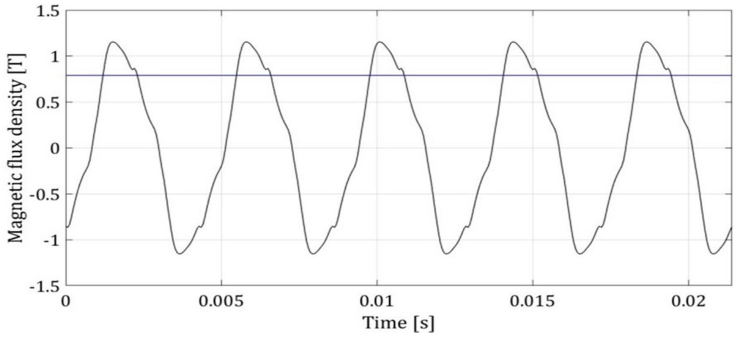

Fig. 4. 32 Magnetic flux density in the air-gap

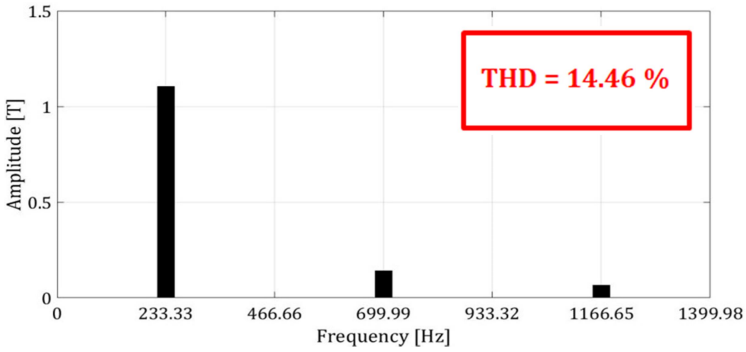

Fig. 4. 33 Magnetic flux density in the air-gap harmonics

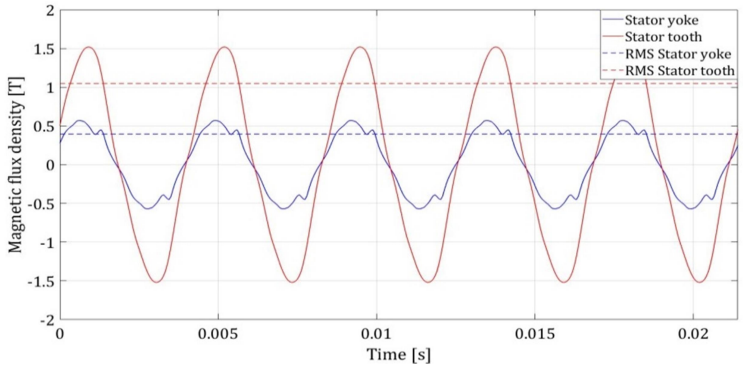

Fig. 4. 34 Magnetic flux density in the stator core

From the waveform point of view, an improvement can be observed in the case of stator yoke, the results of the Fourier analysis being presented in Fig. 4.35.

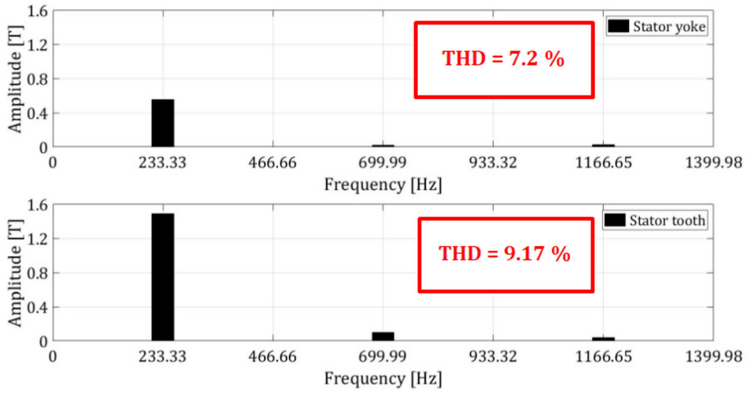

Fig. 4. 35 Magnetic flux density in the stator core harmonics

Another very important parameter of the machine, which was also considered in this analysis, is the motor's inductances. In this regard, the d-axis, respectively the q-axis inductances were computed using JMAG Motor Inductance tool.

Firstly, the d-axis inductance when applying only the d-axis current was computed. The same analysis was implemented for q-axis. In this situation, the two axes are considered completely independent of each other. In other words, the q-axis has no influence on the d-axis, and vice versa. However, in practice, as both axes share the same magnetic circuit, the influence of one on the other one is imminent [23], [24]. This kind of calculation can be implemented with good results when the machine operates below the saturation point. As previously explained in Chapter 4, in this case, the d- and q-axis inductances depend only on the current and flux variations of their own axis. The results of this analysis are highlighted in Fig. 4.36. It can be seen that the quadrature inductance is larger than the direct inductance ($L_q > L_d$). The explanation is based on the fact that the q-axis flux has less air in its path than the d-axis flux. This means that the quadrature reluctance is lower than the direct reluctance. By definition, reluctance is the inverse of inductance, therefore, $L_q > L_d$.

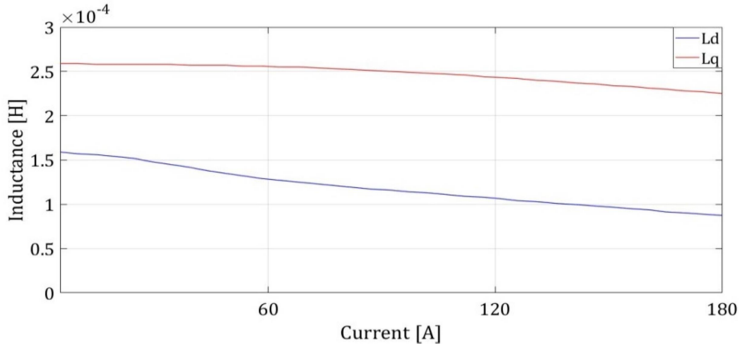

Fig. 4. 36 L_d and L_q when cross-saturation is not considered

If there would be no saturation, the d-axis, respectively q-axis inductances will remain constant, regardless the value of q-, respectively d-axis current.

In order to highlight the cross-saturation effect on L_d, several analysis were performed at different I_q currents, while the direct-axis current varied. The resulting curves are presented in Fig. 4.37. From the figure it can be seen that with the increase of quadrature current, the iron saturates and, as a consequence, the d-axis inductance will decrease.

In addition, for the q-axis, the same procedure was implemented (different values of I_d were applied, while the I_q current was varied) and the results are shown in Fig. 4.38. The interpretation of the results is based on the same observations made in the case of L_d.

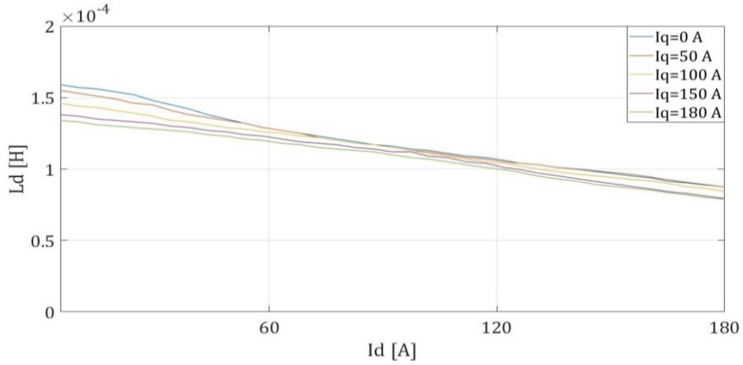

Fig. 4. 37 L_d when cross-saturation is considered

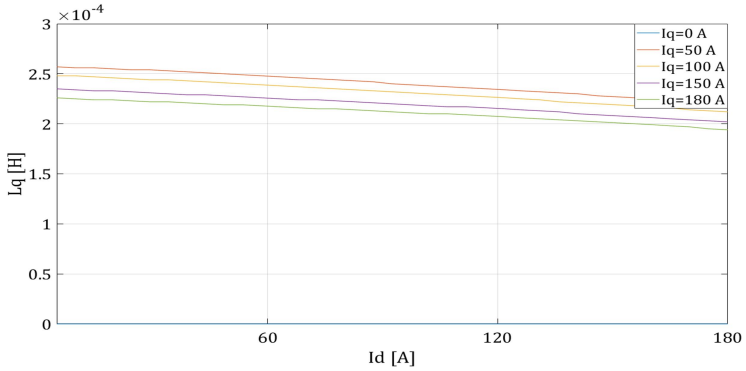

Fig. 4. 38 L_q when cross-saturation is considered

Moreover, to highlight the cross-saturation effect, the d-axis, as well as the q-axis inductances were computed by varying the q-, respectively d-axis currents. The simulations were performed at different d-axis current, respectively q-axis current and the results are presented in Fig. 4.39, for direct inductance, and Fig. 4.40, for quadrature inductance.

As in the previous case, the decreasing of inductance value with the increasing of the current can be observed. Moreover, it can be observed that the cross-saturation effect in the case of L_d is more pronounced than in the case of L_q. This is mainly due to the d-axis flux path.

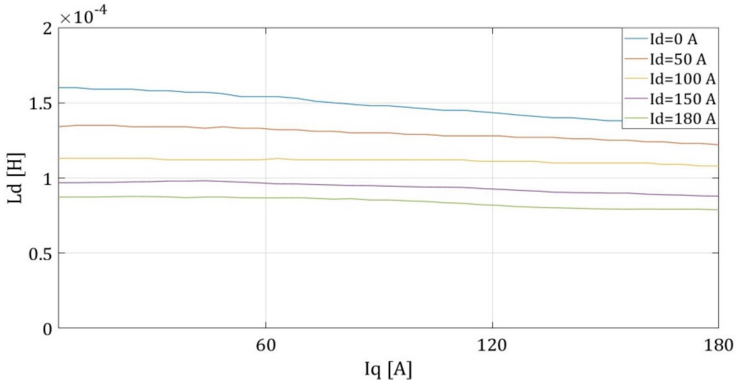

Fig. 4. 39 L_d when cross-saturation is considered

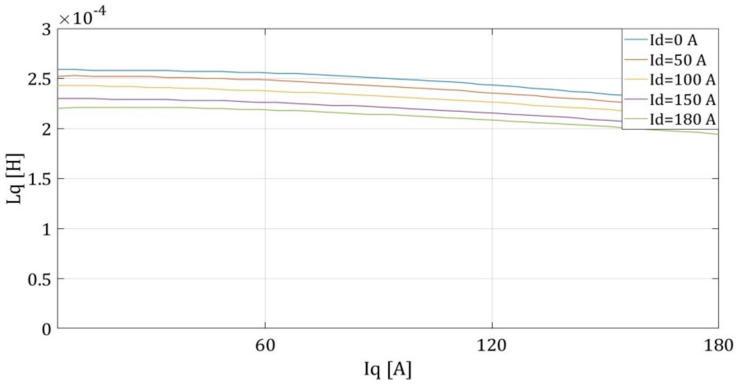

Fig. 4. 40 L_q when cross-saturation is considered

Therefore, in order to obtain an image of the machine under study as accurate as possible, in addition to the d- and q-axis inductances computation when only the direct, respectively the quadrature currents are considered, the parameters should be determined when saturation and cross-saturation phenomena are considered. Thus, the influence of these two phenomena can be fully understood.

In addition, in order to validate the designed model with the requirements, the graph presented in Fig. 4.1 was rebuilt based on the results obtained from the electromagnetic analysis of the machine and shown in the figure below.

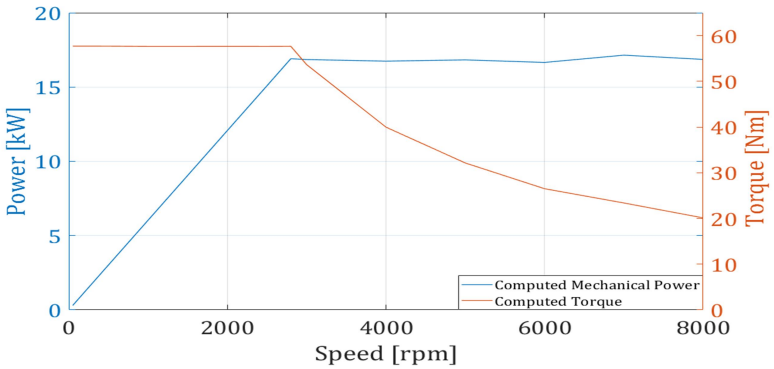

Fig. 4. 41 Computed mechanical power and electromagnetic torque variation vs speed

Comparing the required performances with the computed ones, it can be seen that the designed machine meets the imposed requirements. To highlight the small differences between the required data and computed ones, on Fig. 4.42, the four data sets are superimposed as follows: the required/computed mechanical power, respectively the required/computed torque.

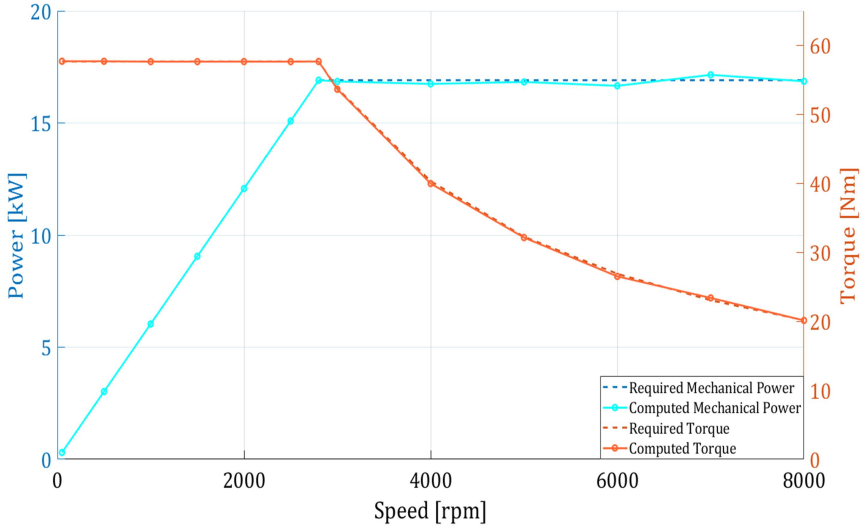

Fig. 4. 42 Required/Computed mechanical power and electromagnetic torque variation vs speed

Regarding the machine's efficiency, Fig. 4.43 shows the efficiency map in the speed range of 0 to 8000 rpm. As it can be seen, at the point of rated operation, the efficiency of the machine is over 91% (91.4%). Moreover, the machine could operate at this efficiency and rated torque, up to a speed of approximately 4000 rpm. It can also be highlighted that, on the curve related to the constant power (Fig.4.44), the machine operates at a favorable efficiency of over 70%, as Fig.4.45 depicts.

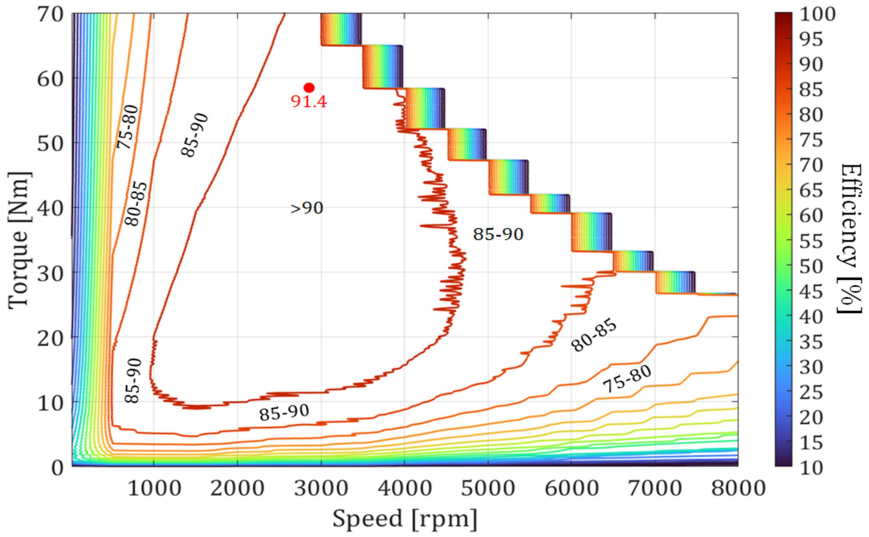

Fig. 4. 43 Efficiency map vs speed

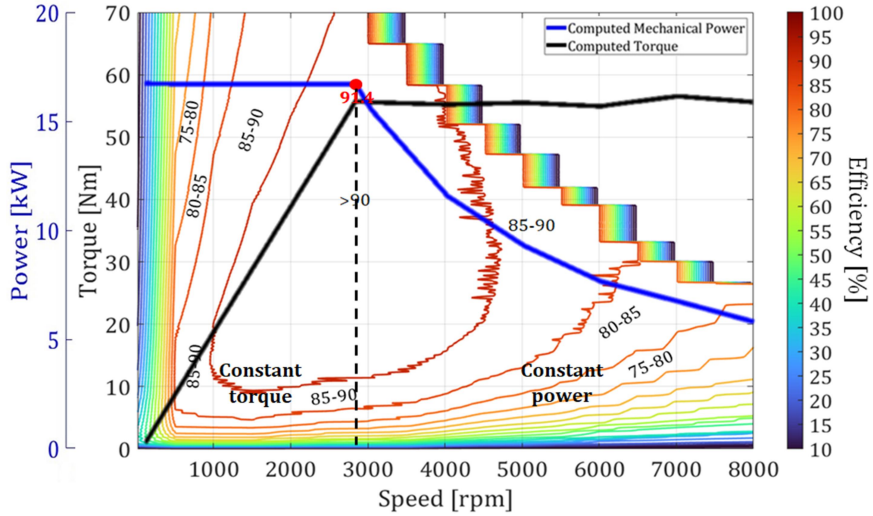

Fig. 4. 44 Efficiency map, computed mechanical power and electromagnetic torque vs speed

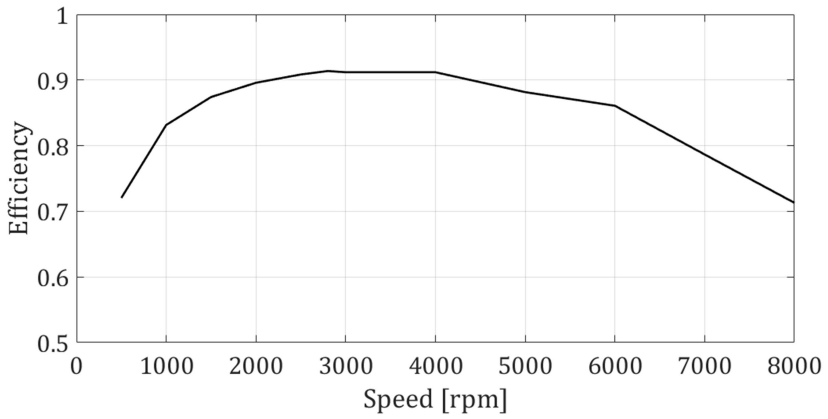

Fig. 4. 45 Efficiency versus speed on the mechanical characteristic

In addition, Fig.4.46 highlights the machine's iron losses, computed in rotor and stator cores. As it can be noticed, the losses increase with the increasing of the machine's speed. Therefore, at rated speed point, the total iron losses are about 350 W.

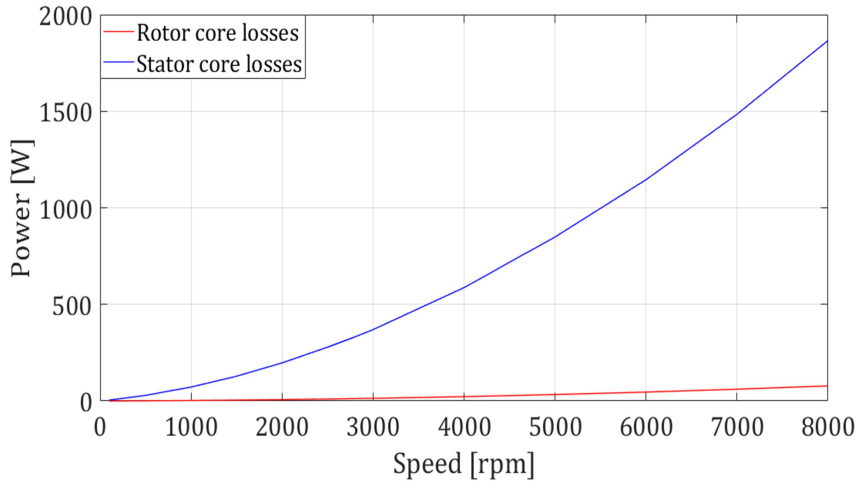

Fig. 4. 46 Iron losses in the machine

In conclusion, by performing all the analyzes previously described, a faithful image of the machine that is the subject of this

thesis was obtained, thus knowing the main parameters and how it behaves in different operating scenarios.

4.6 Thermal analysis

The purpose of electrical machine's thermal analysis is based on increasing its energy efficiency, as well as reducing the costs. As mentioned in Subsection 3.5.2, the thermal analysis can be performed both analytically and numerically.

Therefore, to perform the thermal analysis on the machine that is the subject of this thesis, the FEA method was used through JMAG Designer.

The main thermal characteristics of the materials from which the machine components are made are presented in the table below. It is important to mention that in carrying out the analysis, the main parameter that must be taken into account is the thermal conductivity.

Table 4. 10 Materials thermal properties.

Material	**Thermal conductivity [W/m/°C]**	**Specific heat [J/kg/°C]**
M330-50A (Electrical steel)	23	460
Copper	400	380
N38SH (Sintered NdFeB)	7.6	460

In order to perform the thermal analysis, it is necessary to take into account the machine's losses. This was achieved by including the loss analysis results when defining the simulation conditions related to the heat sources.

In addition, the heat transfer boundary conditions were implemented for each machine's component by taking into account that the machine is cooled with water, and linked to the circuit components. In this regard, the heat transfer coefficient was chosen 1000 $W/m^2/°C$,

considering that the natural convection of water is between 851 and 1703 W/m^2/°C.

Moreover, the heat transfer boundary between stator and gap, respectively rotor and gap was analytical calculated, resulting in 174 W/m^2/°C.

Next, the Contact thermal resistance condition between coils and stator was implemented, as well as between magnets and rotor. This is equal to the maximum value between the thermal conductivities of the considered materials.

Also, the boundary condition was implemented, as well as the initial temperature equal to 20°C. Finally, the machine's motion condition was set, by which the moving parts of the machine, the speed and the initial position of the rotor were defined.

The simulation was run for 3600 s, at rated speed of 2800 rpm and the ambient temperature of 20°C. The results regarding the variation of temperature as function of time, presented in Fig. 4.47 show that the machine does not present any problems from a thermal point of view, as the temperature does not exceed the maximum allowed value.

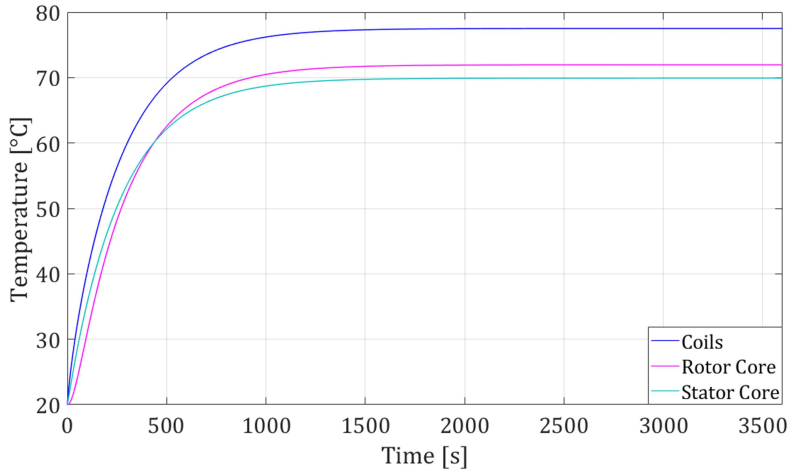

Fig. 4. 47 Temperature variation of the main components of the machine vs time

4.7 Dynamic modelling

In order to complete the analysis of the machine under study, a control strategy will be implemented and tested. In this regard, over the time, different control strategies were developed. The variety of the strategies is due to the fact that a proper control strategy according to the application can considerably improve the drive system performances. Regarding PMSMs, since they are both time-variant and nonlinear, the control strategy is crucial to achieve a high performance drive system, with fast dynamic response and low sensitivity to parameter changes or external factors.

The available control strategies can be broadly divided in two categories, as follows: scalar control and vectorial control.

Scalar control is the simplest control technique and it is based on maintaining the ratio between voltage and frequency, respectively current and frequency constant across the machine's speed range.

It involves the use of an open loop, therefore any feedback from the machine's parameters or the rotor position is not required. Hence the simplicity of this strategy, which is also easy to be implemented with low requirements on the processing capability of the hardware device [25].

However, there are significant drawbacks too. For instance, this strategy has low dynamic performances and, as a consequence, it is mainly used in applications such as pumps or fans. In addition, it may cause the instability of the entire system when the input frequency is too high. To overcome this inconvenience, dumping windings must be included into the rotor, to ensure that it is synchronized with the frequency. Unfortunately, nowadays, due to the fact that they limit a lot from a constructive point of view, most PMSMs are designed without damping windings [26][27].

Fig. 4.48 shows a Simulink model of a scalar control, implemented for a PMSM, from the specialized literature.

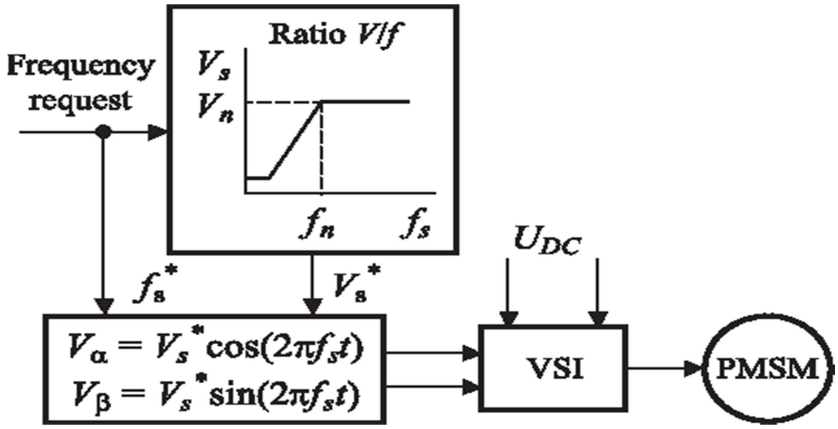

Fig. 4. 48 The scalar control block diagram [28]

The Field Oriented Control (FOC) strategy is an advanced control method that was developed in 1970s.

The idea of developing this strategy started from the simplicity of controlling the DC machine with separate excitation. It is well known that the torque can be expressed as the product between the stator flux and the armature current. In the case of separately excited DC machine these two parameters can be adjusted independently of each other. Moreover, by keeping the stator flux constant, the torque will be influenced only by the variation of the armature current. Thus, in order to obtain a maximum torque, the windings are aligned in such a way that the flux is always orthogonal to the stator current. This assumption is not always valid for AC machines, and, in addition, the flux and the stator current cannot be completely separated. Therefore, the main purpose of FOC strategy is to decouple the flux and the current, so that the torque can be independently controlled. In addition, the produced electromagnetic torque can be controlled to manage the machine's speed, as long as the magnetization is kept at an appropriate level [29][30].

In order to decouple the two previously mentioned parameters, the machine's equations in three-phase reference frame must be

transformed, using Park and Clarke transformations, into the dq reference frame.

Fig. 4.49 shows a literature example of a FOC strategy implementation on a PMSM, using MatLAB Simulink software. As it can be seen, the control is done by comparing the reference speed with the machine's speed. The current controller block compares the estimated current components with the actual input currents and, as a result, the reference values of the supply voltage are obtained. All of these components are expressed in d-q reference frame. Then, the d- and q-axis voltage components are transformed into three-phase reference system before being applied to the machine, using the PWM technique [31].

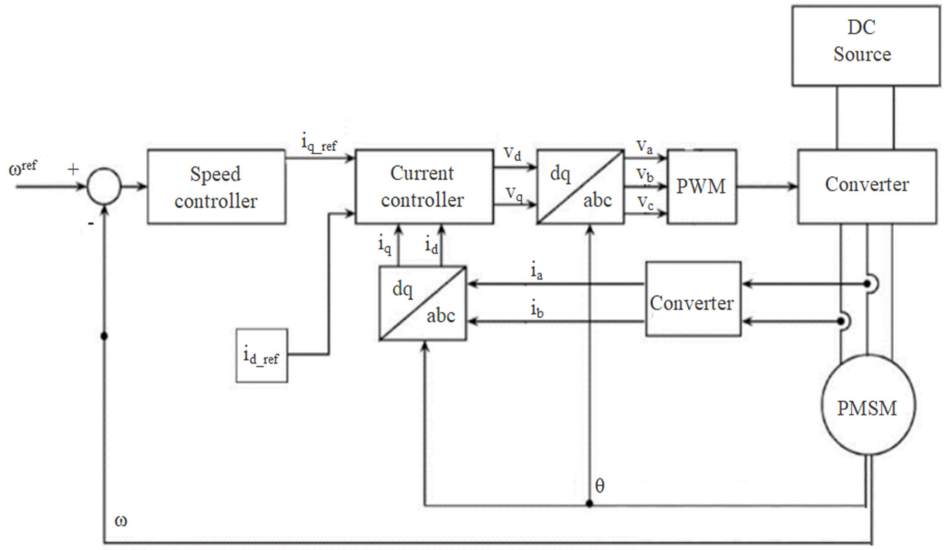

Fig. 4. 49 The FOC strategy block diagram [31]

Regarding the most important advantages of this strategy, the good dynamic response has to be mentioned, as well as the increased efficiency, considering that the torque ripple content can be considerably reduced if the optimal simulation conditions are ensured. On the other hand, among the drawbacks, there is the necessity of using a position sensor, as the rotor position is essential.

In addition, the FOC strategy can be implemented in combination with the Maximum Torque per Ampere (MTPA) strategy, which is, in fact, a current angle control technique that maximizes the electromagnetic torque produced by the machine for a given current, by reducing the machine's copper losses [32].

In order to implement the MTPA control strategy, the machine's torque equation (4.50) should be expressed based on the supply current (i_s).

$$T_e = \frac{3}{2} \cdot p \cdot [\Psi_{PM} \cdot i_q + (L_d - L_q) i_d \cdot i_q] \tag{4.50}$$

Therefore, the d- and q-axis currents can be defined as:

$$i_d = i_s \cdot \cos \alpha \tag{4.51}$$
$$i_q = i_s \cdot \sin \alpha \tag{4.52}$$

where α is the current angle, highlighted in the figure below.

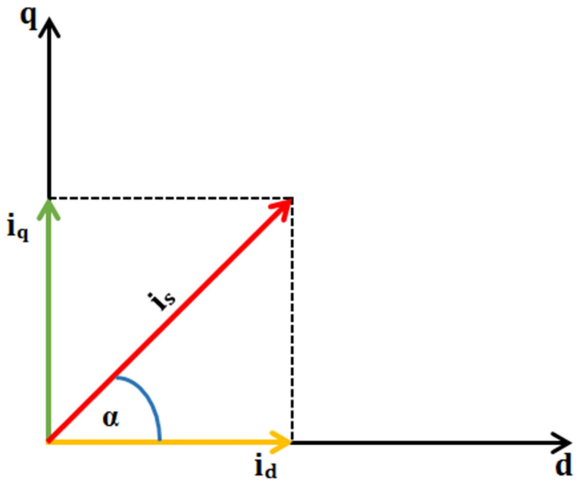

Fig. 4. 50 Stator current components in d-q reference frame

Having the d-, respectively q-axis current components and replacing them in the electromagnetic torque equation it results:

$$T_e = \frac{3}{2} \cdot p \cdot \Psi_{PM} \cdot i_s \cdot \sin\alpha + \frac{3}{4} \cdot p \cdot \left(L_d - L_q\right) \cdot {i_s}^2 \cdot \sin 2\alpha \tag{4.53}$$

$$\frac{T_e}{i_s} = \frac{3}{2} \cdot p \cdot \Psi_{PM} \cdot \sin\alpha + \frac{3}{4} \cdot p \cdot \left(L_d - L_q\right) \cdot i_s \cdot \sin 2\alpha \tag{4.54}$$

Next, the d-axis current component at which the maximum electromagnetic torque is produced can be determined by deriving equation 4.54, considering that the maximum torque value is achieved when $\frac{\partial \frac{T_e}{i_s}}{\partial \alpha} = 0$.

$$\frac{\partial \frac{T_e}{i_s}}{\partial \alpha} = \Psi_{PM} \cdot \cos\alpha + (L_d - L_q) \cdot i_s \cdot (2 \cdot cos^2\alpha - 1) = 0 \tag{4.55}$$

Therefore,

$$\cos\alpha = \frac{-\Psi_{PM} + \sqrt{\Psi_{PM}^2 + 8(L_d - L_q)^2 \cdot i_s^2}}{4(L_d - L_q) \cdot i_s} \tag{4.56}$$

By replacing equation 4.56 in 4.51 and 4.52, the d- and q-axis currents can be determined.

$$i_d = \frac{-\Psi_{PM} + \sqrt{\Psi_{PM}^2 + 8(L_d - L_q)^2 \cdot i_s^2}}{4(L_d - L_q)} \tag{4.57}$$

$$i_q = \sqrt{{i_s}^2 - {i_d}^2} \tag{4.58}$$

Fig. 4.49 highlights a literature example of a FOC strategy implementation combined with MTPA strategy. This is identical to the one shown in Fig. 4.51, except that, in this case, the instantaneous values of d-axis and q-axis reference currents are calculated in the MTPA block. In this regard, the electromagnetic torque is maximized.

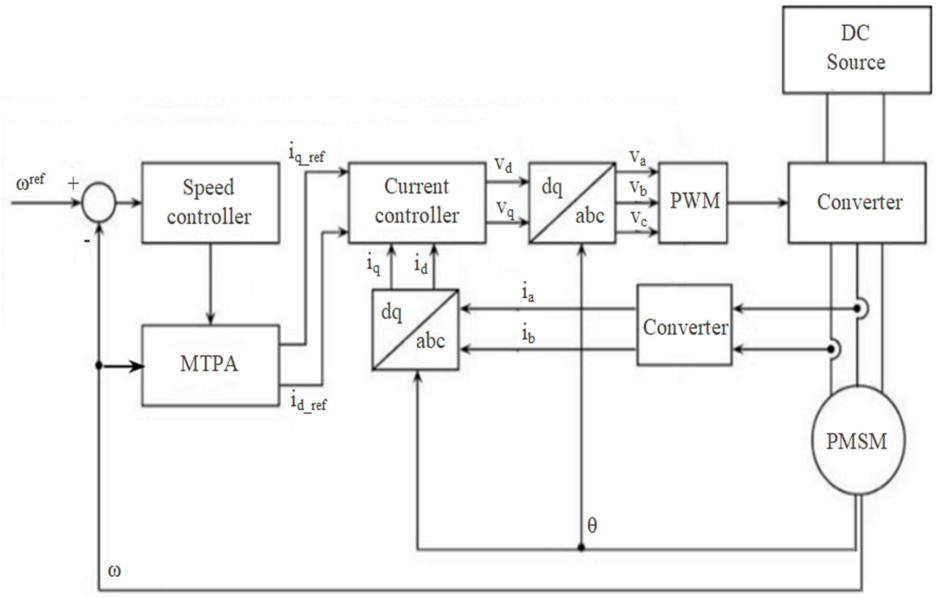

Fig. 4. 51 The FOC strategy block diagram with MTPA [31]

4.6.1. Simulation results

In order to validate the IPMSM model, the MatLAB Simulink software was used. The FOC strategy implemented is based on the available model from the MatLAB library and adapted for the machine under test. This method was chosen due to its simplicity and good accuracy.

In addition, for better performances, the MTPA strategy was introduced too.

The validation of the machine consists in the development of four operating scenarios as follows:

- starting the machine in no load operation mode and operating it at rated speed;
- starting the machine in rated load operation mode and operating it at rated speed;
- starting the machine in rated load operation mode and varying its speed;
- acceleration up to the maximum speed and rated load.

4.6.2.1 No load operation

The IPMSM was firstly tested for no load operation, at rated speed of 2800 rpm. As it can be noticed in the figure below, the machine reaches the rated speed in 0.15 seconds. Also, at that moment it can be seen that the machine reaches the static operation regime. The impact of acceleration can be observed in the case of currents and electromotive force.

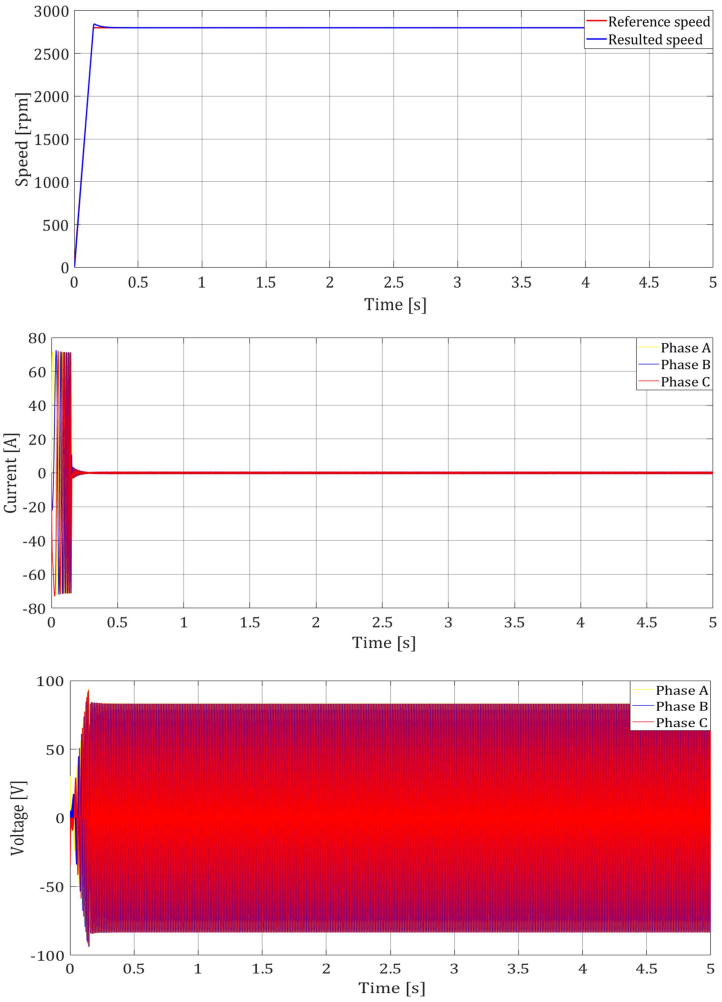

Fig. 4. 52 No load operation

4.6.2.2 Rated load operation

In the case of rated load operation, the machine was tested at rated speed of 2800 rpm and rated torque of 58 Nm. As it can be seen in Fig. 4.53, both speed and torque closely follow the imposed references, therefore, it can be concluded that the machine operates as expected.

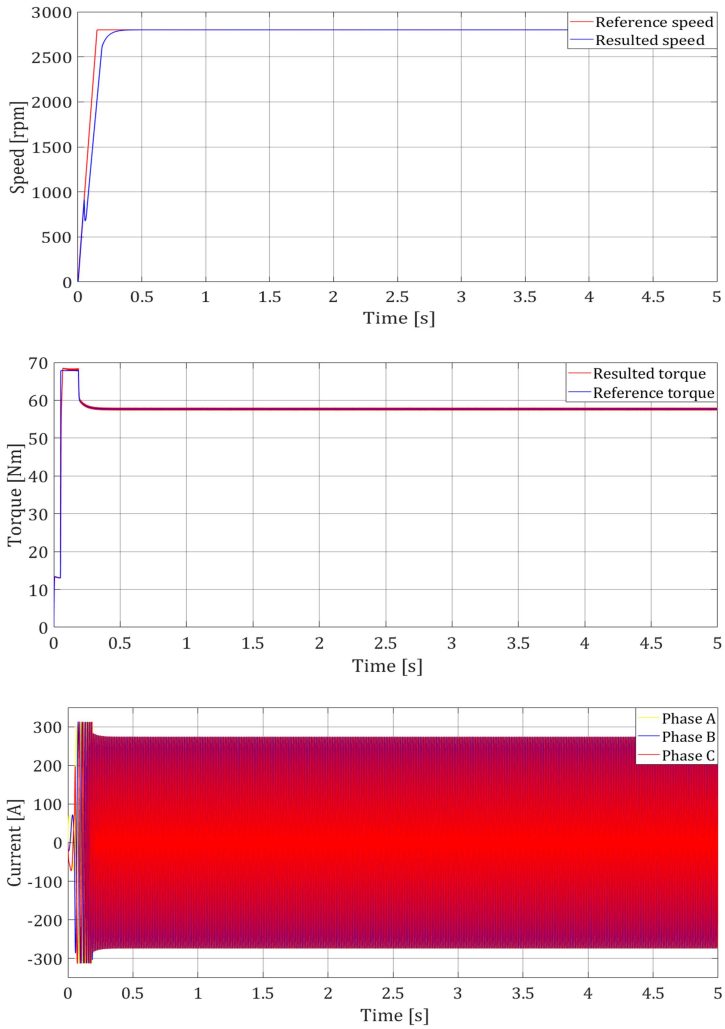

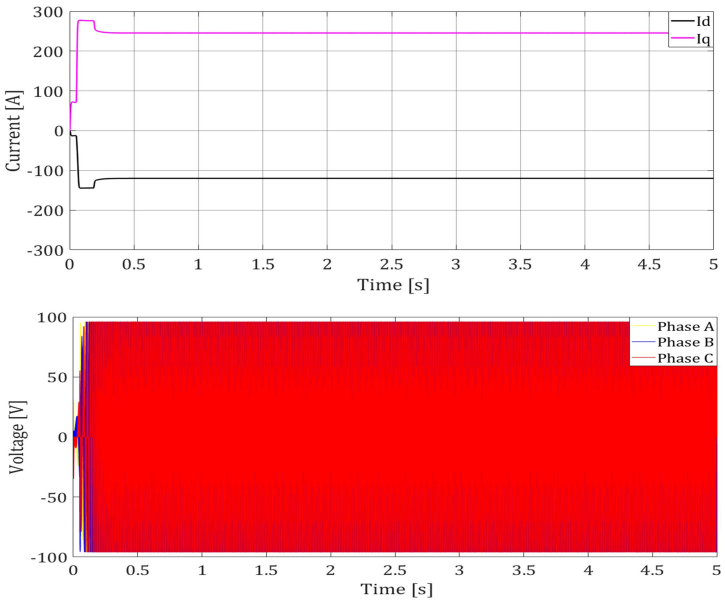

Fig. 4. 53 Rated load operation

4.6.2.3 Rated load and variable speed operation

For this simulation, the speed was increased in steps up to the rated speed of 2800 rpm, while the torque was kept constant at the rated value of 58 Nm. This simulation was performed by implementing the MTPA technique. As it can be noticed in the figure below, the machine operates as intended since it adheres both to the speed and torque profiles. The fluctuations observed in the case of torque and currents are due to the accelerations.

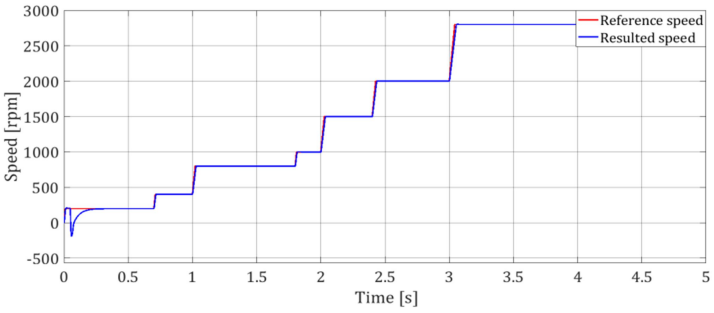

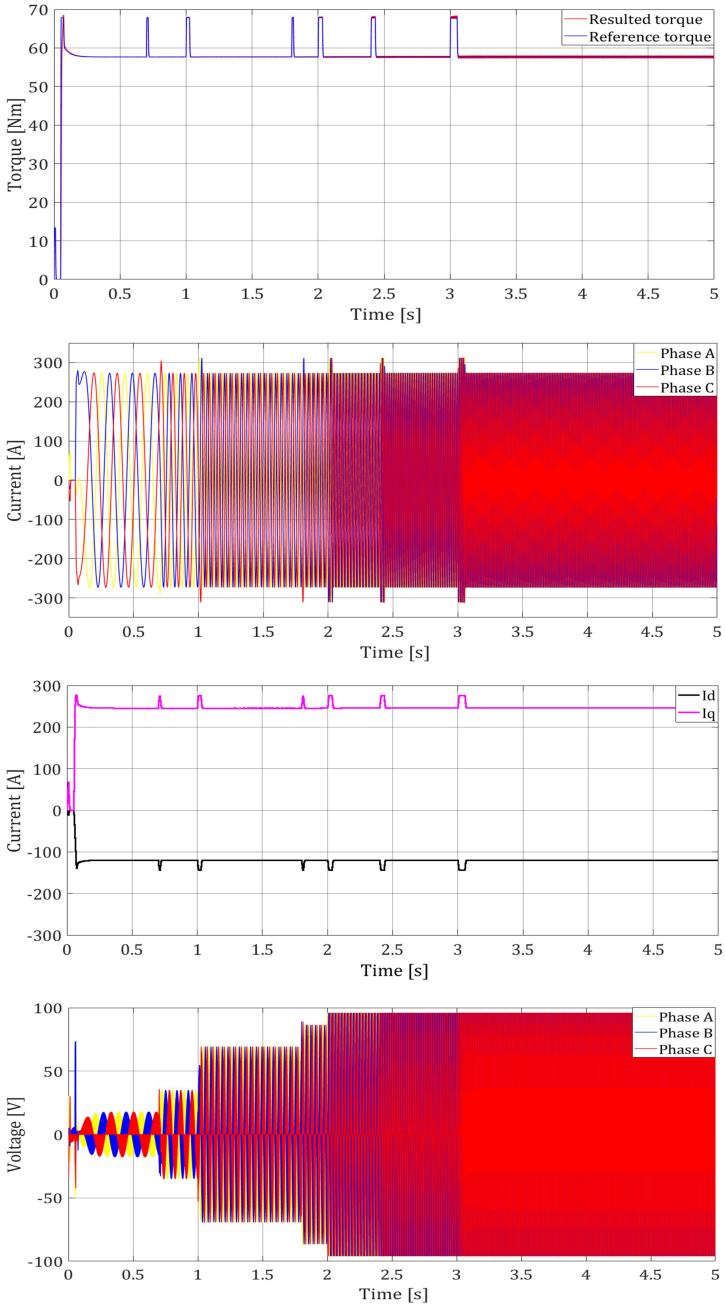

Fig. 4. 54 Rated load and variable speed operation

4.6.2.4 Acceleration up to the maximum speed and rated load operation

This simulation scenario aims to validate the machine's flux weakening operation regime. In this regard, a speed ramp starting from 0 rpm to 7500 rpm was implemented, while the imposed torque was 58 Nm. As it can be observed in the figure below, the torque is kept constant at the imposed value of 58 Nm until the machine reaches the rated speed of 2800 rpm. As the speed increases above the rated value, the torque decreases in order to maintain the mechanical power constant.

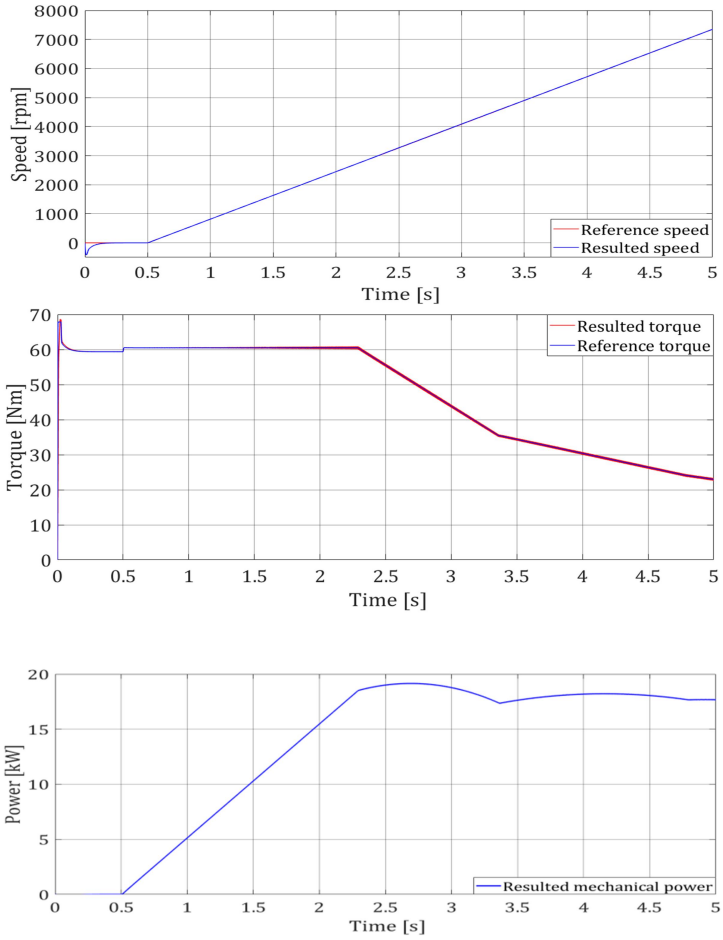

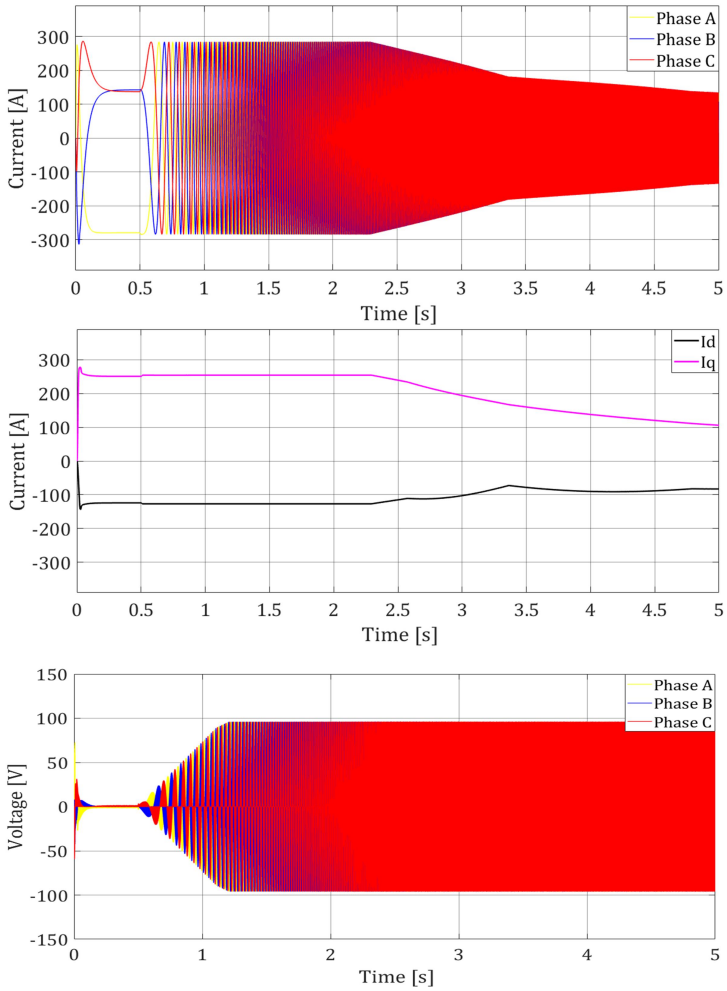

Fig. 4. 55 Acceleration up to the maximum speed

Therefore, upon all the results previously illustrated, it can be concluded that the machine operates as intended since it adheres to imposed scenarios, both in no load and rated load operation.

References

[1] Boran Pikula, Elmedin Mesic, Elmedin Mesic, M. Hodzic „Determination of air drag coefficient of vehicle models”,

Conference: International Congress Motor Vehicles & Motors 2008 - MVM 2008, „Sustainable Development of Automotive Industry“.

[2] Vasilis Pagonis, David Guerra, Sean Chauduri, Brian Hornbecker, Nathan Smith: “Effects of air resistance”, Western Maryland College, Physics Department, Westminster, MD 21157.

[3] **Bilatiu, Cristina** & Moldovan, Tudor & Martis, Claudia-Steluta. (2022). Electromagnetic Analysis and Experimental Validation of an IPMSM. 234-238. 10.1109/EPE56121.2022.9959809.

[4] I. Cioc, N. Bichir, N. Cristea, Maşini electrice. Îndrumar de proiectare vol. 2. Craiova (Romania): Editura Scrisul Românesc, 1981.

[5] S. Huang, J. Luo, F. Leonardi, T.A. Lipo, "A general approach to sizing and power density equations for comparison of electrical machines," *IEEE Transactions on Industry Applications,* vol. 34, no. 1, pp. 92-97, 1998.

[6] I. Boldea, S.A. Nasar, The Induction Machines Design Handbook. Boca Raton (USA): CRC Press, 2018.

[7] Oduyemi, Olufolahan & Chibueze, Kingsley. (2020). Imperatives of Air-Gap Length on the Performance of Electromechanical Devices/Machines. 15-23. 10.9790/1676-1503021523.

[8] Bilatiu, Cristina & Karaisas, Petros & Martis, Claudia-Steluta. (2021). Electromagnetic Analysis and Experimental Validation of an Interior Permanent Magnet Synchronous Motor. 1-6. 10.1109/ATEE52255.2021.9425229.

[9] J.F. Gieras, Permanent Magnet Motor Technology: Design and Applications. New York (USA): Marcel Dekker, 2009.

[10] Szewczyk, K. & Golisz, R. & Walasek, Tomasz & Kucharczyk, Z.. (2011). The influence of an air gap around the permanent magnets with the flux concentrator in Permanent Magnet Synchronous Motor with Internal Magnetic Circuits. 87. 181-183.

[11] R. Măgureanu, N. Vasile, Motoare sincrone cu magneţi permenenţi şi reluctanţă variabilă. Bucureşti (Romania): Editura Tehnică, 1982.

[12] V.B. Honsinger, "Sizing equations for electrical machinery," IEEE Transactions on Energy Conversion, vol. EC-2, no. 1, pp. 116-121, 1987.

[13] F. Ghita, R. Marţiş, F. Pop Pigleşan, C. Marţiş, B. Vărăticeanu, P. Minciunescu, "Soft magnetic composites in the design of permanent magnet synchronous actuators," in Procedings of the International Conference and Exposition on Electrical and Power Engineering (EPE '2018), Iaşi (Romania), 2018, pp. 97-102.

[14] Farnia, David & Hu, Dakai. (2016). Design through simulation of an interior permanent magnet machine and controller. 1-85. 10.1109/ITEC.2016.7520177.

[15] **Bilatiu, Cristina** & Karaisas, Petros & Martis, Claudia-Steluta. (2021). Electromagnetic Analysis and Experimental Validation of an Interior Permanent Magnet Synchronous Motor. 1-6. 10.1109/ATEE52255.2021.9425229.

[16] Bassel Aslan, Eric Semail, Julien Korecki, Jer^ome Legranger. Slot/pole Combinations Choice for Concentrated Multiphase Machines dedicated to Mild-Hybrid Applications. IECON'11, IEEE International Conference On Industrial Applications of Electronics,, Nov 2011, Australia. IEEE, pp.3698-3703, 2011

[17] Hsiao, Chun-Yu & Yeh, Sheng-Nian & Hwang, Jonq-Chin. (2011). A Novel Cogging Torque Simulation Method for Permanent-Magnet Synchronous Machines. Energies. 4. 10.3390/en4122166.

[18] Sun, J.; Ren, J.; Le, Y.; Wang, H. Analysis of Air-Gap Magnetic Field and Structure Optimization Design of Hollow-Cup Motor. *Aerospace* 2022, *9*,549. https://doi.org/10.3390/aerospace9100549.

[19] Zaghdoud, Bellal. (2013). Calculation and evaluation of the magnetic field air gap in permanent magnet synchronous machine.

[20] Dajun, Tao & Liang, & Fei, & Qingpeng, & Jianxiao, & Yutian, & Jibin,. (2020). Magnetic Field Characteristics and Stator Core Losses of High-Speed Permanent Magnet Synchronous Motors. Energies. 13. 535. 10.3390/en13030535.

[21] Wang, Weiye & Ma, Hui & Qiu, Xin & Jianfei, Yang. (2019). A Calculation Method for the On-Load Cogging Torque of Permanent Magnet Synchronous Machine. IEEE Access. PP. 1-1. 10.1109/ACCESS.2019.2929429.

[22] W. Zhao, T. Lipo, and B. Kwon, "Optimal design of a novel asymmetrical rotor structure to obtain torque and efficiency improvement in surface inset pm motors," IEEE Transactions on Magnetics, vol. 51, no. 3, pp. 1-4, March 2015.

[23] Nasui-Zah, Ioana & Nicorici, Andreea-Madalina & Martis, Claudia. (2018). Saturation and cross-saturation in synchronous reluctance machines. 0347-0351. 10.1109/ICEPE.2018.8559766.

[24] Meessen, Koen & Thelin, P. & Soulard, Juliette & Lomonova, E.A.. (2008). Inductance Calculations of Permanent-Magnet Synchronous Machines Including Flux Change and Self- and Cross-Saturations. Magnetics, IEEE Transactions on. 44. 2324 - 2331. 10.1109/TMAG.2008.2001419.

[25] X. Cai, Z. Zhang, J. Wang, R. Kennel, "Optimal control solutions for PMSM drives: a comparison study with experimental assessments," IEEE Journal of Emerging and Selected Topics in Power Electronics, vol. 6, no. 1, pp. 352-362, 2017.

[26] F. Patel, J. Ahir, P. Patel, "Control theory for permanent magnet synchronous motor – A review," Asian Journal For Convergence In Technology (AJCT), vol. 5, no. 1, 2019.

[27] I.C. Proimadis, D.V. Spyropoulos, E.D. Mitronikas, "An alternative for all-electric ships applications: the synchronous reluctance motor," Advances in Power Electronics, vol. 2013, paper #862734, 2013.

[28] Stulrajter, Marek et al. “PERMANENT MAGNETS SYNCHRONOUS MOTOR CONTROL THEORY.” (2007).

[29] B.K. Bose, "The past, present, and future of power electronics," IEEE Industrial Electronics Magazine, vol. 3, no. 2, pp. 7-14, 2009.

[30] I. Boldea, N. Muntean, S.A. Nasar, "Robust low-cost implementation of vector control for reluctance synchronous machines," IEE Proceedings-Electric Power Applications, vol. 141, no. 1, pp. 1-6, 1994.

[31] A. Purwadi, R. Hutahaean, A. Rizqiawan, N. Heryana, N. A. Heryanto and H. Hindersah, "Comparison of maximum torque per Ampere and Constant Torque Angle control for 30kw Interior Interior Permanent Magnet Synchronous Motor," Proceedings of the Joint International Conference on Electric Vehicular Technology and Industrial, Mechanical, Electrical and Chemical Engineering (ICEVT & IMECE), Surakarta, 2015, pp. 253-257.

[32] Caruso, Massimo & Di Tommaso, Antonino & Spataro, C. & Nevoloso, Claudio & Miceli, Rosario & Trapanese, Marco. (2019). Maximum Torque per Ampere Control Strategy for Low-Saliency Ratio IPMSMs. International Journal of Renewable Energy Research. 9. 374-383.

5. Laboratory Testing

5.1 Introduction

The present chapter deals with the experimental validation of the machine under test. In this regard, the test bench on which the machine is mounted is presented. Next, the main electrical parameters of the machine are measured and compared with the theoretical ones. Further, the machine's behaviour is tested on the test bench, for different operating scenarios. All the results are presented and analysed in this chapter.

5.2 The test bench

The IPMSM was built by ICPE București, based on the data obtained from the previously presented calculations and simulations. The two figures below highlight the machine's stator core and the winding distribution, respectively the rotor core.

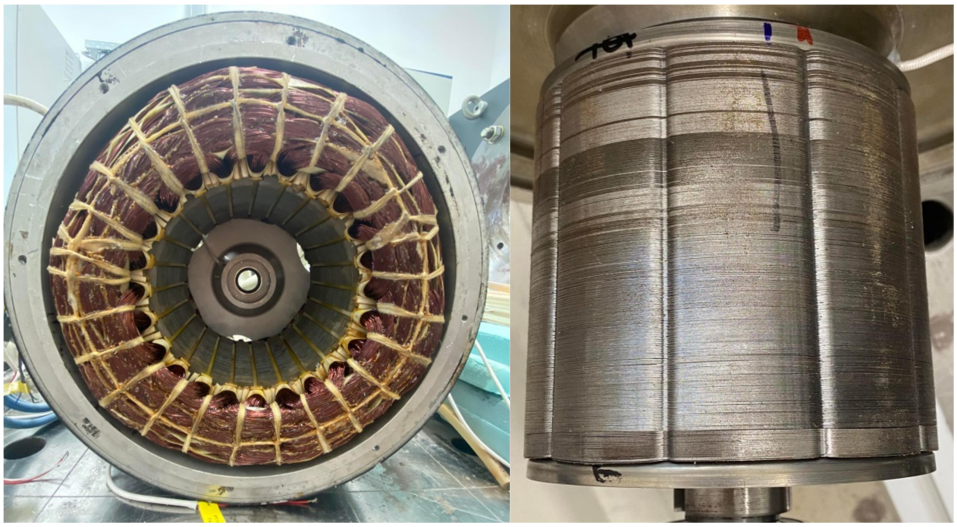

a b

Fig.5. 1 IPMSM prototype a. stator core and winding, b. rotor core

The experimental validation of the IPMSM under test was carried out through hardware-in-the-loop (HiL) simulation testing [1][2][3]. This method was chosen especially because it allows a quick prototyping of the system to be tested, given the fact that the models designed in MatLAB Simulink, for instance, or any other embedded software, can be loaded on the processing unit (in this case, dSpace MicroLab Box). In this way, real time read/write operations can be performed on the inputs and outputs of the processing unit.

Fig. 5.2 highlights the main components of the testing set-up. These include, the 3-phase IPMSM to be tested, an inverter that supplies the necessary AC voltage, the power supply that feeds the inverter, an induction machine used as load, as well as the power supply that feeds the load.

The induction machine that serves as load is controlled using the dSpace processing unit, in order to be able to impose the desired load torque.

In addition, in order to determine the currents, torque and speed of the machine under test, current/torque sensors, respectively an encoder were used. They communicate the collected information to the processing unit.

Regarding the processing unit, as previously mentioned, the dSpace MicroLab Box was used, on which the Permanent Magnet Synchronous Machine control strategy was loaded. MicroLab Box is an all-in-one tool that combines a large number of input/output ports, a high-performance processor, and an FPGA into a single device, to provide users with a complete tool for real-time control applications. The device is equipped with a four cores Intel processor that ensure high performances in terms of computing, while the integrated FPGA that can be programmed in MatLAB Simulink offers high capabilities in terms of signal processing.

For the user interface, ControlDesk software was chosen due to the advantages it offers in terms of data accessibility.

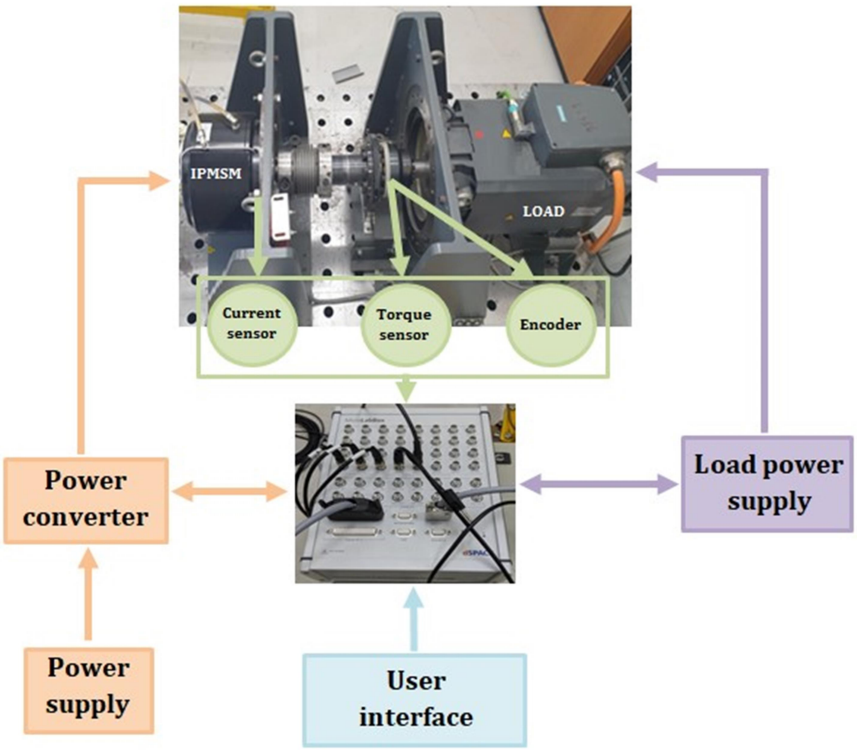

Fig.5. 2 Experimental set-up diagram for IPMSM testing

5.3 L_d, L_q measurement

In order to validate the machine, the d-axis, respectively q-axis inductances should be firstly measured.

The method by which the inductivities were measured is based on machine's circuit time constant (τ) [4].

$$\tau = \frac{L}{R} \tag{5.1}$$

Knowing that:

$$L_d = \frac{2}{3}L, \text{ when d-axis is aligned with phase A} \tag{5.2}$$

$$L_q = \frac{2}{3}L, \text{ when q-axis is aligned with phase A} \tag{5.3}$$

the d-, and q-axis components can be determined using:

$$L_d = \frac{2}{3}\tau R, \text{ when d-axis is aligned with phase A} \quad (5.4)$$

$$L_q = \frac{2}{3}\tau R, \text{ when q-axis is aligned with phase A} \quad (5.5)$$

The circuit time constant can be defined as the time interval from the voltage step start until the winding's current reaches 63.2% of its final value [5]. Therefore, the circuit time constant can be determined by monitoring the winding's current until its value is stabilized and computing the time until 63.2% of its total value is reached.

To compute the inductance on d-axis, the circuit highlighted in Fig. 5.3 must be implemented. Firstly, the phase A is connected to the positive potential of the source, while B, respectively C phases are connected to the negative potential of the source. Now, the machine's rotor is aligned with phase A and the machine is supplied with a low voltage. Next, the rotor shaft must be locked, phase A must be linked to the negative terminal, while phases B and C must be linked to the positive terminal (see Fig. 5.3 b).

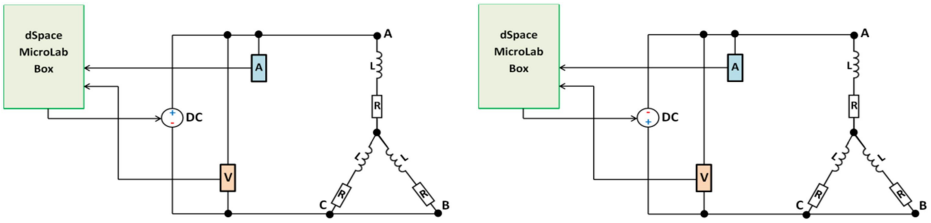

(a) (b)

Fig.5. 3 d-axis circuit (a) positive supply, (b) negative supply

Several tests were carried out at different DC voltage levels, starting with 0.2 V, up to 6 V, increasing the voltage with 0.2 V/test. Thus, the current was monitored, and for each case the time until the current reaches 63.2% of its final value was determined, therefore the circuit time constant for d-axis is known.

In order to determine the q-axis inductance, the same principle was applied, with the main difference that, in this case, the rotor was aligned with the q-axis. The circuit used for this situation is presented in Fig. 5.4. Now, the phase B is connected to the positive potential of the DC source, while phase C to the negative one. As it can be noticed in Fig. 5.3 a, phase A is floating. The rotor shaft must be locked when the rotor is aligned with the q-axis, phase A should be connected to the positive potential, while phases B and C must be linked to the negative terminal (see Fig. 5.4 b). Next, the same tests as in the previous case are carried out, in order to determine the circuit time constant for q-axis.

The measurements at higher voltages aim to determine how the saturation and cross-saturation phenomena influence the machine's inductances.

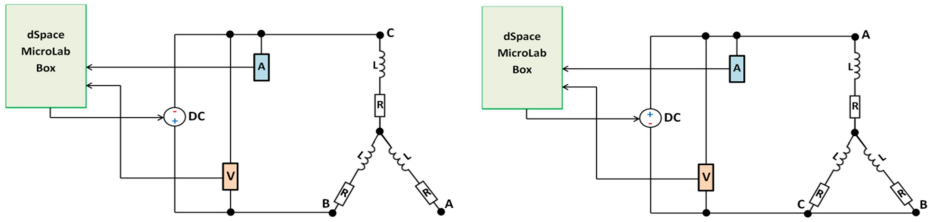

(a) (b)

Fig.5. 4 q-axis circuit (a) positive supply, (b) negative supply

Fig. 5.5 shows the measured d-, and q-axis inductances versus current, compared with the computed values. The differences between the measured and simulated values can be observed especially in the case of direct axis inductance, at higher currents. The measured d-axis inductance is higher than the computed one, and it is almost constant. Regarding the q-axis inductance, the differences between the measured and simulated values are small, and the measured values are lower than the computed ones.

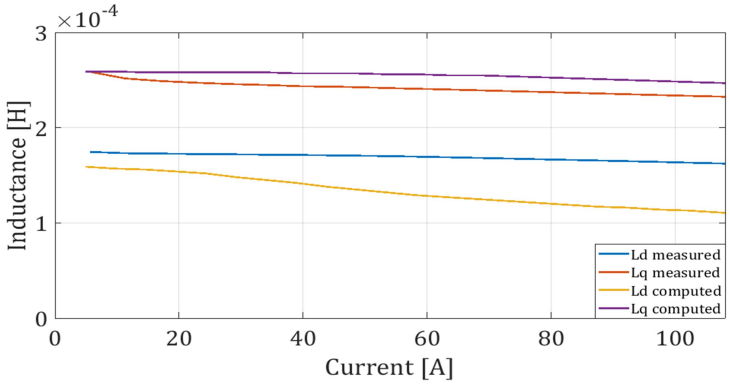

Fig.5. 5 Measured and computed d-, and q-axis inductances vs current

It can be noticed that the measured values for Lq are closer to the computed ones, while for measured Ld the values are decreasing more with the increasing of the phase current compared to the computed ones. This is due to the manufacturing tolerances. The current values went up to 60% of the current rated value, in order to avoid the demagnetization of the permanent magnets.

5.4 Testing the machine at no load operation

Firstly, the no load operation of the machine was tested. In this regard, the IPMSM was tested at different speeds (250 rpm, 500 rpm, 1500 rpm, 1733 rpm, and 2000 rpm) and the results were compared with the simulated results.

Next, the most significant results obtained at the previously mentioned speed values are given. In all the cases the plots versus time of the measured/simulated speed, phase currents, measured/simulated direct and quadrature currents, and measured induced electromotive force are depicted.

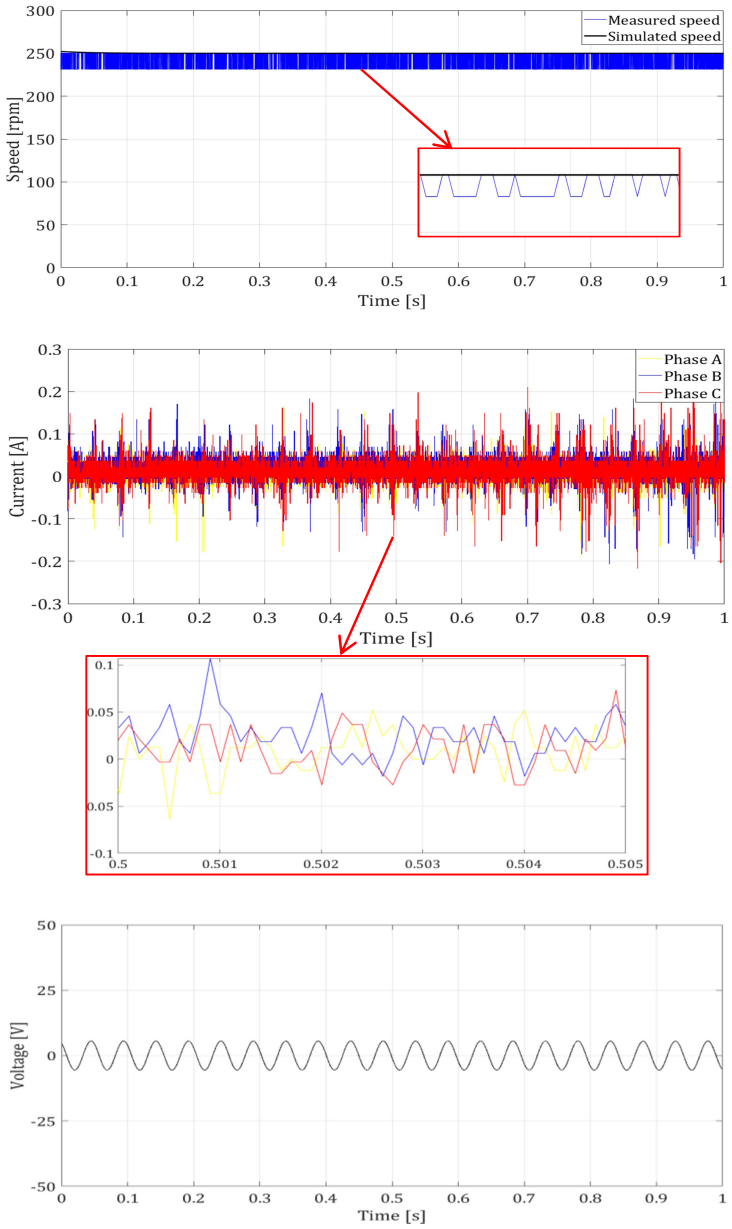

Fig.5. 6 No load operation – 250 rpm

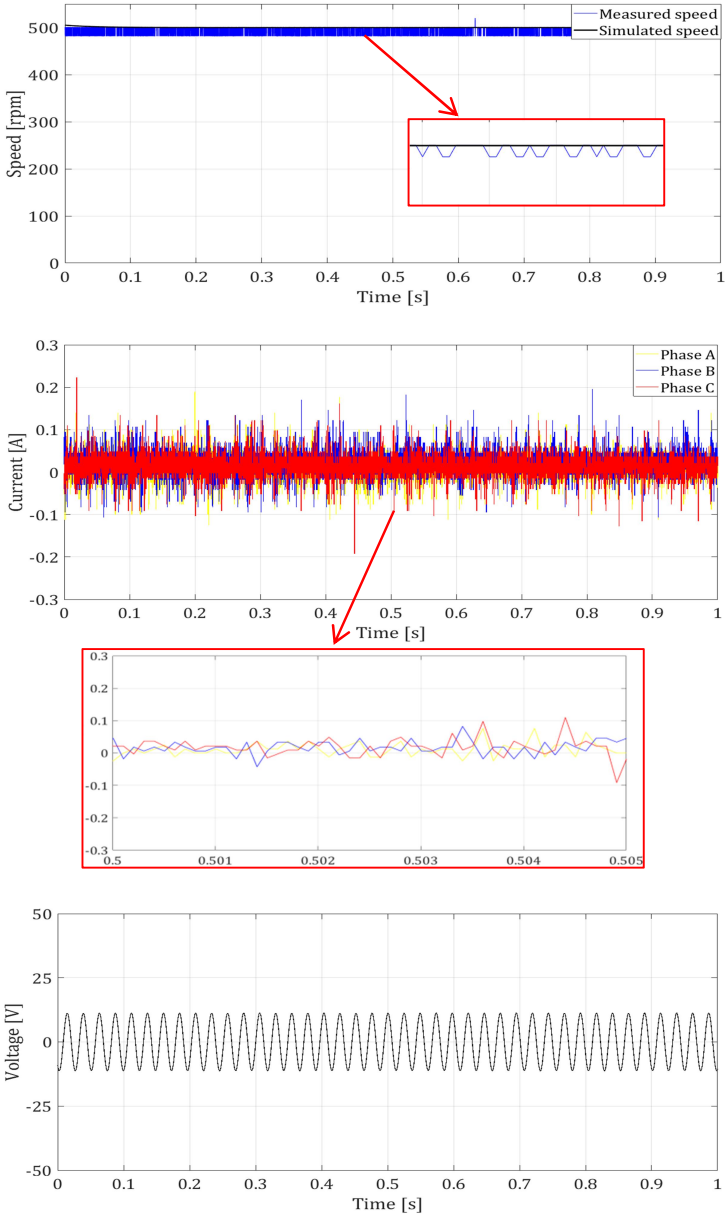

Fig.5. 7 No load operation – 500 rpm

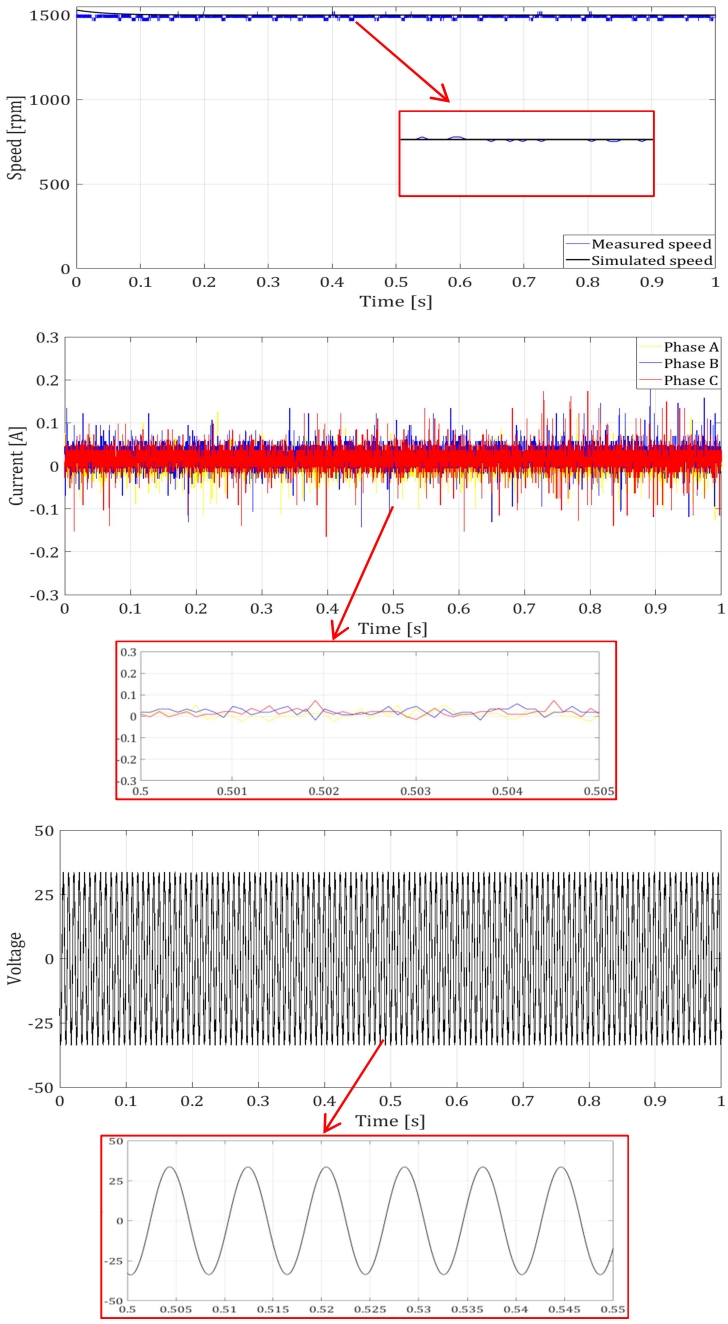

Fig.5. 8 No load operation – 1500 rpm

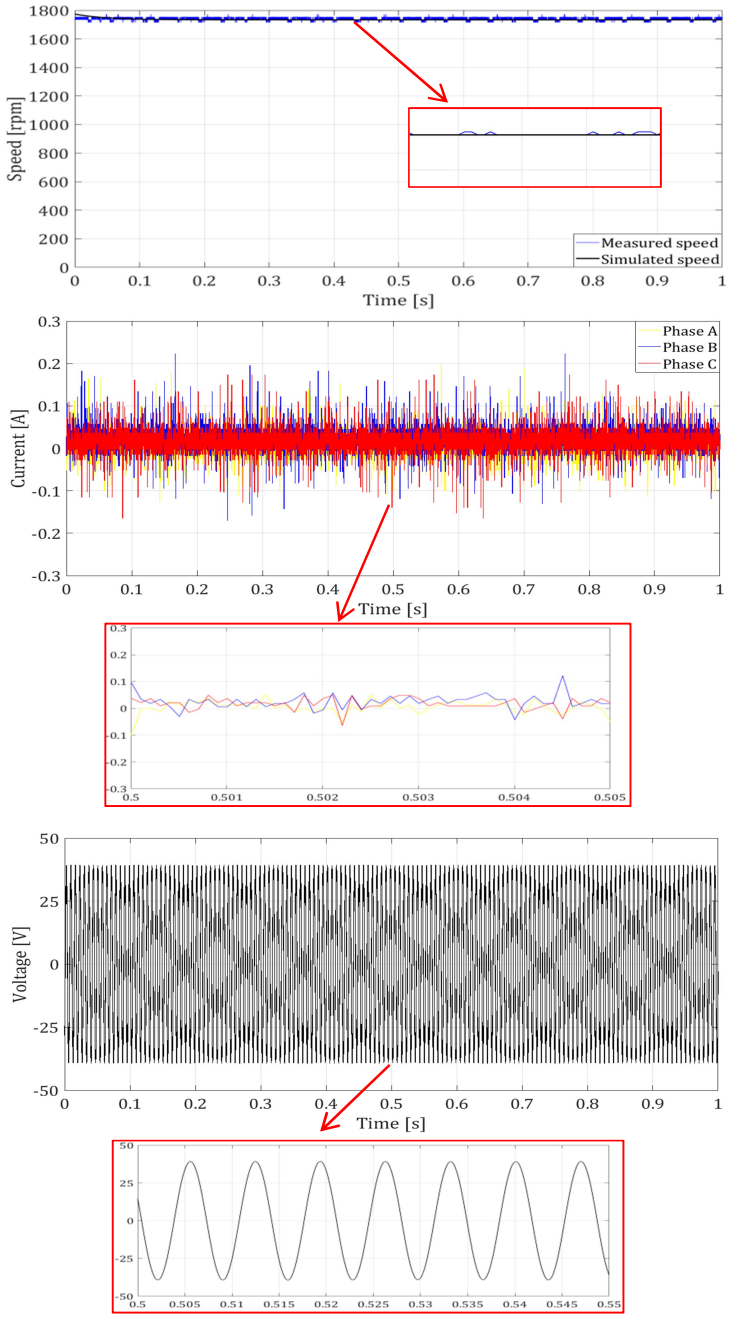

Fig.5. 9 No load operation – 1733 rpm

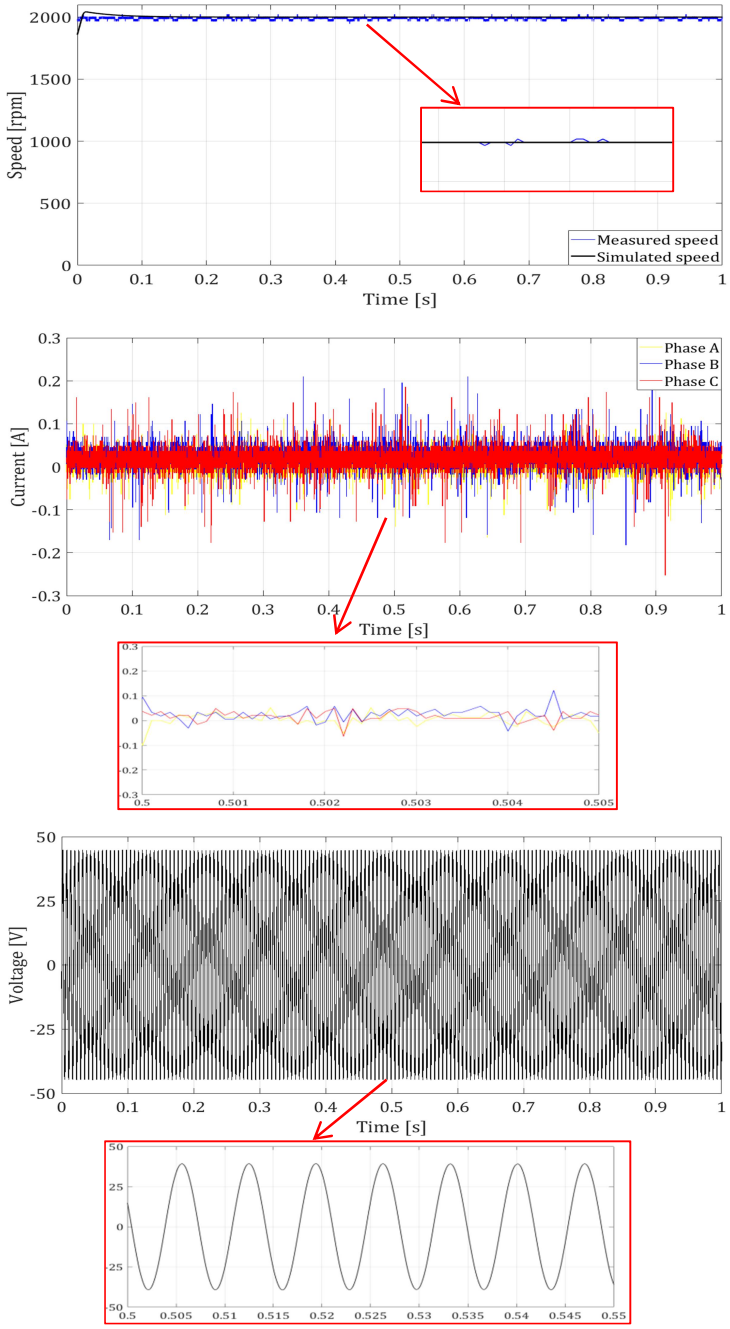

Fig.5. 10 No load operation – 2000 rpm

Table 5. 1 The RMS values of the measured vs. simulated phase current and voltage.

	250 [rpm]	**500 [rpm]**	**1500 [rpm]**	**1733 [rpm]**	**2000 [rpm]**
$I_{RMS\_measured}$ [A]	0.0253	0.0225	0.219	0.0243	0.0231
$I_{RMS\_simulated}$ [A]	0.05	0.097	0.21	0.21	0.24
$U_{RMS\_measured}$ [V]	3.93	7.93	23.87	27.84	31.77
$U_{RMS\_simulated}$ [V]	2.96	5.81	21.63	26.98	31.59

5.5 Testing the machine at constant torque and variable speed

In order to perform this test, the machine's torque was kept constant, at 30Nm, while the speed was varied in steps, from 800 rpm to 2800 rpm. In the figures below it can be seen that the IPMSM operates as expected, the results being comparable to those obtained in simulations.

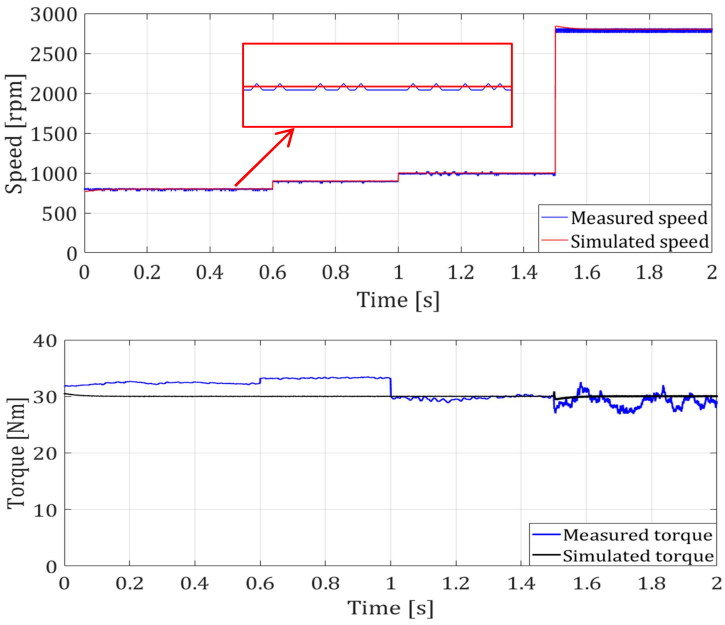

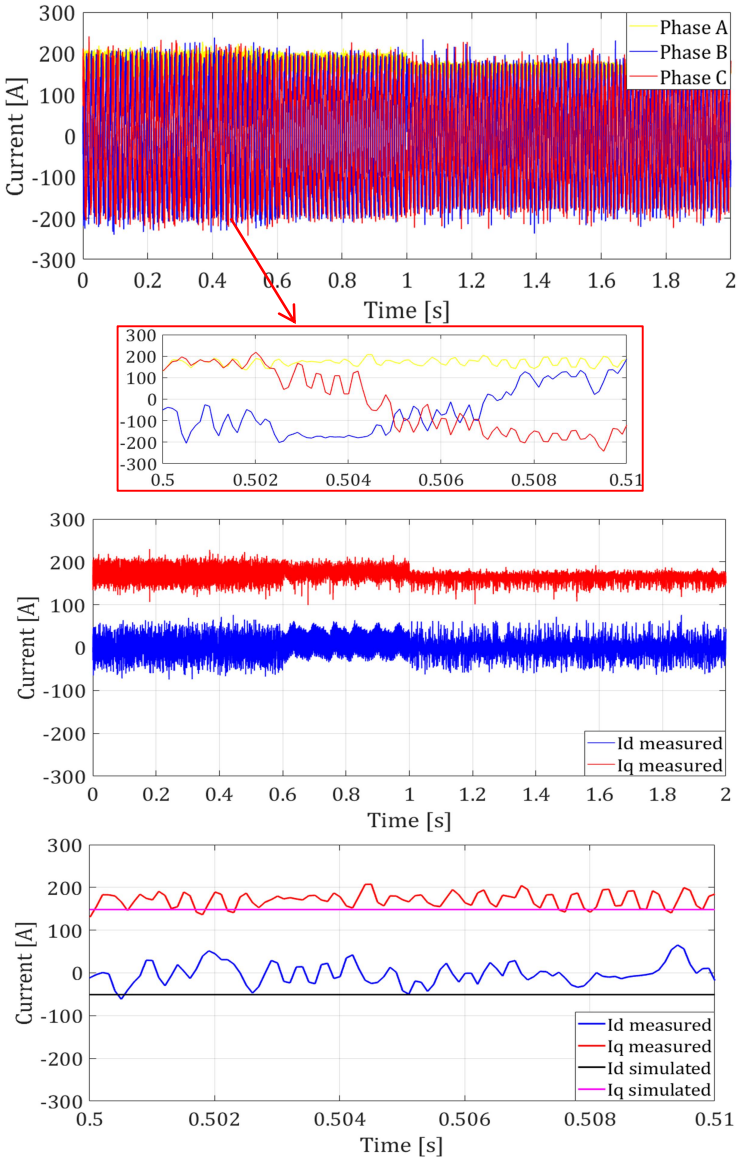

Fig.5. 11 Constant torque operation

5.6 Testing the machine at constant speed and variable torque

The following measurement was carried out with the machine operating at speed of 490 rpm, while the torque was varied in three steps, at 7.94 Nm, 12.49 Nm, and 14.33 Nm, respectively.

The following figures depict the most important results extracted from the performed measurement. As it can be noticed, the measured results correspond to the simulated values, the machine under test closely respecting the given profile.

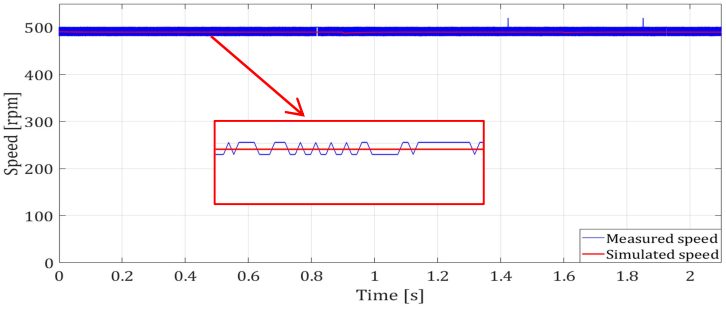

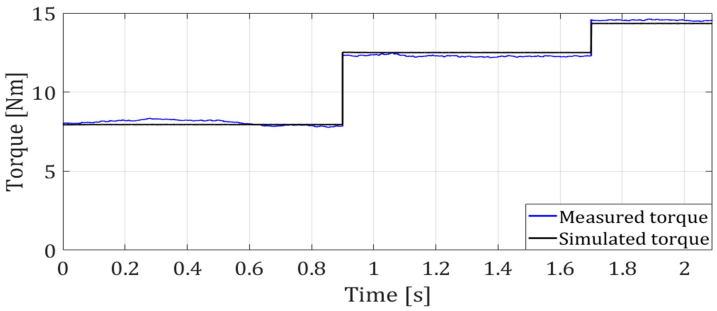

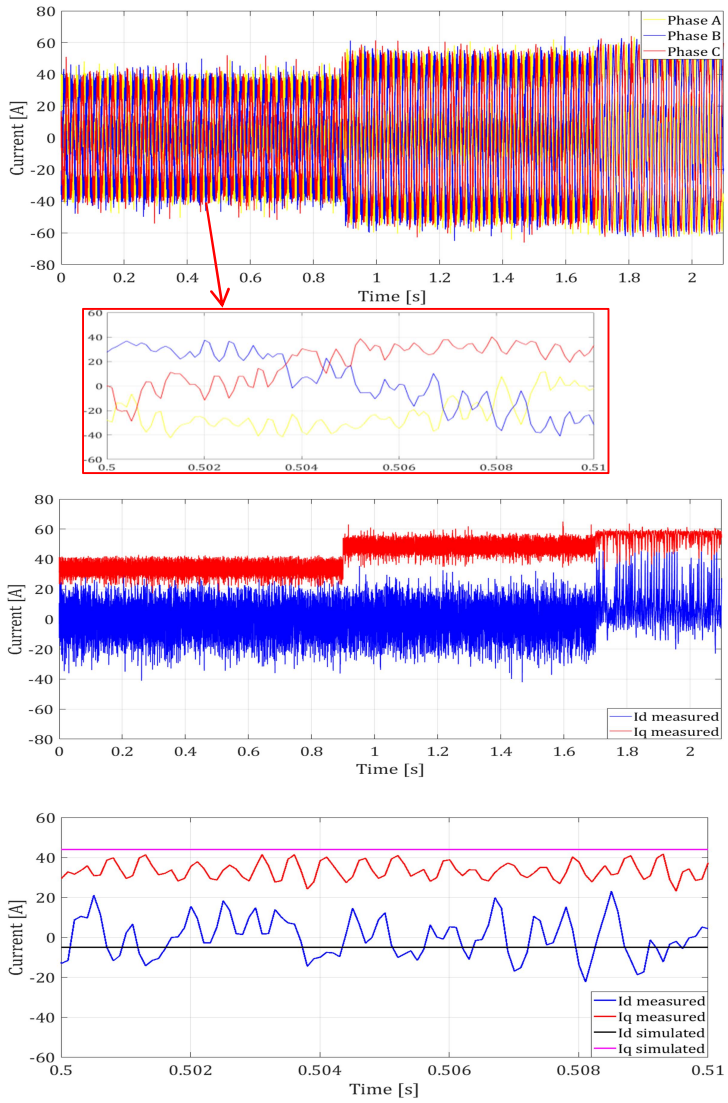

Fig.5. 12 Constant speed operation

This chapter was intended to validate the developed IPMSM experimental model. In conclusion, by performing all the analyzes previously described, the theoretical results were validated by the experimental measurements, as the machine operates as expected on the test bench.

References

[1] Boran Pikula, Elmedin Mesic, Elmedin Mesic, M. Hodzic „Determination of air drag coefficient of vehicle models", Conference: International Congress Motor Vehicles & Motors 2008 - MVM 2008, „Sustainable Development of Automotive Industry".

[2] **Bilatiu, Cristina** & Karaisas, Petros & Martis, Claudia-Steluta. (2021). Electromagnetic Analysis and Experimental Validation of an Interior Permanent Magnet Synchronous Motor. 1-6. 10.1109/ATEE52255.2021.9425229.

[3] T. Moldovan, R. Inţe, R. -O. Nemeş, M. Ruba and C. Marţiş, "Typhoon HIL Real-Time Validation of Permanent Magnet Synchronous Motor's Control," 2021 9th International Conference on Modern Power Systems (MPS), Cluj-Napoca, Romania, 2021, pp. 1-6, doi: 10.1109/MPS52805.2021.9492619.

[4] Hwang, Seon-Hwan & Kim, Jang-Mok & Khang, Huynh Van & Ahn, Jin-Woo. (2010). Parameter Identification of a Synchronous Reluctance Motor by using a Synchronous PI Current Regulator at a Standstill. Journal of Power Electronics. 10. 10.6113/JPE.2010.10.5.491.

[5] Viktor Bobek ''PMSM Electrical Parameters Measurement'' Document number AN4680, 02/2013.

6. Conclusions, Contributions, and Future work

6.1 Final conclusions

The main purpose of this thesis is to design an IPMSM for the propulsion system of an electrical vehicle. The first chapter highlights the context of the work by presenting the PMSM, its particularities, advantages, and disadvantages compared to other available machines on the market, the principle of operation, as well as the constructive elements and variants.

Regarding this particular application, a set of requirements were imposed. The author had to transform these requirements in specifications of the propulsion system in order to be able to design an electrical machine suitable for the given application.

Once the machine's specifications were established, the IPMSM pre-sizing stage began. In this regard, a pre-sizing algorithm was developed, based on which the main dimensions of the machine were determined, the materials from which the main elements of the machine will be built, as well as details such as: the slots-poles combination or the winding configuration. In addition, to determine the main dimensions of the machine to be designed, the limitations imposed by the manufacturing company were also taken into account.

Next, the electromagnetic analysis of the machine was performed using JMAG Designer software package. Based on the results obtained in the pre-sizing stage, the machine's model was built. Firstly, the machine's rotor and stator were modelled, followed by the winding's modelling. Then, the materials from each part is built were assigned, as well as the conditions of the analyses. Next steps consisted in implementing the machine's circuit, setting the mesh and the simulations parameters.

After all the steps above mentioned have been completed, the electromagnetic analysis of the machine was performed. For the simulations, two scenarios (no-load operation, rated-load operation) were considered.

For the no-load analysis the magnetic flux density distribution, the magnetic flux lines, the cogging torque, the induced electromagnetic force and its harmonics, as well as the magnetic flux density in the air-gap and other different point of the machine and their harmonics were taken into account.

On the other hand, for rated-load operation, flux density distribution, the magnetic flux lines, the electromagnetic torque with its components and the torque ripple content, the magnetic flux density in the air-gap and other different point of the machine and their harmonics were analysed. In addition, the machine's parameters, such as the d- and q-axis inductances were computed. Moreover, to compute the machine's inductances, the saturation and cross-saturation phenomena were taken into account in order to analyse the influence of these phenomena on machine's behaviour.

Furthermore, the efficiency map of the machine was computed in the speed range of 0-8000 rpm (the maximum speed). This was aimed at identifying the efficiency of the machine on the mechanical characteristic, thus, the following was concluded:

- the machine's efficiency at rated speed and torque is over 91% (the imposed efficiency by requirements);
- the machine could operate at this efficiency and rated torque up to a speed of 4000 rpm;
- on the curve related to constant power, the machine's efficiency is over 70%.

Moreover, the thermal analysis of the machine was performed and the results show that the machine does not present any problems from a thermal point of view, as the temperature does not exceed the maximum allowed value.

In addition, in order to obtain to complete the analysis of the machine under study, a control strategy will be implemented and tested. For this particular case, the FOC strategy was chosen because of its advantages and simplicity. In addition, to maximize the control performances, FOC was combined with MTPA technique. Upon the performed simulations, it can be concluded that the machine operates as intended since it adheres to the requirements. Moreover, the results of these simulations validate the results obtained in JMAG Designer, being very similar to them.

Next, to validate the machine's prototype, a laboratory test bench was built in the Electrical Machines Research Laboratory of the Technical University of Cluj-Napoca. The first measurement was performed to determine the d- and q-axis inductances, and the obtained measurements were compared with the simulated one. It was concluded that the small differences between data are related both to the material imperfections and manufacturing process. After that, the machine was tested on the test bench. In this regard, three operation scenarios were implemented (no load operation at different speed, constant torque and variable speed operation, constant speed and variable torque operation) and the results are presented in Subsections 5.4 to 5.6.

By comparing both theoretical and experimental results, it was concluded that the designed IPMSM works properly and as expected.

Therefore, it can be concluded that the proposed design, namely the IPMSM having a configuration of 10 poles and 24 slots, meets all the application requirements. In addition, all the analysis, applied techniques, and devices were completely competent to validate the proposed design.

6.2 Personal contributions

The main contributions of this work are summarized below, as follows:

- performing a comprehensive literature review regarding the Permanent Magnet Synchronous Machines used for electrical vehicles propulsion system, based on the available specialized books and papers;
- identifying the main requirements of a propulsion system for electrical vehicles;
- identifying the best-fitted electrical machine for the given application, by reviewing the literature;
- defining the specifications of the electrical machine to be designed;
- defining the IPMSM design algorithm;
- pre-sizing the electrical machine, including the computation of the main dimensions of the machine (such as, the inner/outer stator/rotor diameter, the machine's length, the PMs/slots dimensions , the choice of the optimal combination between the number of poles and number of stator slots, the materials from which the machine's components are made, etc.);
- analysing the influence of winding configuration on the machine's performances;
- development of the Interior Permanent Magnet Synchronous model in JMAG Designer;
- performing the electromagnetic analysis of the machine;
- analysing the influence of saturation and cross-saturation phenomena on the machine's performances;
- performing the thermal analysis of the machine;
- implementing the FOC and MTPA strategies to validate the machine;
- testing the machine on the test bench;
- interpreting the results obtained, comparing them with the simulated results and validating the machine.

6.3 Future work

Regarding the future work, the following items should be implemented:

- performing a 3D analysis and comparing the results obtained via 2D and 3D simulations;
- performing structural analysis of the machine;
- performing the optimization of the machine under test;
- designing new models and analysing the differences between them and the machine that make the object of this thesis in terms of performances;
- improving the laboratory set-up to obtain a wider spectrum of experimental results.

LIST OF FIGURES

LIST OF TABLES

LIST OF PUBLICATIONS

[1] Cosman, Sorin & Moldovan, Cristina & Iusan, Rares & Oprea, Claudiu & Martis, Claudia. (2019). Development of an automated system to optimize greenhouse resource consumption. 1-7. 10.1109/MPS.2019.8759727.

[2] Cosman, Sorin & Bilatiu, Cristina & Martis, Claudia. (2019). Development of an Automated System to Monitor and Control a Greenhouse. 1-4. 10.1109/EMES.2019.8795186.

[3] Bilatiu, Cristina & Cosman, Sorin & Martis, Radu-Andrei & Martis, Claudia & Morariu, Silvan. (2019). Identification and Evaluation of Electric and Hybrid Vehicles Propulsion Systems. 1-5. 10.1109/EV.2019.8892965.

[4] Cosman, Sorin & Iulia, Vascan & Bilatiu, Cristina & Dranca, Marius & Alexandru, Rares & Martis, Claudia. (2020). EDM cutting for rapid prototyping of a PMBG. 1-5. 10.1109/ELEKTRO49696.2020.9130365.

[5] Cosman, Sorin-Iulian & Iulia, Vascan & Bilatiu, Cristina & Tintelecan, Adriana & Martis, Claudia & Zorlescu, Bica. (2020). Design and Analysis of a Heating, Ventilation and Air Conditioning System for Electric Vehicles. 305-310. 10.1109/SPEEDAM48782.2020.9161970.

[6] Cosman, Sorin & Bilatiu, Cristina & Martis, Radu-Andrei & Martis, Claudia & Morariu, Silvan. (2020). Identifying the Propulsion System Characteristics for a Battery Electric Vehicle. 093-097. 10.1109/EPE50722.2020.9305526.

[7] Bilatiu, Cristina & Karaisas, Petros & Martis, Claudia-Steluta. (2021). Electromagnetic Analysis and Experimental Validation of an Interior Permanent Magnet Synchronous Motor. 1-6. 10.1109/ATEE52255.2021.9425229.

[8] Bilatiu, Cristina & Moldovan, Tudor & Martis, Claudia-Steluta. (2022). Electromagnetic Analysis and Experimental Validation of an IPMSM. 234-238. 10.1109/EPE56121.2022.9959809.

[9] BILAȚIU Cristina-Adina, MARȚIȘ Claudia-Steluța -Technical University of Cluj-Napoca, Romania, Permanent Magnet Synchronous Machines Design Aspects, JOURNAL OF COMPUTER SCIENCE AND CONTROL SYSTEMS - Vol. 15, nr. 1, May 2023